This document is downloaded from DR-NTU (https://dr.ntu.edu.sg)
Nanyang Technological University, Singapore.

Mechanics of materials characterization of lead-free solders

Xiong, Bingshou

2005

Xiong, B. S. (2005). Mechanics of materials characterization of lead-free solders. Doctoral thesis, Nanyang Technological University, Singapore.

https://hdl.handle.net/10356/5423

https://doi.org/10.32657/10356/5423

Nanyang Technological University

Downloaded on 17 Aug 2022 06:09:06 SGT

ATTENTION: The Singapore Copyright Act applies to the use of this document. Nanyang Technological University Library

a365086

Mechanics of Materials Characterization of Lead-Free Solders

Xiong Bingshou

School of Mechanical and Aerospace Engineering

A thesis submitted to the Nanyang Technological University
in fulfillment of the requirement for the degree of
Doctor of Philosophy

2005

TS
610
X6
2005

ATTENTION: The Singapore Copyright Act applies to the use of this document. Nanyang Technological University Library

ABSTRACT

Lead-free solders will replace tin-lead solders in electronic products due to European Union laws to restrict the use of toxic materials like lead (Pb) in electronic equipment by July 1st, 2006. Legislation to ban the use of lead (Pb) is forcing the electronic industry to use lead-free solders. Solder interconnections serve as electrical connections and also as the mechanical support to hold the IC component in position on the printed circuit board (PCB). It is important to characterize the mechanical properties of lead-free solders. NEMI (National Electronic Manufacturing Initiative) recommends Sn-3.9Ag-0.6Cu(±0.2%) for reflow soldering process and Sn-0.7Cu solder alloy for wave soldering. The scope of this study includes the two NEMI recommended Pb-free solder alloys, namely Sn-3.8Ag-0.7Cu and Sn-0.7Cu. A mechanics of materials characterization of the elastic-plastic-creep properties and low cycle fatigue behavior is reported. A new visco-plastic constitutive model and fatigue model is presented and used to model the thermal fatigue behavior of a Micro-BGA assembly.

A systematic mechanics of materials study of Sn-3.8Ag-0.7Cu and Sn-0.7Cu lead-free solders is reported in this thesis. Firstly, tensile tests at four different temperatures (-40°C, 25°C, 75°C and 125°C), and at each temperature, three different strain rates (5.6×10^{-4}, 5.6×10^{-3} and 5.6×10^{-2}) were conducted to study the temperature and strain rate effect on tensile properties of Sn-3.8Ag-0.7Cu and Sn-0.7Cu solder alloys. Empirical equations for temperature and strain rate dependent elastic modulus, yield stress and UTS were developed. Visco-plastic constitutive models for both lead-free solders were also presented.

ATTENTION: The Singapore Copyright Act applies to the use of this document. Nanyang Technological University Library

Secondly, creep tests were conducted at four different temperatures (-40°C, 25°C, 75°C and 125°C), and at each temperature, several different stress levels were tested to study the effect of temperature and stress level on the steady state creep strain rate behavior. Creep constitutive models were developed for Sn-3.8Ag-0.7Cu and Sn-0.7Cu.

Thirdly, low cycle fatigue tests were conducted at three different temperatures (25°C, 75°C and 125°C), and at each temperature, different strain range and frequencies were tested to study the effect of temperature and frequency on the fatigue behavior. Both strain-based and energy-based low cycle fatigue life prediction models were developed.

Fourthly, new research contributions have been achieved in the following areas,

(a) A new visco-plastic constitutive model was developed. The new model can accurately simulate strain-stress response with temperature, strain rate and hardening-softening effects.

(b) A new fatigue model was developed, which makes the fatigue lives at different temperatures and frequencies have a master curve with the load drop rate.

(c) Impact tests at three different strain rates (7×10^2, 9×10^2 and 1.3×10^3 s^{-1}) were conducted to study the strain rate effect on impact properties of lead-free solder alloys at room temperature. Yield stress equations over a wide strain rate range (from 10^{-4} to 10^3 s^{-1}) were developed based on impact test results.

Finally, micro-deformation analysis of a Micro-BGA assembly with Sn-3.8Ag-0.7Cu was investigated using in-situ Digital Image Correlation (DIC) measurement. FEA simulation based on the new visco-plastic model was investigated. The measured test data compared well with the FEA results.

ATTENTION: The Singapore Copyright Act applies to the use of this document. Nanyang Technological University Library

Acknowledgement

The author would like to acknowledge and express his sincere appreciation and gratitude to the following people:

A/P Pang Hock Lye, John, the project supervisor, for his invaluable advice and constant encouragement during this project.

Dr. Zhang Xueren, Dr. Liu Qingjun, Dr. Kithva Prakash Hariram, Mr. Mao Xiaohai and Mr. Low Tse Hoong, for their helpful discussion.

All technicians in the Strength of Materials Lab for providing technical support.

Finally, the author would like to express his gratitude to his parents, for their support and encouragement.

ATTENTION: The Singapore Copyright Act applies to the use of this document. Nanyang Technological University Library

Table of Contents

Chapter 1 Introduction 1

1.1 Background 1

1.2 Lead-Free Solder..2

1.3 Reliability Problem of Soldered Assemblies..3

1.4 Objective of the Study..5

1.5 Dissertation Outline..6

Chapter 2 Literature Review 9

2.1 Constitutive Models..9

2.1.1 Elastic-Plastic-Creep Approach..10

2.1.2 Visco-plastic Approach..14

2.2 Low Cycle Fatigue Models..17

2.2.1 Total Life Approach..17

2.2.2 Crack Initiation and Propagation Approach..25

Chapter 3 Experimental Procedure 29

3.1 Tensile Test..29

3.2 Creep Test..34

3.3 Low Cycle Fatigue Test..36

3.4 Split Hopkinson Pressure Bar Impact Test..40

ATTENTION: The Singapore Copyright Act applies to the use of this document. Nanyang Technological University Library

Chapter 4 Tensile Test Data & Analysis 43

4.1 Tensile Test Result....43

4.1.1 95.5Sn-3.8Ag-0.7Cu solder alloy results....43

4.1.2 99.3Sn-0.7Cu solder alloy results....50

4.1.3 Comparison with other reported results....51

4.2 Analysis of Tensile Test Result....57

4.2.1 Strain rate and temperature dependent tensile properties....57

4.2.2 Application to Anand visco-plastic model....60

Chapter 5 Creep Test Data & Analysis 65

5.1 Creep Test Result....65

5.1.1 Creep behavior of lead-free solders....65

5.1.2 95.5Sn-3.8Ag-0.7Cu solder alloy results....68

5.1.3 99.3Sn-0.7Cu solder alloy results....70

5.1.4 Comparison with other reported results....72

5.2 Creep Models....77

Chapter 6 Low Cycle Fatigue Test Data & Analysis 81

6.1 Low Cycle Fatigue Test Result....81

6.1.1 Cyclic stress-strain behavior....81

6.1.2 Effect of temperature on low cycle fatigue behavior....84

6.1.3 Effect of frequency on low cycle fatigue behavior....86

6.1.4 Comparison with other reported results....89

6.2 Low Cycle Fatigue Models....94

ATTENTION: The Singapore Copyright Act applies to the use of this document. Nanyang Technological University Library

Chapter 7 Research on New Visco-plastic Model, Fatigue Model and Impact Yield stress for 95.5Sn-3.8Ag-0.7Cu solder **100**

7.1 New Visco-plastic Model for 95.5Sn-3.8Ag-0.7Cu Solder.........................100

7.1.1 Model Formulation...100

7.1.2 Parameter determination..106

7.2 New Load Drop Rate Fatigue Model for 95.5Sn-3.8Ag-0.7Cu Solder...........111

7.2.1 Strain range, temperature and frequency dependent load drop rate.........111

7.2.2 Load drop rate damage model...116

7.3 Impact Properties and High Strain Rate Model For Sn-3.8Ag-0.7Cu Solder.....120

Chapter 8 Micro-Deformation Analysis of Micro-BGA Assembly **125**

8.1 In-situ Measurements Under Thermal Loading....................................125

8.1.1 Test vehicle...125

8.1.2 Micro-DISC system..126

8.1.3 In-situ thermal deformation measurement....................................128

8.2 FEA Application of New Visco-Plastic Model....................................132

Chapter 9 Conclusion & Recommendation **137**

References **143**

Appendix A USERMAT Subroutine Code **155**

Appendix B FEA Simulation of Simple Tension Displacement Case Study **162**

Appendix C List of Journal Publication **165**

ATTENTION: The Singapore Copyright Act applies to the use of this document. Nanyang Technological University Library

NOMENCLATURE

Sn	Tin
Ag	Silver
Cu	Copper
Pb	Lead
SMT	Surface mount technology
EPA	Environmental Protection Agency
NEMI	National Electronic Manufacturing Initiative
PCB	Printed circuit board
DFR	Design for reliability
FEA	Finite element analysis
WLCSP	Wafer-level chip-scale package
UTS	Ultimate tensile strength
SHPB	Split Hopkinson pressure bar
BGA	Ball grid array
DISC	Digital image speckle correlation
$\frac{d\Phi}{dN}$	Load drop rate
T_m	Melting temperature (K)
σ	Normal stress (MPa)
ε_{ij}	Total normal strain
ε_{ij}^{e}	Elastic normal strain
ε_{ij}^{p}	Plastic normal strain
ε_{ij}^{c}	Creep normal strain
γ	Shear strain
τ	Shear stress (MPa)
E	Elastic modulus (GPa)
G	Shear modulus (GPa)
$d\varepsilon_{in}/dt$	Inelastic strain rate
Q	Activation energy
R	Universal gas constant
b	Burgers vector
k	Boltzmann's constant (J/K)
d	Grain size
D_0	Diffusion constant
T	Absolute temperature (K)
ΔH_{GB}	Activation energy for grain boundary,
ΔH_{MC}	Activation energy for matrix creep
Q_c	Activation energy for the core-diffusion
Q_l	Activation energy for lattice-diffusion
$\Delta\varepsilon_p$	Plastic strain range

ATTENTION: The Singapore Copyright Act applies to the use of this document. Nanyang Technological University Library

g	Equilibrium or back stress
c	Fatigue exponent
ε'_f	Fatigue ductility coefficient
N_f	Fatigue life
σ'_f	Fatigue strength coefficient
b	Fatigue strength exponent
$\Delta\gamma_{mc}$	Strain range due to matrix creep
TSOP	Thin small outline package
N_p	Number of cycles to failure due to plastic fatigue
N_c	Number of cycles to failure due to the creep fatigue
SRP	Strain range partitioning method
f	Frequency (Hz)
$\Delta\overline{W}_{total}$	Total strain energy (J)
ν	Poisson's ratio
J	J integral
LCF	Low cycle fatigue
ASTM	American society for testing and materials
σ_{dr}	Dynamic recovery parameter
σ_{ss}	Saturation stress
$h'(\varepsilon)$	Strain hardening function
ε_i	Initial strain
σ_{h-s}	Hardening-softening parameter
TEC	Thermoelectric coolers
DNP	Displacement from neutral point

ATTENTION: The Singapore Copyright Act applies to the use of this document. Nanyang Technological University Library

Chapter 1. Introduction

Electronic packaging is a challenging research area due to the introduction of new materials, development of packaging design, minimization of structures, and many challenges driven by technological, environmental and economic considerations. For electronic products, reliable fatigue design is required for long-term reliability, especially when dealing with lead-free solder materials, where constitutive models and fatigue analysis are needed.

1.1 Background

Interest in advanced solder alloys arises from the increase use of surface mount technology (SMT) in electronic assemblies. Surface mount technology was developed to overcome the limitations of pin-through-hole (PTH) assembly technology. SMT can achieve more Input/Output (I/Os) and lower volumes compared to PTH technology. Development of surface mount devices moves from SMT-peripheral (such as QFP) to SMT- Area Array (such as BGA), and onto chip scale packaging (CSP) due to industry tends to minimize package size and increase solder joint I/Os. Hence, the electronics industry focused their attention on research and development of solder based manufacturing technologies [1]. In Singapore, the electronics sector is one of the most important industries and the production of high-quality and reliable electronic products are dependent on the advances in electronic packaging technology. As this industry advances, the demand in manufacturing efficiency, increased device

ATTENTION: The Singapore Copyright Act applies to the use of this document. Nanyang Technological University Library

function and reliability is expected. Solder joint reliability research for lead-free solder alloys is urgently needed as the industry will have to adjust to lead-free electronic manufacturing in the coming years.

1.2 Lead-Free Solder

Tin-lead solders are the primary materials used for interconnecting electronic components for many reasons, such as low cost, good soldering properties, known metallurgical and fatigue resistance properties. However, lead (Pb) in solders has been cited by the Environmental Protection Agency (EPA) in the USA as one of the materials posing a health and environment problem. Untreated or inadequately treated water containing lead from waste dumping is a major health concern. The European Commission introduced two legislations, WEEE (Waste Electrical and Electronic Equipment) and ROHS (Reduction of Hazardous Substances) to minimize the risks and impact that the production, use, treatment and disposal of waste electrical and electronic equipment has on human health and the environment. The European Parliament has approved the ban on hazardous substances including lead (Pb) to take effect on July 1st, 2006.

The main substitutes for traditional tin-lead (Sn-Pb) solders are Sn-Ag-Cu, Sn-Cu, and Sn-Ag lead-free solder alloys [2-3]. The National Electronic Manufacturing Initiative (NEMI) recommends using Sn-3.9Ag-0.6Cu(±0.2%) solder for reflow soldering and Sn-0.7Cu solder alloy for wave soldering [4]. Tin-lead solders have been studied for more than 40 years, while research on lead-free or Pb-free solders is

ATTENTION: The Singapore Copyright Act applies to the use of this document. Nanyang Technological University Library

active in recent years. Mechanics of materials characterization of lead-free solders are needed for understanding and developing reliable SMT assemblies with lead-free solders.

1.3 Reliability Problem of Soldered Assemblies

In SMT soldered assemblies, solder joints provide electrical connections and function as structural members to join the IC components to the printed circuit boards (PCBs). That means the solder alloys serve not only as an interconnect material for electrical connections but also as the mechanical support to hold the component in position on the PCBs. The assemblies contain materials with different coefficients of thermal expansion and generate high cyclic strain in the solder joints when subjected to cyclic thermal loading. The thermal loadings may be caused by either changes in the external temperature or internal heat generation and dissipation by operating devices. The temperature fluctuation may be large, for example, from -55°C to 125°C for automotive electronic components; or small, for computers in climate-controlled environment. Even small temperature fluctuations can have a large effect, depending upon the size of the package and solder joint, and the difference in the thermal expansion of the materials.

The majority of current reliability test methodologies are based on empirical analysis of reliability test data [5]. That means, the solder joints on an actual product are exposed to conditions of accelerated thermo-mechanical fatigue, the lifetime prediction will be extrapolated based on the accelerated fatigue data. Such test

ATTENTION: The Singapore Copyright Act applies to the use of this document. Nanyang Technological University Library

methods for thermal cycling are time consuming and expensive to use for extensive parametric studies. In order to study the reliability problem of solder in SMT assemblies more fundamentally, a fatigue life prediction method employing a Design For Reliability (DFR) approach is needed. The schematic illustration of the DFR methodology is shown in Fig. 1-1. The stress-strain relationship and creep properties highlighted in the figure must be obtained from tensile and creep tests and expressed as mechanics models in Finite Element Analysis (FEA) to calculate the plastic strain range or strain energy density in the solder material. These failure parameters can then be used in fatigue models, which are developed based on low cycle fatigue tests of solder alloys, to predict the fatigue life of solder joints.

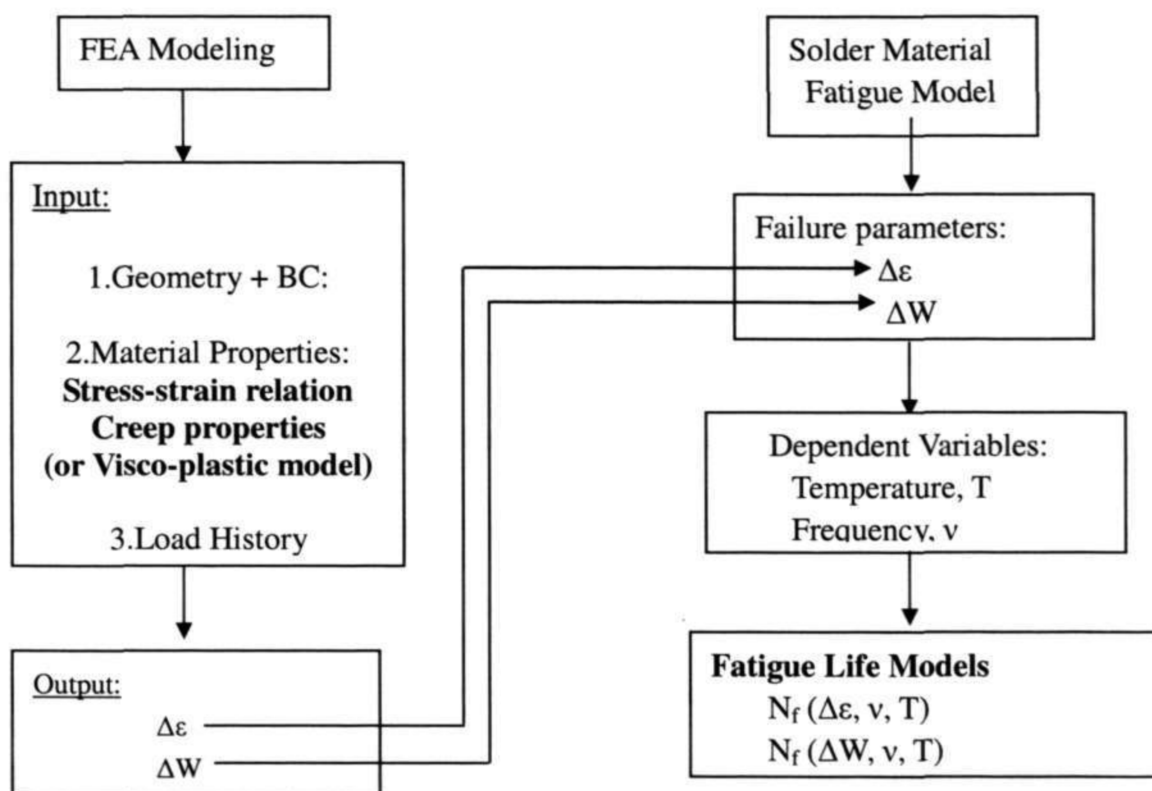

Fig. 1-1 Schematic illustration of Design for Reliability Methodology

ATTENTION: The Singapore Copyright Act applies to the use of this document. Nanyang Technological University Library

1.4 Objective of the Study

The objective of this study is to characterize the mechanical properties of two lead-free solder alloys (Sn-3.8Ag-0.7Cu and Sn-0.7Cu) and develop new constitutive and fatigue models for these lead-free solder alloys. Mechanics of materials characterization of the elastic-plastic-creep properties and low cycle fatigue behavior were investigated. A new visco-plastic constitutive model was developed and applied to FEA simulation of a Micro-BGA assembly subjected to thermal loading. A new load-drop fatigue model was developed to improve on the existing low cycle fatigue analysis of solder materials.

The specific research objectives are:

(i) Develop temperature and strain rate dependent tensile properties and stress-strain relations for Pb-free solders.

(ii) Develop creep constitutive model for Pb-free solders.

(iii) Develop low cycle fatigue model for Pb-free solders, study the effects of temperature and frequency.

(iv) Develop new visco-plastic constitutive model for Pb-free solders.

(v) Develop new fatigue model based on a load-drop parameter.

(vi) Application of developed constitutive models to a Micro-BGA packaging assembly subject to thermal loading.

ATTENTION: The Singapore Copyright Act applies to the use of this document. Nanyang Technological University Library

1.5 Dissertation Outline

The dissertation is organized into nine chapters. The structure of each chapter is summarized in the following.

Chapter one introduces the need for mechanics of materials research of lead-free solders.

Chapter two review and categorize the published constitutive and fatigue models of solder alloys.

Chapter three introduces the experimental procedure in this study. The specimen geometry, test machine and test conditions for tensile, impact, creep and fatigue tests are described.

Chapter four investigates the mechanical properties at different temperature and strain rate for the two lead-free solders (Sn-3.8Ag-0.7Cu and Sn-0.7Cu), and the data were compared with other reported results. The apparent elastic modulus, yield stress and ultimate tensile strength (UTS) will be presented as function of temperature and strain rate. The test data were applied to the Anand visco-plastic model for both lead-free solders.

Chapter five studies the creep behavior at different temperature and stress level for the two lead-free solders (Sn-3.8Ag-0.7Cu and Sn-0.7Cu). The creep data are compared with other reported results. The steady state creep strain rate of lead-free solders is characterized by the established hyperbolic sine creep model.

Chapter six studies the low cycle fatigue behavior for the two lead-free solders (Sn-3.8Ag-0.7Cu and Sn-0.7Cu), and the fatigue data are compared with other

ATTENTION: The Singapore Copyright Act applies to the use of this document. Nanyang Technological University Library

reported results. The fatigue test results for the two lead-free solders are described by low cycle fatigue models, where temperature and frequency dependent constants were determined. Frequency-modified low cycle fatigue models are developed to characterize the fatigue behavior of the lead-free solders over wide range of frequencies.

Chapter seven focus on new research contributions for Sn-3.8Ag-0.7Cu solder. Firstly, a new visco-plastic constitutive model is formulated and applied to model the tensile test results and shows good agreement. Secondly, a new fatigue parameter (load drop rate, $\frac{d\Phi}{dN}$) is introduced to overcome the difficulties encountered in conventional low cycle fatigue models employed earlier. Thirdly, high strain rate impact tests on Sn-3.8Ag-0.7Cu lead-free solder are investigated. The yield stress equation over a wide range of strain rate (from 10^{-4} to 10^{3}) is developed.

Chapter eight applies the developed models in Finite Element Analysis (FEA) to simulate a Micro-BGA assembly with Sn-3.8Ag-0.7Cu lead-free solder subject to thermal loading. The thermal loading was applied to Micro-BGA assembly from 25°C to 125°C. In-situ measurement is conducted by a Micro-DISC (Digital Image Speckle Correlation) system. The displacement and strain field of the solder joint at 75°C and 125°C were measured. The results from the in-situ measurements are compared to the FEA results. The FEA simulation employed the new constitutive visco-plastic model. A subroutine code was programmed and integrated into the ANSYS finite element analysis software. The comparison between the in-situ measurement strain and FEA simulated strain are made.

ATTENTION: The Singapore Copyright Act applies to the use of this document. Nanyang Technological University Library

Chapter nine concludes with the key results, contributions made and suggestions for future research study.

ATTENTION: The Singapore Copyright Act applies to the use of this document. Nanyang Technological University Library

Chapter 2. Literature Review

Solder materials are usually subjected to thermo-mechanical loadings at the high operating temperatures, 0.5 to 0.8 times T_m of the alloy, and deformation induced are non-linear and consist of plastic and creep effects. The stress, strain or strain energy density during the thermal-mechanical loading will not be directly measured or controlled in the field situation. However, these quantities are quite important for fatigue life prediction and estimated by calculations or simulations. Therefore, the constitutive models to calculate these quantities are the basis of the solder fatigue life prediction methodology. In this chapter, constitutive and fatigue models for solder alloys will be reviewed.

2.1 Constitutive Models

Due to the low melting temperature, solders have complex mechanical phenomena, both the time-independent plastic strain and time-dependent creep strain are significant parts of the solder deformation. The published constitutive models for solder alloys behavior can be categorized into elastic-plastic-creep approach and visco-plastic approach.

ATTENTION: The Singapore Copyright Act applies to the use of this document. Nanyang Technological University Library

2.1.1 Elastic-plastic-creep approach

Elastic-plastic-creep approach treats the total strain as the sum of the phenomenological components of elastic strain, time independent plastic strain and time dependent creep strain as shown below,

$$\varepsilon_{ij} = \varepsilon_{ij}^{e} + \varepsilon_{ij}^{p} + \varepsilon_{ij}^{c} \tag{2.1.1}$$

where ε_{ij} , ε_{ij}^{e} , ε_{ij}^{p} and ε_{ij}^{c} are total, elastic, time-independent plastic and time-dependent creep strain tensors, respectively. The formation of elastic and plastic strain is the same for all models. While the formulation for creep strain differs depending on the creep mechanism model used as shown in Fig. 2-1. Depending on temperature and applied stress, dislocation glide, dislocation recovery, Nabarro-Herring creep and dislocation glide-climb mechanisms may be the dominant creep deformation mechanism. At low temperature and high stress level, dislocation glide is the dominant mechanism; however, at high temperature and low stress level, Nabarro-Herring creep mechanism occurs by diffusional mass transport will dominate the creep deformation.

ATTENTION: The Singapore Copyright Act applies to the use of this document. Nanyang Technological University Library

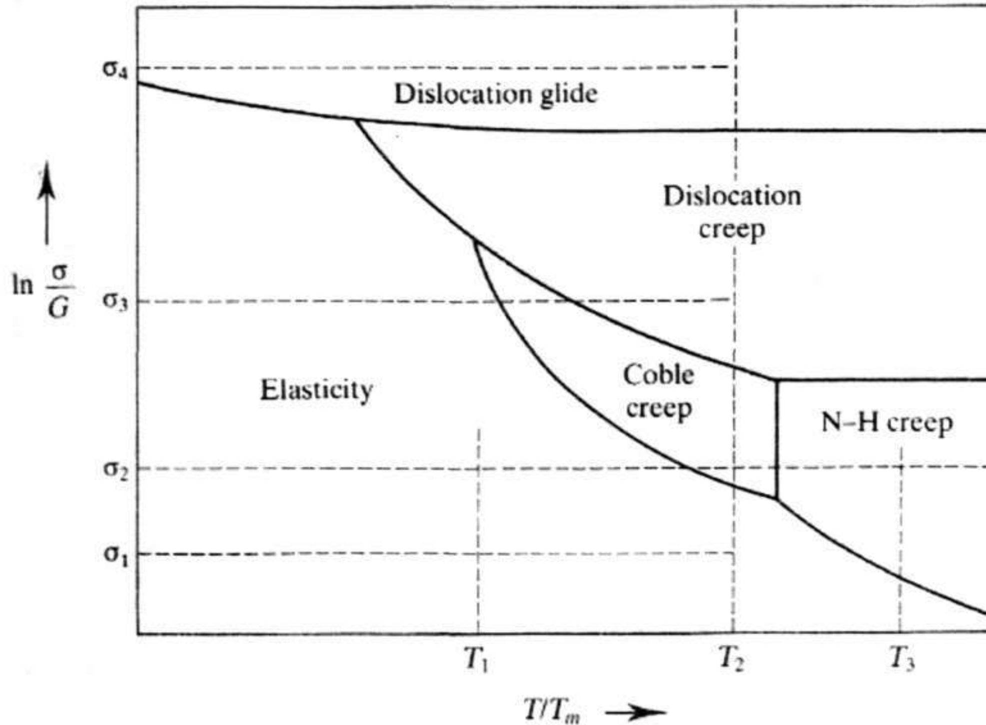

Fig. 2-1 Schematic of deformation mechanism map

Some of the creep and plastic strain forms will be discussed in the following parts:

Knecht and Fox [6] proposed a constitutive relation based on total shear strain rate. For time dependent creep strain rate, the Integrated Matrix Creep (IMC) model was introduced, accounts for the effects of equivalent grain boundary creep and the equivalent matrix creep by utilizing a creep strain rate equation in the form of two power laws:

$$\dot{\gamma}_{cr} = C_1 \exp\left(\frac{-\Delta H_{GB}}{kT}\right)\tau^{n_{GB}} + C_2 \exp\left(\frac{-\Delta H_{MC}}{kT}\right)\tau^{n_{MC}} \tag{2.1.2a}$$

where C_1 and C_2 are material constants, ΔH_{GB} is the activation energy for grain boundary, ΔH_{MC} is the activation energy for matrix creep, k is Boltzmann's constant, T is absolute temperature, τ is the shear stress, n_{GB} and n_{MC} are grain boundary creep

ATTENTION: The Singapore Copyright Act applies to the use of this document. Nanyang Technological University Library

and matrix creep exponents, respectively. The time-independent elastic and plastic strain part is,

$$\gamma_{e+p} = \frac{\tau}{G} + \left(\frac{\tau}{\tau_p}\right)^n \tag{2.1.2b}$$

where γ_{e+p} is the time-independent elastic and creep strain, G is the shear modulus and τ_p is plasticity parameter.

Darveaux [7] proposed a model based on inelastic strain, which neglected the time independent elastic strain, shown in the following equations below.

$$\varepsilon_{in} = \varepsilon_c + \varepsilon_P \tag{2.1.3a}$$

$$\varepsilon_c = \frac{d\varepsilon_s}{dt} t + \varepsilon_T \left(1 - \exp\left(-B \frac{d\varepsilon_s}{dt}\right)\right) \tag{2.1.3b}$$

$$\varepsilon_p = C_p \left(\frac{\sigma}{G}\right)^{m_p} \tag{2.1.3c}$$

where ε_c and ε_p are the creep and plastic strain, respectively. For creep strain, Darveaux included the transient creep strain (ε_T) in the model. The transient creep strain will occur immediately after the stress is applied and before a steady state creep stage is reached, the transient creep strain will be more dominant when the stress level is low. While $d\varepsilon_s/dt$ is the steady creep rate, B is the transient creep coefficient, ε_p is the time-independent plastic strain, G is shear modulus, and C_p and m_p are material constants.

Akay, et al [8-9] used only the creep part to represent the total inelastic strain, the creep law is shown as,

$$\frac{d\gamma_s}{dt} = \frac{CGb}{kT}\left(\frac{b}{d}\right)^p \left(\frac{\tau}{G}\right)^n D_0 \exp\left(\frac{-\Delta H}{kT}\right) \tag{2.1.4}$$

ATTENTION: The Singapore Copyright Act applies to the use of this document. Nanyang Technological University Library

where dγ/dt is steady-state shear strain rate, G is shear modulus, b is Burgers vector. k is Boltzmann's constant, d is grain size, τ is applied stress, D_0 is diffusion constant, ΔH is activation energy for the deformation process, p is grain size exponent, C is a constant characteristic of the underlying micro-mechanism. Akay's model correlates the macro material behavior with microstructure. The stress exponent, n, is dependent on the rate controlling mechanism. At low stresses, n=1 for diffusion creep, n=2 for grain boundary sliding. At intermediate stresses, n=3 to 4 dislocation glide controlled kinetics, and n=5 to 7 for dislocation climb process. At high stresses, the strain rate is an exponential function of stress. The intermediate-to-high stress power law breakdown region can be described by a hyperbolic-sine expression [10]:

$$\frac{d\gamma_s}{dt} = C_1 \frac{G}{kT}\left[\sinh\left(\alpha\frac{\tau}{G}\right)\right]^n \exp\left(\frac{-\Delta H}{kT}\right) \tag{2.1.5}$$

where α prescribes the stress level at which the power dependence break down and C_1 is a constant.

Shi et al [11] also proposed a creep model to describe the creep flow of the solder and the model is capable of explaining the issues of stress and temperature dependent stress exponent and activation energy in the Arrhenius power-law model, shown as

$$\dot{\gamma} = C_1 \frac{G}{T}\left(\frac{\tau}{G}\right)^n \left[1 + C_2 \exp\left(-\frac{(Q_c - Q_l) - (\alpha - \beta)(\tau / G)}{RT}\right)\right] \exp\left(-\frac{Q_l - \alpha(\tau / G)}{RT}\right) \tag{2.1.6}$$

where C_1, C_2, α, β are material constants, Q_c and Q_l are the activation energy for the core-diffusion and that for lattice-diffusion, respectively. τ is shear stress, G is shear modulus, T is absolute temperature, R is gas constant.

ATTENTION: The Singapore Copyright Act applies to the use of this document. Nanyang Technological University Library

Elastic-plastic-creep approach is a phenomenological way to describe the constitutive behavior of solder alloy, since the elastic, plastic and creep strains represent different deformation stages. All types of strain have been studied very well, for example, many creep models for high temperature metals can be used for solder creep modeling. However, during the thermal-mechanical loading, the time-independent plastic strain and time-dependent creep strain is difficult to distinguish. From the non-linear deformation modeling point of view, the mechanism of the creep and plastic strain may be related to dislocation motion. In order to study the constitutive behavior from a state variable visco-plastic approach, the creep and plastic strain may be combined into inelastic strain, accumulated over a deformation history.

2.1.2 Visco-plastic approach

The visco-plastic approach follows the materials science perspective that dislocation motion is the cause of both creep and plastic deformation, and combined them into a state variable inelastic strain. The total strain is expressed as,

$$\varepsilon_{ij} = \varepsilon_{ij}^{e} + \varepsilon_{ij}^{in} \tag{2.1.7}$$

where ε_{ij}^{in} is the inelastic strain tensor. Some of the visco-plastic models will be described next.

One visco-plastic model commonly used for solder is the Anand model, which was reported by Anand [12]. The Anand model [13] consists of two coupled differential equations that relate the inelastic strain rate to the rate of deformation resistance. The strain rate equation is represented by,

ATTENTION: The Singapore Copyright Act applies to the use of this document. Nanyang Technological University Library

$$\frac{d\varepsilon_{in}}{dt} = A\left[\sinh\left(\xi\frac{\sigma}{s}\right)\right]^{\frac{1}{m}}\exp(-Q/RT) \tag{2.1.8a}$$

and the rate of deformation resistance equation by

$$\dot{s} = \left\{h_0(|B|)^{a}\frac{B}{|B|}\right\}\frac{d\varepsilon_p}{dt} \tag{2.1.8b}$$

$$B = 1 - \frac{s}{s^*} \tag{2.1.8c}$$

$$s^* = \hat{s}\left[\frac{1}{A}\frac{d\varepsilon_p}{dt}\exp(-Q/RT)\right] \tag{2.1.8d}$$

where $d\varepsilon_{in}/dt$ is the effective inelastic strain rate, σ is effective true stress, s is the deformation resistance, T is the absolute temperature, A is the pre-exponential factor, ξ is the stress multiplier, m is the strain rate sensitivity of stress, Q is the activation energy, R is the universal gas constant, h_0 is the hardening/softening constant, $\hat{s}$ is the coefficient for deformation resistance saturation value, n is the strain rate sensitivity of saturation value, and α is strain rate sensitivity of hardening or softening. In order to curve-fit the nine material constants in the Anand model, the incremental form shown in Eq. (2.1.8) should be integrated into integral form, which is shown in Eq. (2.1.9).

$$\sigma^* = \frac{\hat{s}}{\xi}\left(\frac{\dot{\varepsilon}_p}{A}e^{Q/RT}\right)^{n}\sinh^{-1}\left[\left(\frac{\dot{\varepsilon}_p}{A}e^{Q/RT}\right)^{m}\right] \tag{2.1.9a}$$

$$\sigma = \sigma^* - [(\sigma^* - cs_0)^{(1-a)} + (a-1)ch_0\sigma^{*(-a)}\,\varepsilon_p]^{1/(1-a)} \tag{2.1.9b}$$

ATTENTION: The Singapore Copyright Act applies to the use of this document. Nanyang Technological University Library

The creep test results can be used to curve-fit the constants in Eq.(2.1.9a), which is the flow equation; while stress-strain curves from tensile tests are used to fit the material constants in Eq.(2.1.9b). The Anand model has been coded into the ANSYS Finite Element software and has been widely used for simulation of the solder joint deformation under thermal-mechanical loading.

Other visco-plastic models were also developed for solder alloys. Tachibana Y. and Krempl E. [14-16] proposed their visco-plastic model based on overstress, called VBO model. VBO model contains a state variable called the equilibrium (back) stress. Bor [17] modified VBO model and applied it into Sn-Pb solder. Unified creep-plasticity (UCP) models are also proven to be successful methods to model the solder material at high homologous temperatures. McDowell D.L. [18] introduced a thermo-viscoplastic internal state variable model to simulate the solder alloys. Wen et al [19] incorporated the damage effect into UCP model, and applied it to Sn-Ag lead-free solder. Busso et al [20] proposed another UCP model, which assumes that the inelastic strain is the result from the release of the dislocations. Other constitutive models were also developed to describe the stress-strain behavior for high temperature metals and other materials. Yaguchi M. [21-23] proposed the model for nickel-base super alloy.

Although the Anand model is widely used for solder joint reliability analysis, its dynamic hardening term h combines the dynamic recovery and strain hardening effects and loses the physical meaning of h. New visco-plastic constitutive model is needed to overcome this concern.

ATTENTION: The Singapore Copyright Act applies to the use of this document. Nanyang Technological University Library

2.2 Low Cycle Fatigue Models

Low cycle fatigue behavior of solders is an important property for fatigue life prediction analysis of thermal cycling tests for soldered assemblies. Typically, thermal cycling test failures fall between 1000 to 10,000 cycles, which is related to low cycle fatigue behavior. Over the years, generally there are two types of approaches to model the fatigue life of structures. They are the total life approach, and the crack initiation and propagation approach. For total life approach, some fatigue parameters, such as strain or strain energy density are used to predict the total fatigue life. However, the crack initiation and propagation approach will predict the fatigue life with a pre-existing crack, the fatigue life is the number of cycles to propagate this crack to a critical size.

2.2.1 Total life approach

Total life approach can be divided into three major methods, based on the fatigue driving force parameter used to characterize the fatigue damage process. These three parameters are (a) plastic strain range, (b) creep strain range and, (c) inelastic energy density or plastic work. In the strain range based fatigue approach, strain controlled loading have been reported by many researchers [24-37]. The strain range based fatigue approach can be further divided into plastic strain range and creep strain range methods. Plastic strain deformation focuses on the time-independent plastic effect, while creep strain accounts for the time-dependent effects. The energy-based fatigue models employ the stress-strain hysteresis energy density of the solder specimen.

ATTENTION: The Singapore Copyright Act applies to the use of this document. Nanyang Technological University Library

2.2.1.1 Plastic Strain Range Fatigue Models

The Coffin-Manson fatigue model [38-39] is perhaps the best-known and most widely used approach. The total number of cycles to failure, N_f, is depicted as being dependent on the plastic strain range, $\Delta\varepsilon_p$, the fatigue ductility coefficient, ε'_f, and the fatigue ductility exponent, c, given in the expression below:

$$\frac{\Delta\varepsilon_p}{2} = \varepsilon'_f (2N_f)^c \qquad (2.2.1)$$

The fatigue ductility coefficient, ε'_f, is approximately equal to the true fracture ductility, ε_f. The fatigue ductility exponent, c, varies between –0.5 and –0.7 for tin-lead solder (Dieter, 1986 [40]; Kilinski, 1991 [41]), and experimental data are required to determine the constants. Actual solder joint fatigue tests, however, are often time consuming and the results are usually applicable only to the specific geometry of the solder joint. For small solder joints, FEA modeling can be used to determine the plastic strain, which is then used to predict the fatigue life. This version of the Coffin-Manson relation assumes that fatigue failure is strictly due to plastic deformation and that elastic strains contribute only a small portion to fatigue failure.

Because the Coffin-Manson equation considers only plastic deformations, it is commonly combined with the Basquin's equation to account for elastic deformation as well [41]. The resulting equation is known as the total strain equation, and is given below:

$$\frac{\Delta\varepsilon}{2} = \frac{\sigma'_f}{E} (2N_f)^b + \varepsilon'_f (2N_f)^c \qquad (2.2.2)$$

ATTENTION: The Singapore Copyright Act applies to the use of this document. Nanyang Technological University Library

where $\Delta\varepsilon$ is the strain gauge, σ'_f is the fatigue strength coefficient, E is the elastic modulus, ε'_f is the fatigue ductility, b is the fatigue strength exponent (Basquin's exponent), and c is the fatigue ductility exponent. This fatigue model is an improvement over the Coffin-Manson equation in that it also accounts for the elastic contribution to fatigue failure.

Solomon's low cycle fatigue model [42] relates the plastic shear strain range to fatigue life cycles is given below:

$$\Delta\gamma_p N_p^{\alpha} = \theta \qquad (2.2.3)$$

$\Delta\gamma_p$ is the plastic shear strain range. N_p is the number of cycles to failure, θ is the inverse of the fatigue ductility coefficient, and α is a material constant. Typical hysteresis loop is shown in Fig. 2-2.

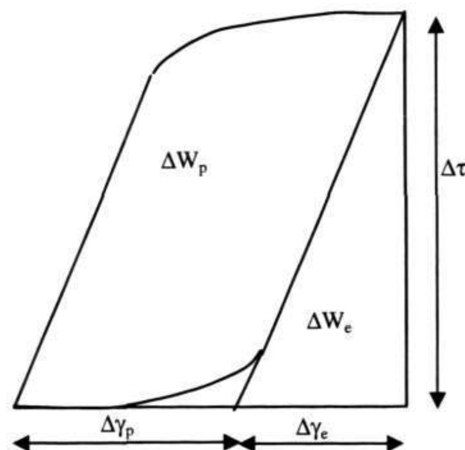

Fig. 2-2 Typical hysteresis loop

ATTENTION: The Singapore Copyright Act applies to the use of this document. Nanyang Technological University Library

2.2.1.2 Creep Strain Range Fatigue Models

Creep strain range fatigue models account strictly for the cyclic creep deformation in the solder joints. Early attempts at modeling creep were made by isolating the elastic and plastic deformation mechanisms. Creep, as mentioned previously, can be separated into two possible mechanisms, matrix and grain boundary creep. Knecht and Fox [43] proposed a simple matrix creep fatigue model relating the solder microstructure and the matrix creep shear strain range given below,

$$N_f = \frac{C}{\Delta\gamma_{mc}} \tag{2.2.4}$$

The number of cycles to failure, N_f, is related to a constant C, which is dependent on failure criteria and solder microstructure. $\Delta\gamma_{mc}$ is the strain range due to matrix creep.

The second creep mechanism, grain boundary sliding, is incorporated with matrix creep into a fatigue model presented by Syed [44-45]. In this model, creep strain is partitioned into two parts as shown [44],

$$N_f = \left([0.022D_{gbs}] + [0.063D_{mc}]\right)^{-1} \tag{2.2.5}$$

Here, D_{gbs} and D_{mc} are the accumulated equivalent creep strain per cycle for grain boundary sliding and the matrix creep, respectively. Results published by Syed on thin small outline package (TSOP) parts indicated that the dominant mechanism changes from grain boundary sliding to matrix creep for faster ramp rates, stiffer assemblies, and lower temperature controlling the lower temperature ranges.

ATTENTION: The Singapore Copyright Act applies to the use of this document. Nanyang Technological University Library

2.2.1.3 Creep-Fatigue Interaction Model

By applying Miner's linear superposition principal, both plastic and creep strain can be accounted for in strain-based fatigue model. This model combines the Solomon fatigue model with the Knecht and Fox creep model, and is given below:

$$\frac{1}{N_f} = \frac{1}{N_p} + \frac{1}{N_c} \tag{2.2.6}$$

where N_p refers to the number of cycles to failure due to plastic fatigue and is obtained directly from the Solomon's fatigue model. N_c refers to the number of cycles to failure due to the creep fatigue and is obtained from the Knecht and Fox's creep fatigue model. This fatigue model relates the fatigue behavior to the plastic shear strain imposed on the specimen, and requires data collection or determination of the experimental plastic strain range. The model has been applied to ceramic BGA and underfilled flip chip assemblies subjected to thermal cycling loading [46-49]. However, this model does not account for frequency effects.

A similar approach is the Strain Range Partitioning (SRP) approach [41]. In SRP, a typical hysteresis loop can be separated into four components, the plastic strain in tension and compression (PP), the creep strain in tension and compression (CC), the creep strain in tension-plastic strain in compression (CP) and the plastic strain in tension-creep strain in compression (PC), as shown in Fig. 2-3. The SRP equation is given below:

$$\frac{1}{N_f} = \frac{F_{pp}}{N_{pp}} + \frac{F_{cc}}{N_{cc}} + \frac{F_{cp}}{N_{cp}} + \frac{F_{pc}}{N_{pc}} \tag{2.2.7}$$

where F_{ij} is the fraction of the total inelastic strain range of the hysteresis loop. The

ATTENTION: The Singapore Copyright Act applies to the use of this document. Nanyang Technological University Library

contributions to each part are determined from other fatigue models and from cyclic stress-strain test. Though the SRP model is a good approach to study the creep-fatigue interaction, it may be difficult for application.

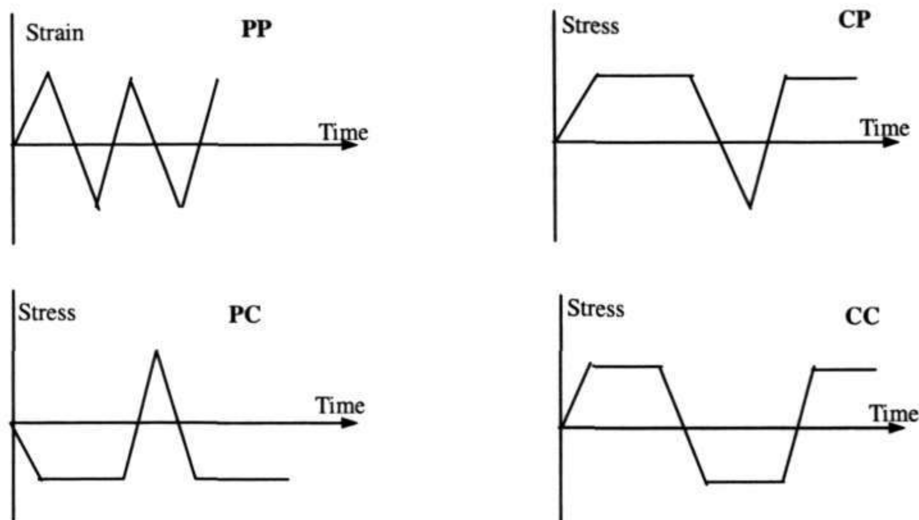

Fig. 2-3 Schematic of the Strain Range Partitioning Method

2.2.1.4 Total Strain Range Fatigue Model

The Engelmaier fatigue model [50] is shown in Eq. (2.2.8), the total number of cycles to failure is related to the total shear strain, $\Delta\gamma_t$, the fatigue ductility coefficient, ε'_f, and the variable, c, which is a function of frequency and temperature.

$$N_f = \frac{1}{2}\left[\frac{\Delta\gamma_t}{2\varepsilon'_f}\right]^{1/c} \tag{2.2.8}$$

where $c=-0.442-6\times10^{-4}T_s+1.74\times10^{-2}\ln(1+f)$ for Sn-Pb solders. T_s is the mean cyclic solder joint temperature in °C, and f is the cyclic frequency in cycles/day. This fatigue model improves on Soloman's and Coffin-Manson by including cyclic frequency and temperature effects.

ATTENTION: The Singapore Copyright Act applies to the use of this document. Nanyang Technological University Library

2.2.1.5 Frequency Modified Plastic Strain Range Method

The constants in the Coffin-Manson model are dependent on temperature and cyclic frequency. Shi et al. [51] proposed a modified Coffin-Manson model for eutectic tin-lead solder given below:

$$\left[N_f \nu^{(k-1)}\right]^m \Delta\varepsilon_p = C \tag{2.2.9}$$

where $\nu^{(k-1)} =$

$$\begin{cases} \nu^{(k_1-1)} & for\ 1Hz \geq \nu \geq 10^{-3}\,Hz \\ \left[\dfrac{\nu}{10^{-3}}\right]^{(k_2-1)} \left(10^{-3}\right)^{(k_1-1)} & for\ 10^{-3}\,Hz > \nu \geq 10^{-4}\,Hz \end{cases}$$

where k_1, k_2, m and C are dependent on temperature. The frequency effect was compensated by this frequency-modified model. However, the temperature effect of low cycle fatigue behavior is still a problem.

2.2.1.6 Energy-Based Models

Energy-based fatigue models are used to predict fatigue failure based on measured hysteresis energy volume-weighted average strain energy density history. Fatigue energy is typically calculated using some correlation to the energy under the stress-strain hysteresis loop. Akay et al [8-9] has proposed the following fatigue model, based on the total strain energy,

$$N_f = \left(\frac{\Delta \overline{W}_{total}}{W_0}\right)^{1/k} \tag{2.2.10}$$

where N_f is the mean cycles to failure, $\Delta \overline{W}_{total}$ is the total strain energy, W_0 and k are fatigue coefficients. They used this model on an LLCC leaded package fatigue

ATTENTION: The Singapore Copyright Act applies to the use of this document. Nanyang Technological University Library

behavior.

Darveaux et. al [10] used strain energy to predict crack initiation and crack growth, the equations are given below:

$$N_0 = K_1 \Delta W^{K_2} \tag{2.2.11}$$

$$\frac{da}{dN} = K_3 \Delta W^{K_4} \tag{2.2.12}$$

where ΔW is strain energy, K_1, K_2, K_3, and K_4 are material constants. When this model was used in finite element analysis, the strain energy ΔW is normalized by the volume of the element:

$$\Delta W_{ave} = \frac{\sum \Delta W \bullet V}{\sum V} \tag{2.2.13}$$

where ΔW_{ave} is the average strain energy, V is the volume of each element.

Shi et al. [52] proposed a modified energy-based low cycle fatigue model, given below:

$$\left[N_f \nu^{(k-1)}\right]^m \frac{W_p}{2\sigma_f} = C \tag{2.2.14}$$

where $\nu^{(k-1)} =$

$$\begin{cases} \nu^{(k_1-1)} & for\ 1Hz \geq \nu \geq 10^{-3}\,Hz \\ \left[\dfrac{\nu}{10^{-3}}\right]^{(k_2-1)} \left(10^{-3}\right)^{(k_1-1)} & for\ 10^{-3}\,Hz > \nu \geq 10^{-4}\,Hz \end{cases}$$

where k_1, k_2, m and C are dependent on temperature. This model has been used for fatigue life prediction of PBGA and flip chip solder joint reliability evaluations [47].

ATTENTION: The Singapore Copyright Act applies to the use of this document. Nanyang Technological University Library

2.2.2 *Crack initiation and propagation approach*

Crack initiation and propagation approach characterizes the fatigue crack growth phases during the fatigue life. Some research work on applying fracture mechanics to tin-lead solder had been reported by Pao [53] and Lau [54]. Fatigue crack growth behavior under creep-fatigue conditions have been reported for solders and other metals (Bernstein, 1982 [55]; Kordisch, 1996 [56]; Mcdowell, 1996 [57]; Pidaparti, 1996 [58]; Nguyen, 2000 [59]; Liu, 2000 [60]; Mutoh, 2001 [61]; Zhao 2002 [62]). Because of the low melting point of solder, the material is at high homologous temperature. Under low cycle fatigue (LCF) condition, it is known that the time-dependent creep deformation is likely to occur together with cyclic fatigue crack growth under creep-fatigue interaction conditions. Creep failure is characterized by intergranular cracking due to grain boundary sliding, while fatigue failure occurs due to formation of surface cracks and then propagation. The creep-fatigue failure can be viewed as interaction of grain boundary cracks with the fatigue cracks. Therefore, failure would be transgranular at high frequencies and become intergranular at low frequencies due to transition from fatigue to creep controlled mechanisms (See Fig. 2-4). Hence, the fatigue crack growth behavior can be separated as: fatigue dominated region and creep-dominated region.

ATTENTION: The Singapore Copyright Act applies to the use of this document. Nanyang Technological University Library

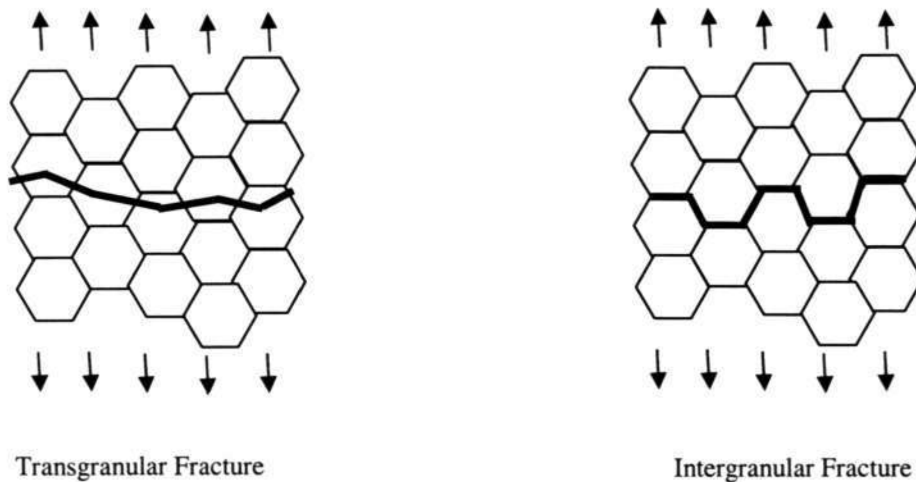

Fig. 2-4 Transgranular and Intergranular Fracture

For fatigue-dominated region, the crack growth is cycle dependent, the failure mechanism is transgranular, and many researchers [61-62] use ΔJ to predict fatigue crack growth rate in this region, given below:

$$da/dN = A(\Delta J)^{m} \tag{2.2.15}$$

where a is crack length, N is cycle, A and m are material constants, and ΔJ-value can be calculated according to the following equation:

$$\Delta J = \frac{S_p}{B(W-a)} f(a,W) \tag{2.2.16}$$

where S_p is the area under the load verses load-line displacement curve with consideration of crack closure. B, W and a are the thickness, the width and the crack length, respectively. f (a, W) is the function of geometry determined by a and W.

ATTENTION: The Singapore Copyright Act applies to the use of this document. Nanyang Technological University Library

For creep dominated region, the crack growth is time dependent, the failure mechanism is intergranular, and C* can be used to predict the crack growth in this region, shown as:

$$da/dt = B(C^*)^n \tag{2.2.17}$$

where a is crack length, B and n are material constants, and C*-value is estimated by using the following equation:

$$C^* = \frac{P\dot{V}_c}{BW}\left[\frac{n}{n+1}\left(\frac{2}{1-a/W}+0.522\right)\right] \tag{2.2.18}$$

where P is the applied load (P_{max} was used in cyclic loading condition), $\dot{V}_c$ is the load-line displacement rate, B, W and a are the specimen thickness, width and crack length, respectively. n is the creep exponent. However, there are some practical difficulties in applying this approach to thermal fatigue problems.

The total life approach is most widely used. However, its fatigue exponent m and ductility coefficient C will dependent on test temperatures and frequencies. Shi et al [51-52] proposed the frequency-modified Coffin-Manson and Morrow's model, and solved the frequency dependent problem, it is still difficult to characterize the temperature and frequency dependent low cycle fatigue behavior of solder alloys in the thermal-mechanical loading conditions. Furthermore, the plastic strain range or inelastic strain energy density used in Coffin-Manson or Morrow's model is derived at a representative "stable" hysteresis loop. Kanchanomai [35] noted that there is no

ATTENTION: The Singapore Copyright Act applies to the use of this document. Nanyang Technological University Library

"stable" hysteresis loop during the fatigue tests of lead-free solder alloys. The plastic strain range will increase, while the stress range will decrease with the cycles. It may not be reasonable to use only one representative "stable" loop information to characterize the long period of fatigue life. Hence, new fatigue model is needed to overcome this problem.

ATTENTION: The Singapore Copyright Act applies to the use of this document. Nanyang Technological University Library

Chapter 3. Experimental Procedure

To characterize the mechanical and creep properties of lead-free solder alloys, tensile and creep tests over a wide range of test conditions were conducted. Low cycle fatigue tests were conducted to characterize the fatigue resistances at different temperatures and frequencies. Thermal cycling loading is the major concern of solder alloys; however, drop impact loading is also very important. Hence, impact tests were conducted to characterize the mechanical properties of solder alloys at high strain rate. In this chapter, the experimental procedure and details for a comprehensive mechanics test program is described. This includes the specimen geometry, test conditions and matrix, test machine and procedure used.

3.1 Tensile test

The tensile test method was employed to measure the mechanical properties of 95.5Sn-3.8Ag-0.7Cu and 99.3Sn-0.7Cu solder alloys. Dog bone-shaped bulk solder specimens for uni-axial tensile test were machined from solder bar. The specimen has a total length of 65mm, a gage length of 15mm, and a diameter of 3mm (See Fig.3-1), which is following the ASTM standard [63]. The specimens were annealed for 24 hours at 60°C in vacuum to eliminate the surface residual stresses.

ATTENTION: The Singapore Copyright Act applies to the use of this document. Nanyang Technological University Library

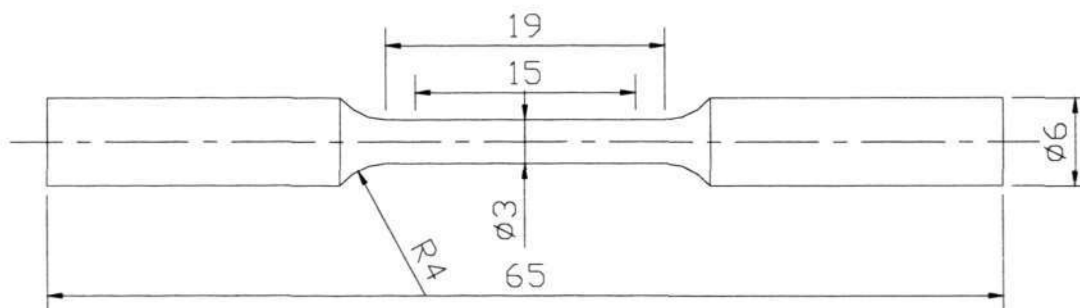

Fig.3-1 Geometry of tensile and creep specimen (in mm)

The tensile tests were carried out on a universal testing machine, Instron model 5569, at four different temperatures (-40°C, 25°C, 75°C and 125°C). At each temperature, three different displacement rates were used (0.5mm/min, 5mm/min and 50mm/min). The test matrix for Sn-3.8Ag-0.7Cu and Sn-0.7Cu are shown in Table 3-1 and 3-2. In order to perform the test over the range from -40°C to 125°C, it was conducted within a thermally insulated chamber. A non-contact video extensometer was employed in the specimen gauge section to measure the true extension of the specimen. Two lines were marked on the gauge length of the specimen as shown in Fig. 3-2(a), and are detected by the system as shown in Fig. 3-2(b). When test is in progress, the distance between these two points can be measured and the strain of the specimen can be calculated. A computer with the data acquisition software was used to collect the data.

ATTENTION: The Singapore Copyright Act applies to the use of this document. Nanyang Technological University Library

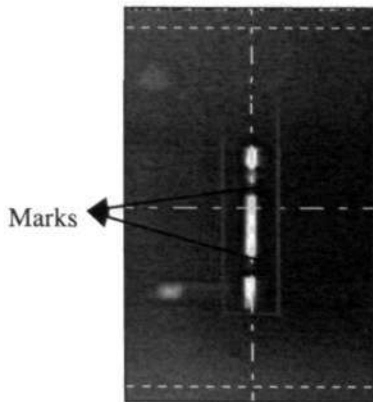

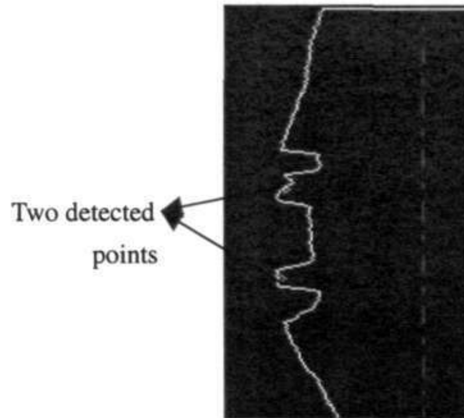

Fig. 3-2(a) Image of video extensometer

Fig. 3-2(b) Detected points

Table 3-1 Tensile test matrix for Sn-3.8Ag-0.7Cu

	-40°C	25°C	75°C	125°C
0.5mm/min	×1	×3	×3	×3
5mm/min	×1	×3	×3	×3
50mm/min	×1	×3	×3	×3

Table 3-2 Tensile test matrix for Sn-0.7Cu

	-40°C	25°C	75°C	125°C
0.5mm/min	-	×3	×2	×2
5mm/min	-	×2	×2	×2
50mm/min	-	×2	×2	×2

ATTENTION: The Singapore Copyright Act applies to the use of this document. Nanyang Technological University Library

After the specimen grips and environmental chamber reached thermal equilibrium, the specimen was fixed in grips within the chamber for a minimum of half an hour prior to testing. The specimen temperature was monitored by a thermal-couple. A feed back control was used to regulate the test temperature. An example of the specimen for Sn-3.8Ag-0.7Cu solder before and after testing (at 125°C and 0.5mm/min) is shown in Fig. 3-3. The load and displacement curves for three repeated tests at 125°C and 0.5mm/min are given in Fig. 3-4. In order to calculate the modulus and yield stress accurately, initial parts of the load and displacement curves are plotted in Fig. 3-5. Using Fig. 3-5 and following the method in ASTM standard, the Elastic modulus, yield stress at certain condition can be calculated.

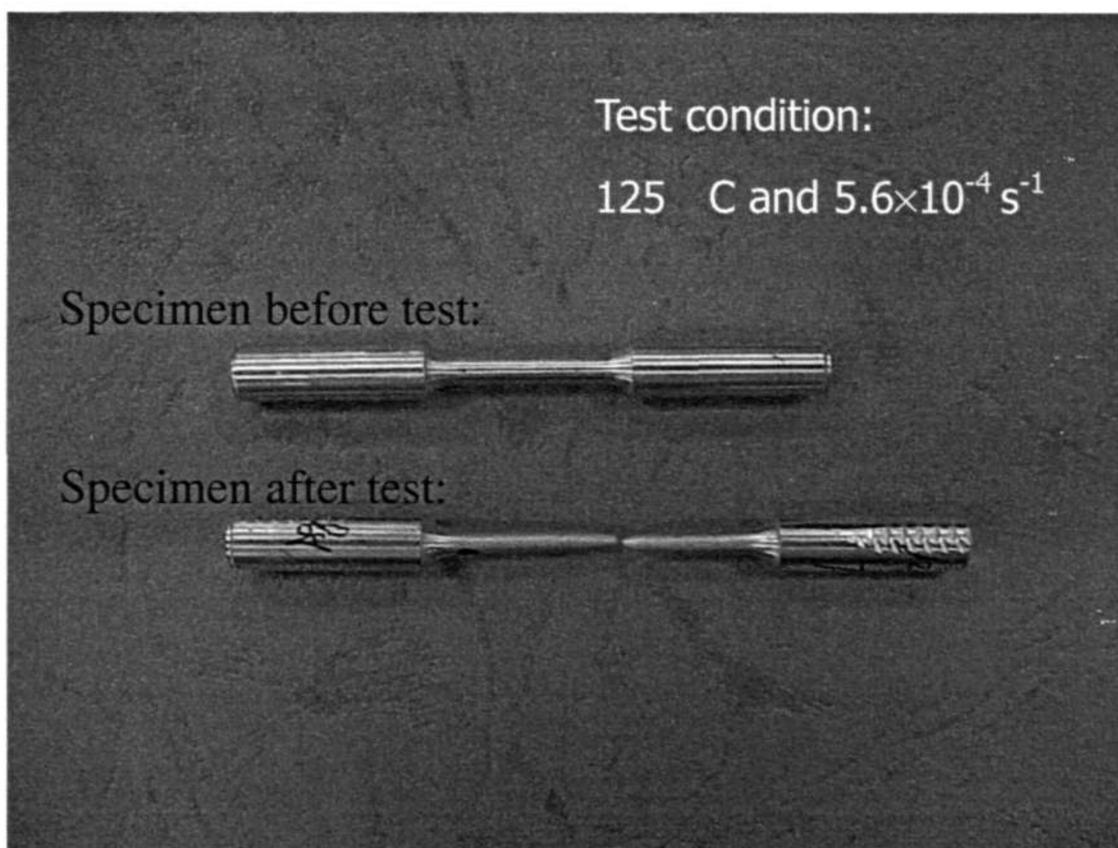

Fig. 3-3 Tensile specimen before and after testing

ATTENTION: The Singapore Copyright Act applies to the use of this document. Nanyang Technological University Library

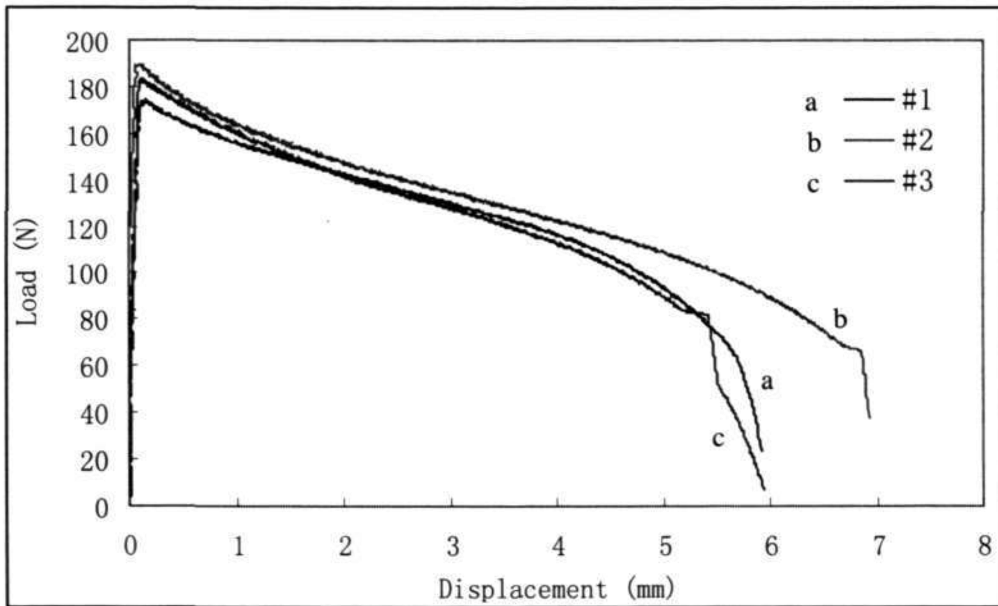

Fig. 3-4 Load-displacement curves at 125°C and 0.5mm/min

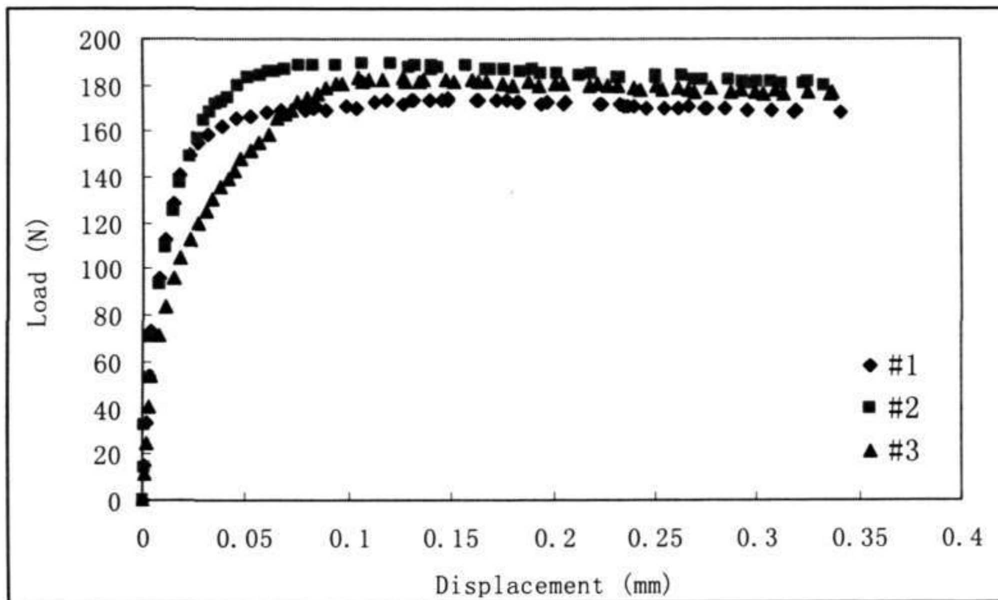

Fig. 3-5 Initial parts of load and displacement curves at 125°C and 0.5mm/min

ATTENTION: The Singapore Copyright Act applies to the use of this document. Nanyang Technological University Library

3.2 Creep Test

The specimen used for tensile test for 95.5Sn-3.8Ag-0.7Cu and 99.3Sn-0.7Cu solder alloy was also used for the creep test program. The specimens were also annealed for 24 hours at 60°C in vacuum to eliminate the surface residual stresses. The creep tests were carried out on a universal testing machine, Instron model 5569, the machine has the capability to hold the load constant. A thermal chamber was used for creep test over a wide range of test temperatures. In the creep test, specimen was deformed in tension at constant load. The non-contact video extensometer was employed to measure the strain. Creep tests were carried out at four different temperatures (-40°C, 25°C, 75°C and 125°C), with constant stress set at different values (3, 4, 5, 7, 10, 15, 20, 25, 30, 35, 40, 50, 60 and 70 MPa). The test matrix for Sn-3.8Ag-0.7Cu and Sn-0.7Cu are shown in Table 3-3 and 3-4. After the specimen grips and chamber reached thermal equilibrium, the specimen was placed into the chamber for a minimum of half an hour prior to testing. The specimen temperature was monitored by a thermal-couple, which is used to regulate the testing temperature in the chamber. For example, specimen for Sn-3.8Ag-0.7Cu solder, before and after testing (at 125°C and 10MPa) is shown in Fig. 3-6.

ATTENTION: The Singapore Copyright Act applies to the use of this document. Nanyang Technological University Library

Table 3-3 Creep test matrix for Sn-3.8Ag-0.7Cu

	-40°C	25°C	75°C	125°C
2MPa	-	-	-	×1
3MPa	-	-	-	×1
5MPa	-	×1	×1	×2
7MPa	-	-	×1	×1
10MPa	-	×1	×1	×2
15MPa	-	×2	×1	×1
20MPa	-	×1	×1	×2
25MPa	×1	×2	×2	-
30MPa	×1	×1	-	-
35MPa	-	×2	×1	
40MPa	×1	×1	-	-
50MPa	×1	-	-	-
60MPa	×1	-	-	-
70MPa	×1	-	--	-

Table 3-4 Creep test matrix for Sn-0.7Cu

	25°C	75°C	125°C
3MPa	-	×1	×1
4MPa	-	-	×1
5MPa	×1	×1	×2
7MPa	×1	×1	×1
10MPa	×2	×2	×2
15MPa	×1	×1	×1
20MPa	×2	×1	×2
25MPa	×1	×1	-
30MPa	×2	×1	-
35MPa	×1	-	-

ATTENTION: The Singapore Copyright Act applies to the use of this document. Nanyang Technological University Library

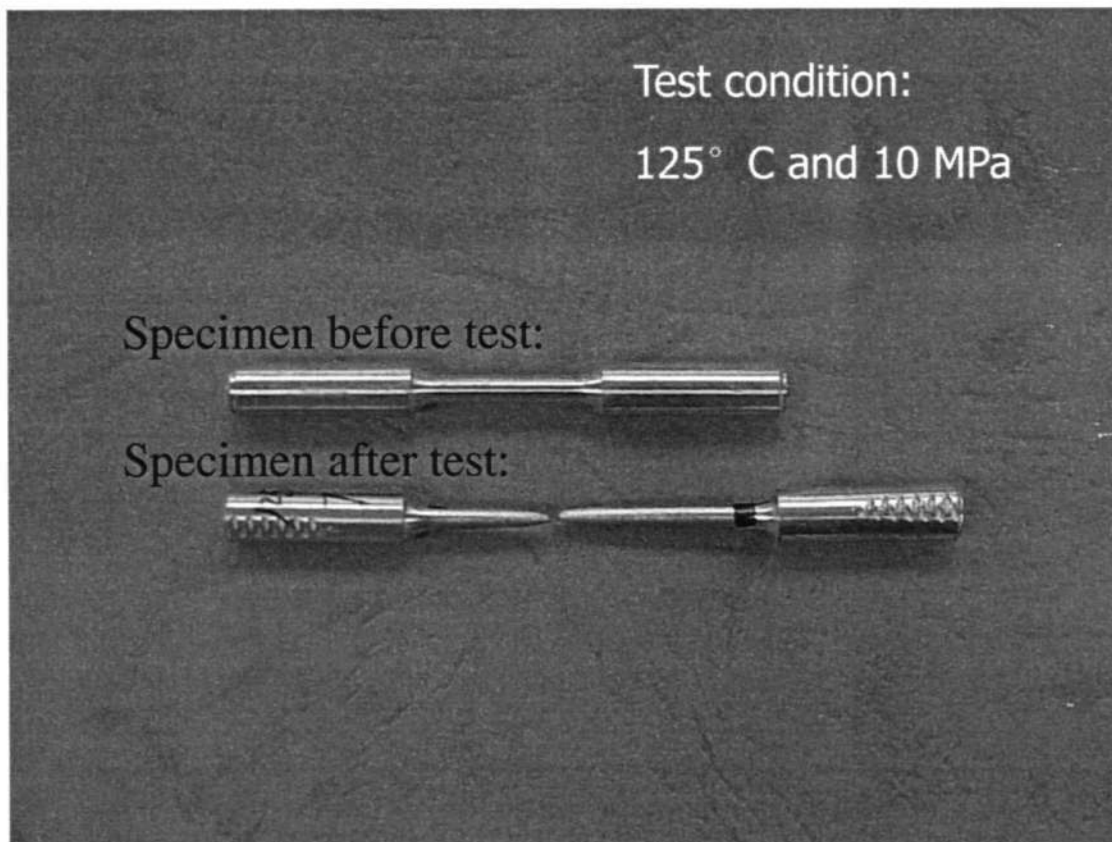

Fig. 3-6 Creep specimen before and after testing

3.3 Low Cycle Fatigue Test

The low cycle fatigue test specimens for 95.5Sn-3.8Ag-0.7Cu and 99.3Sn-0.7Cu solder alloy were machined from the solder bar as well. The configuration of the fatigue specimens has a diameter of 6mm at the two grip ends, a center diameter of 3mm, and a gauge length of 4.5mm with a radius of curvature of 50mm. The geometry of the specimen follows the ASTM standard [64] and is shown in Fig. 3-7.

The low cycle fatigue tests were conducted on a micro-force materials test system. Chuck grips were used to fix the solder specimen for tension-compression fatigue test. The tests were run under a symmetrical uni-axial tension-compression loading with

ATTENTION: The Singapore Copyright Act applies to the use of this document. Nanyang Technological University Library

total displacement control over a range of test frequencies. The sine waveform was employed for all fatigue tests. The total strain was calculated from the crosshead displacement divided by the gauge length. The tests were carried out at three different frequencies (10^{-3}, 10^{-2} and 1Hz) and at three different temperatures (25, 75 and 125°C) with total strain set at four different values (2, 3.5, 5 and 7.5%). The test matrix of fatigue test for Sn-3.8Ag-0.7Cu and Sn-0.7Cu are shown in Table 3-5 and 3-6. The fatigue failure was defined as 50% reduction of maximum tensile load. The specimen of Sn-3.8Ag-0.7Cu solder before and after testing at 75°C, 1Hz and 3.5% total strain is shown in Fig. 3-8.

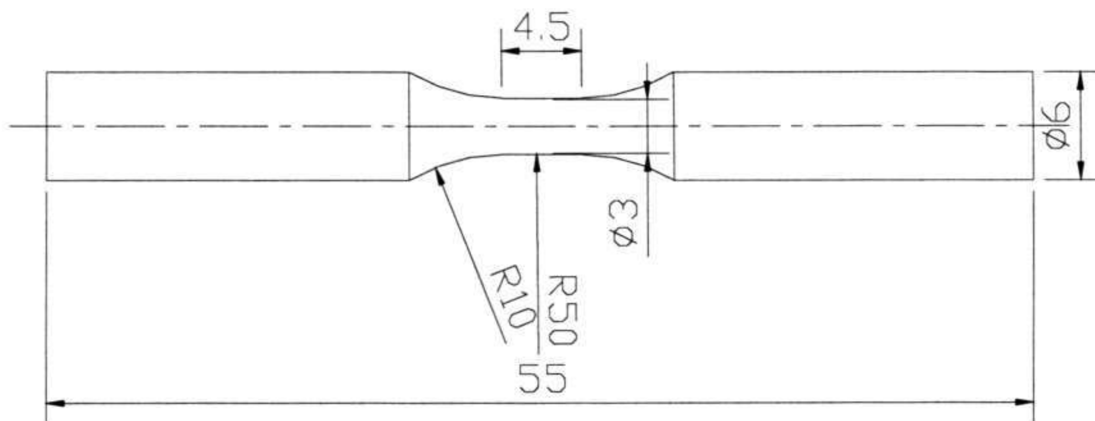

Fig. 3-7 Geometry of fatigue specimen(in mm)

ATTENTION: The Singapore Copyright Act applies to the use of this document. Nanyang Technological University Library

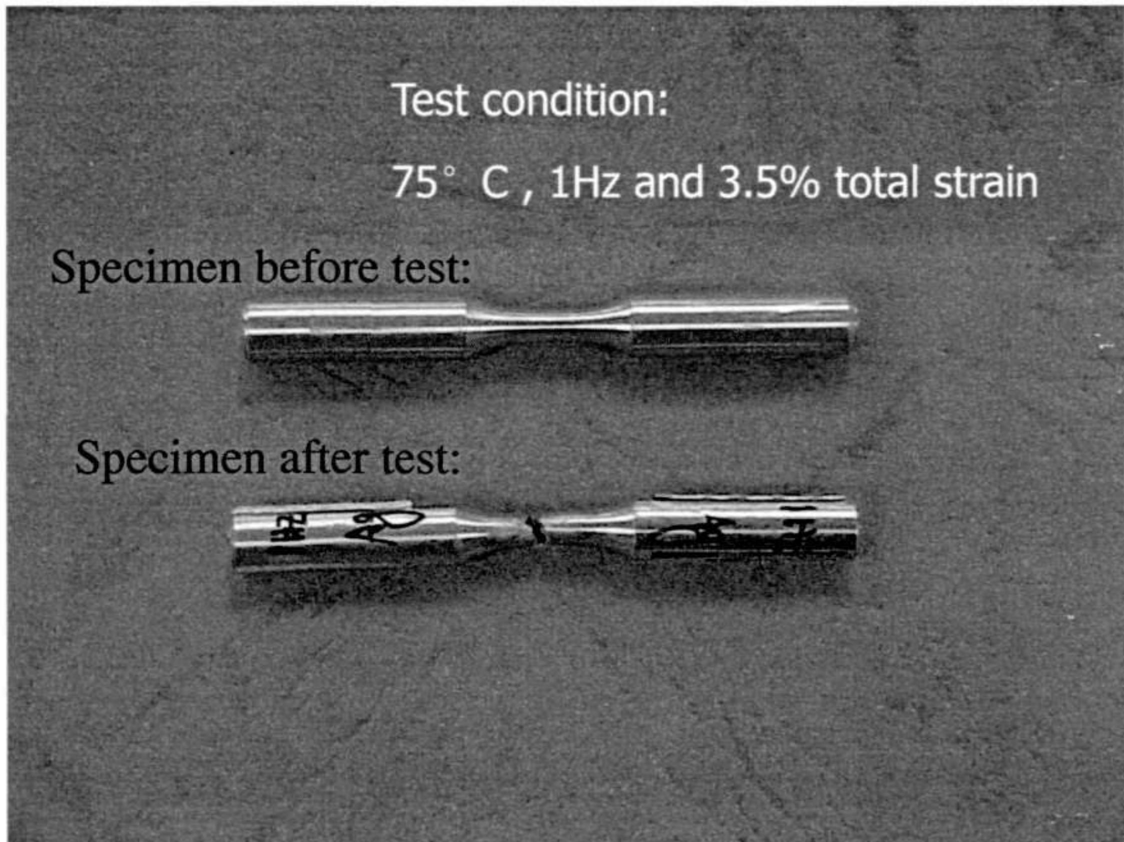

Fig. 3-8 Fatigue specimen before and after testing

Table 3-5 Fatigue test matrix for Sn-3.8Ag-0.7Cu

		25°C	75°C	125°C
2%	1Hz	×2	×1	×2
	0.01Hz	×2	×1	×2
	0.001Hz	×1	×1	×1
3.5%	1Hz	×1	×1	×1
	0.01Hz	×1	×1	×1
	0.001Hz	×1	×1	×1

ATTENTION: The Singapore Copyright Act applies to the use of this document. Nanyang Technological University Library

5%	1Hz	×1	×1	×1
	0.01Hz	×1	×1	×1
	0.001Hz	×1	×1	×1
7.5%	1Hz	×2	×1	×2
	0.01Hz	×2	×1	×2
	0.001Hz	×1	×1	×1

Table 3-6 Fatigue test matrix for Sn-0.7Cu

		25°C	75°C	125°C
2%	1Hz	×1	×1	×1
	0.01Hz	×1	×1	×1
	0.001Hz	-	-	×1
3.5%	1Hz	×1	×1	×1
	0.01Hz	×1	×1	×1
	0.001Hz	-	-	×1
5%	1Hz	×1	×1	×1
	0.01Hz	×1	×1	×1
	0.001Hz	-	-	×1
7.5%	1Hz	×1	×1	×1
	0.01Hz	×1	×1	×1
	0.001Hz	-	-	×1

ATTENTION: The Singapore Copyright Act applies to the use of this document. Nanyang Technological University Library

3.4 Split Hopkinson Pressure Bar Impact Test

Impact test method was employed to determine the mechanical properties of 95.5Sn-3.8Ag-0.7Cu solder alloys at high strain rate. Dog bone-shaped bulk solder specimens for impact tensile test were machining from solder bars. The specimen has a total length of 50mm, a gage length of 10 mm, and a diameter of 4mm (See Fig. 3-9). The specimen was threaded at both ends and screwed to the test system.

Impact tests were conducted with a Split Hopkinson pressure bar (SHPB). The Hopkinson bar test system commonly used to study the dynamic response of materials. The basic theory of the SHPB is based on the theory of stress wave propagation in elastic bar and interaction between a stress pulse and the specimen of different impedance. The data acquisition system collects and analyzes the output waveforms from the SHPB tests. A schematic illustration of the SHPB and recording system is shown in Fig. 3-10. The solder specimen was assembled between the incident and transmitted bars (ie: input and output bars). Strain gages at the mid-span of both the incident and transmitted bars were used to measure the dynamic response. The strain gages used on the bars are 120Ω and connected in a full bridge circuitry arrangement. Data acquisition is performed with a TML DC-92D dynamic strain meter and a DL 1540 digital oscilloscope. The strain meter will amplify the pulse signals and the oscilloscope will display the input and output waveforms.

ATTENTION: The Singapore Copyright Act applies to the use of this document. Nanyang Technological University Library

The pressure pulse was initiated by axial impact from the striker bar that was accelerated to the desired impact velocity by the pressure chamber. The striker bar impacts on the anvil bar, which was connected to the input bar, so the pulse can travel via the input bar to the specimen. This manner of loading produces a loading pulse in the input bar with an amplitude that is proportional to the impact velocity of the striker. The impact mechanical properties can be calculated from the strain gauge readings. The test matrix is shown in Table 3-7.

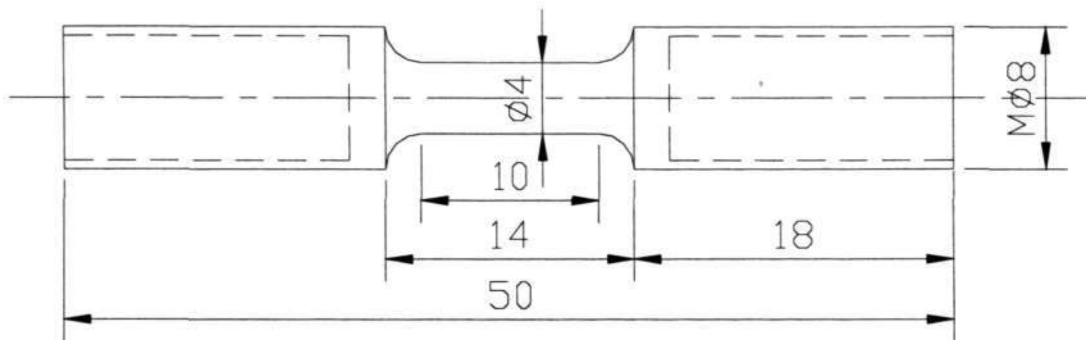

Fig. 3-9 Geometry of impact specimen (in mm)

Table 3-7 Impact test matrix for Sn-3.8Ag-0.7Cu

Strain rate	25°C
$7 \times 10^{2}\ s^{-1}$	×3
$9 \times 10^{2}\ s^{-1}$	×2
$1.3 \times 10^{3}\ s^{-1}$	×3

ATTENTION: The Singapore Copyright Act applies to the use of this document. Nanyang Technological University Library

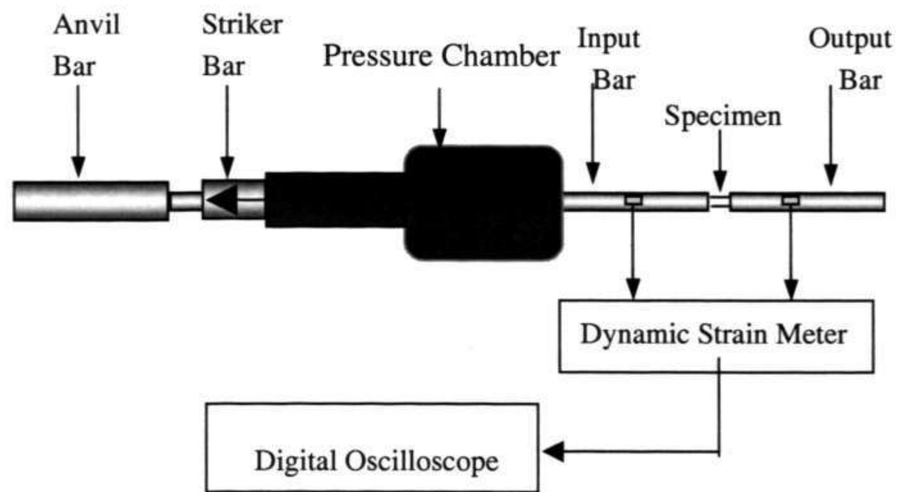

Fig. 3-10 Dynamic tensile test using SHPB testing system

ATTENTION: The Singapore Copyright Act applies to the use of this document. Nanyang Technological University Library

Chapter 4. Tensile Test Data & Analysis

In this chapter, mechanical properties will be presented for different temperatures and strain rates for the two NEMI recommended lead-free solder alloys. Temperature and strain rate dependent expression for stress-strain properties was developed and non-linear curve-fitting to use Anand model will also be presented.

4.1 Tensile test result

4.1.1 95.5Sn-3.8Ag-0.7Cu solder alloy results

The effects of strain rate and temperature on the 95.5Sn-3.8Ag-0.7Cu tensile properties were evaluated and the stress-strain curves for the three different strain rates at a constant temperature of 25°C are shown in Fig 4.1-1. The test result for the three strain rate conditions at temperature of 125°C is given in Fig 4.1-2. The strain rate was calculated using displacement rate of machine divided by the gauge length of specimen. It can be seen that the mechanical properties of 95.5Sn-3.8Ag-0.7Cu is strongly dependent on the test temperature and strain rate parameters [65-67]. For the same temperature, strength of the material will increase with strain rate, ultimate strength increase from about 40MPa for strain rate of 5.6×10^{-4} s^{-1} to 60MPa for 5.6×10^{-2} s^{-1} at 25°C (See Fig. 4.1-1); However, at the same strain rate, the strength will decrease with temperature, for example, in Fig. 4.1-1 and 4.1-2, both line (c) indicate the strain rate of 5.6×10^{-4} s^{-1}, while the strength will decrease from 40MPa at 25°C to 20MPa at 125°C.

ATTENTION: The Singapore Copyright Act applies to the use of this document. Nanyang Technological University Library

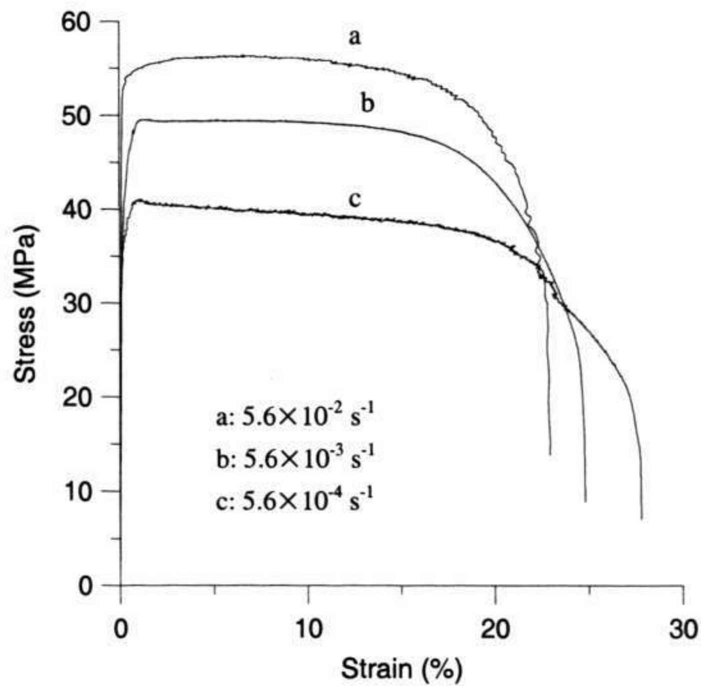

Fig. 4.1-1 Tensile test results at constant temperature of 25°C

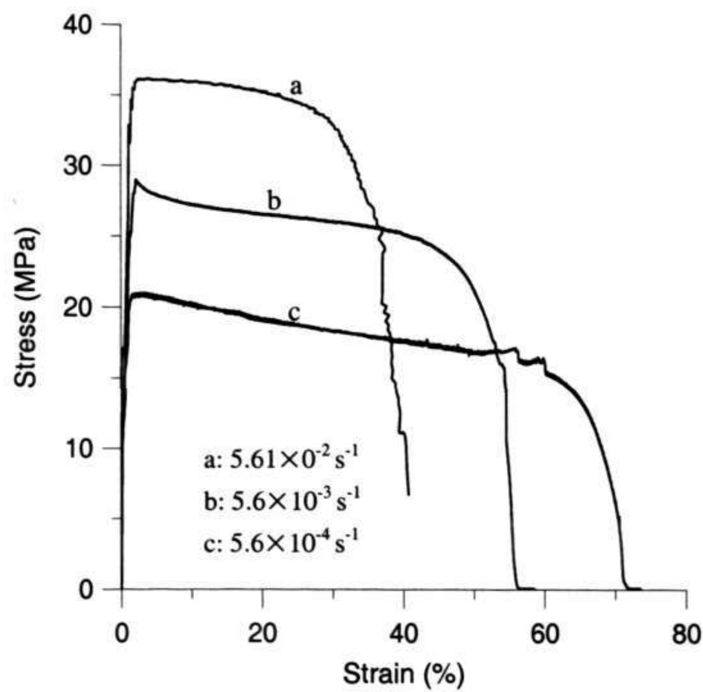

Fig. 4.1-2 Tensile test results at constant temperature of 125°C

ATTENTION: The Singapore Copyright Act applies to the use of this document. Nanyang Technological University Library

Based on the stress-strain curves obtained from tensile test, the Elastic modulus, yield stress and UTS can be derived. Fig. 4.1-3 illustrate the calculation method.

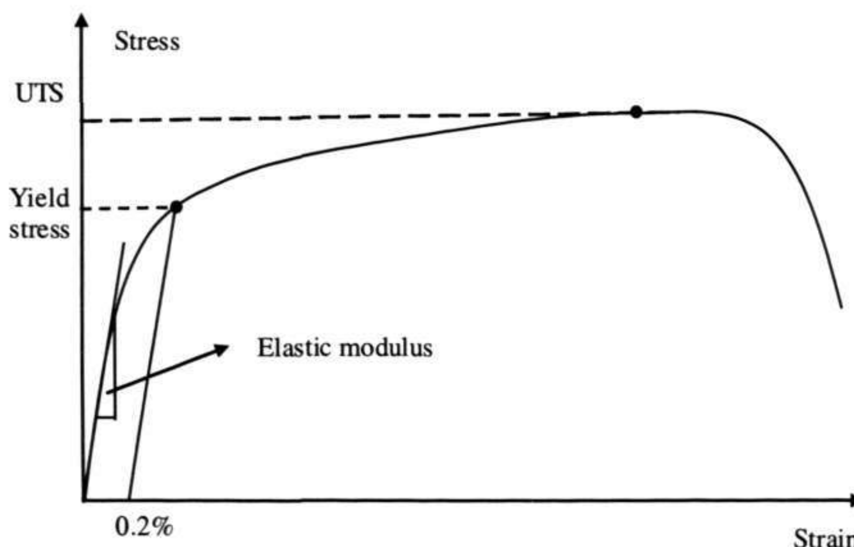

Fig. 4.1-3 Illustration of calculating elastic modulus, yield stress and UTS

The result of the effect of temperature on elastic modulus is shown in Fig. 4.1-4. It can be seen that the curves demonstrate linear relationship between the elastic modulus and the temperature and elastic modulus decrease with the increase of temperature. The effect of strain rate on elastic modulus was presented by plotting the graph of elastic modulus versus strain rate as shown in Fig. 4.1-5. The plot shows approximately straight lines with a constant slope for any given temperature. This is expected as the elastic modulus has a linear function of logarithmic strain rate and elastic modulus increase with increase in strain rate.

ATTENTION: The Singapore Copyright Act applies to the use of this document. Nanyang Technological University Library

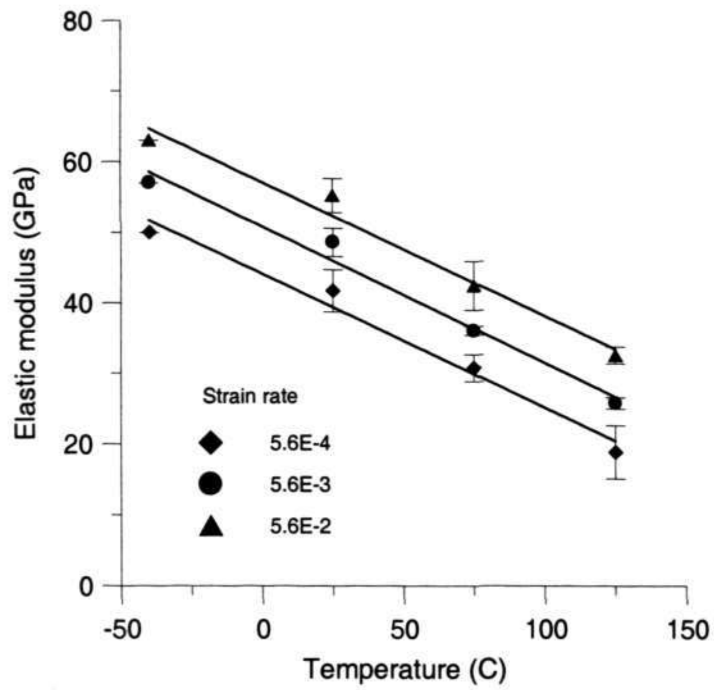

Fig.4.1-4 Effect of temperature on elastic modulus

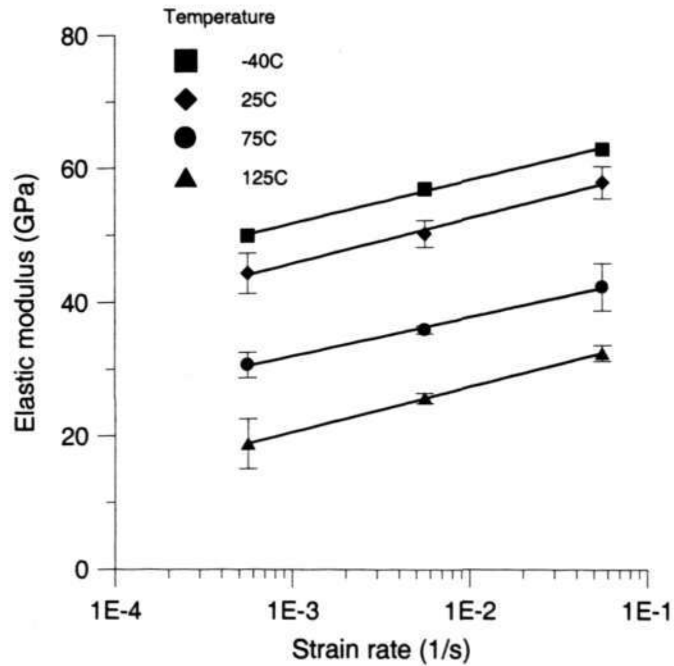

Fig.4.1-5 Effect of strain rate on elastic modulus

ATTENTION: The Singapore Copyright Act applies to the use of this document. Nanyang Technological University Library

The yield stress was computed from the stress-strain curve at 0.2 percent plastic strain. The effects of test temperature and strain rate on the yield stress are given in Figs 4.1-6 and 4.1-7, respectively. There is a linear relationship between the yield stress versus temperature plot, and Yield Stress versus logarithmic strain rate. The yield stress increases with faster strain rate, and decreases with increase in temperature.

The corresponding results for the ultimate tensile stress (UTS) are given in Figs 4.1-8 and 4.1-9, respectively. The UTS results follow a similar trend as the yield stress results. UTS increases with increase in strain rate, and decreases with increase in temperature.

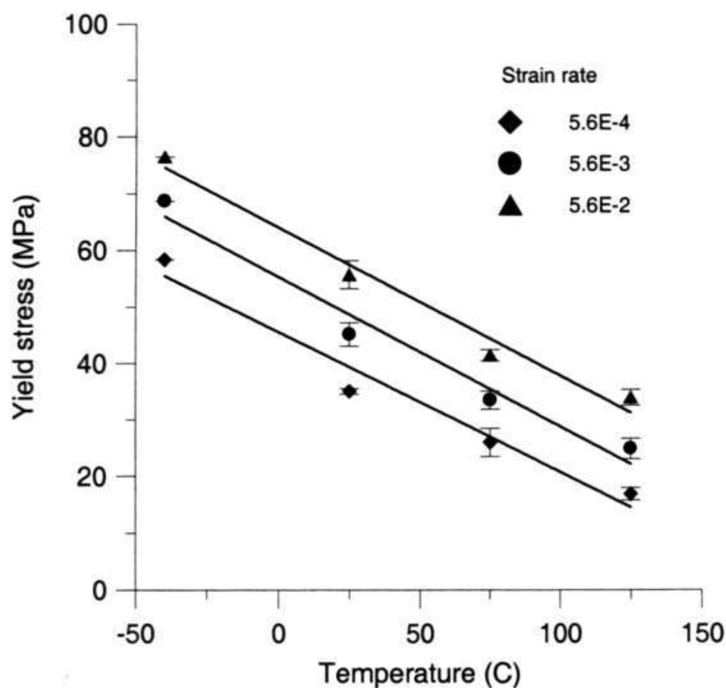

Fig. 4.1-6 Effect of temperature on yield stress

ATTENTION: The Singapore Copyright Act applies to the use of this document. Nanyang Technological University Library

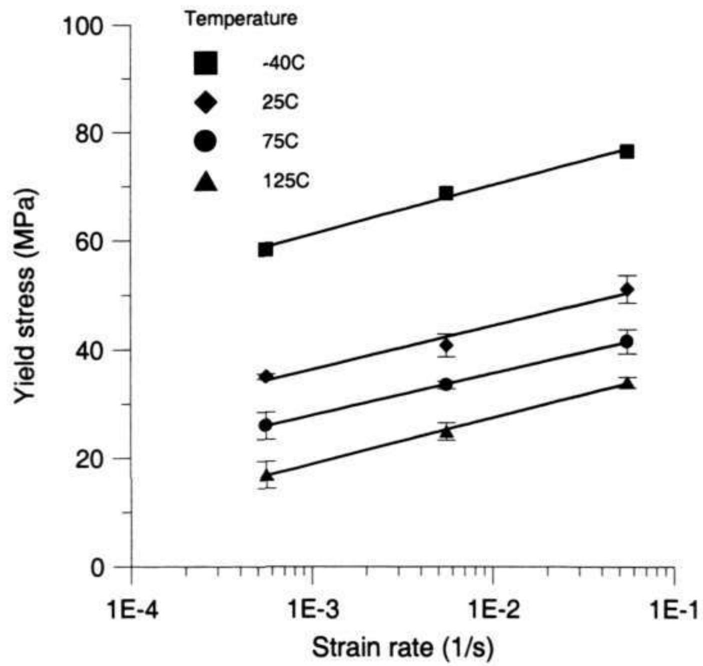

Fig. 4.1-7 Effect of strain rate on yield stress

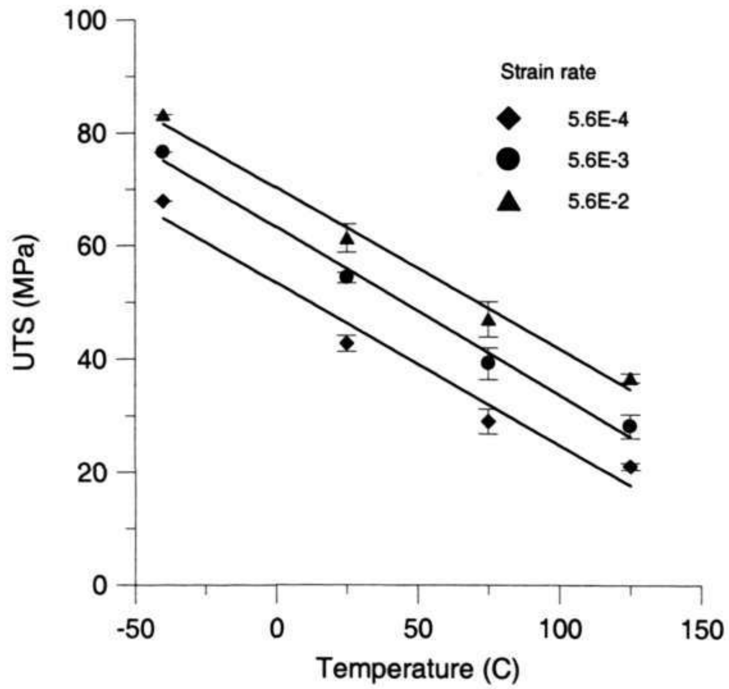

Fig.4.1-8 Effect of temperature on UTS

ATTENTION: The Singapore Copyright Act applies to the use of this document. Nanyang Technological University Library

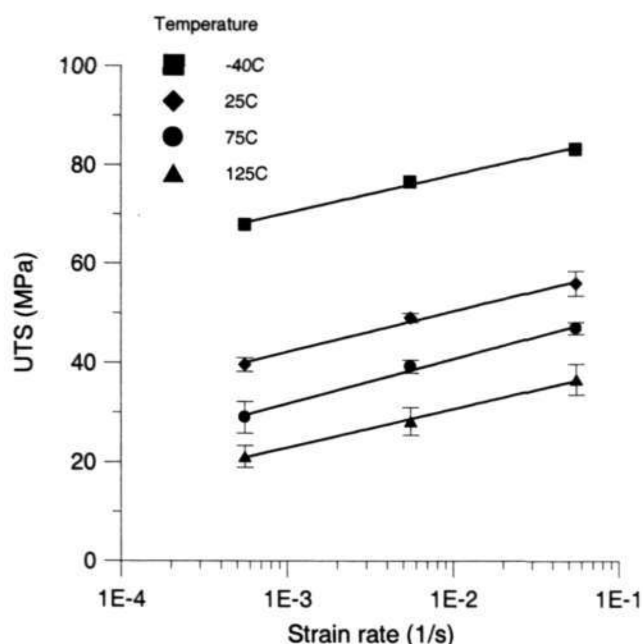

Fig.4.1-9 Effect of strain rate on UTS

The temperature and strain rate dependent elastic modulus, yield stress and UTS for the bulk 95.5Sn-3.8Ag-0.7Cu solder tensile test results are summarized in Table 4.1-1. The variance range of test data was also shown to evaluate the repeatability of test results.

Table 4.1-1: Summary of Tensile Test Results for Sn-Ag-Cu Solder

	E (GPa)	Yield (MPa)	UTS (MPa)
25°C			
5.6×10^{-4}	41.8 ± 3.0	35.1 ± 0.5	40.6 ± 1.4
5.6×10^{-3}	48.3 ± 2.1	42.9 ± 2.1	49.0 ± 0.9
5.6×10^{-2}	55.1 ± 2.4	52.8 ± 1.5	58.0 ± 2.5
75°C			
5.6×10^{-4}	30.7 ± 1.9	25.6 ± 2.5	29.0 ± 3.2
5.6×10^{-3}	36.0 ± 0.6	33.5 ± 0.7	38.8 ± 3.3
5.6×10^{-2}	42.4 ± 3.5	41.5 ± 1.2	47.0 ± 3.5
125°C			
5.6×10^{-4}	18.8 ± 3.8	16.7 ± 0.5	19.7 ± 0.4
5.6×10^{-3}	26.1 ± 0.8	23.9 ± 1.6	27.2 ± 1.8
5.6×10^{-2}	32.5 ± 1.2	34.0 ± 1.0	39.7 ± 0.5

ATTENTION: The Singapore Copyright Act applies to the use of this document. Nanyang Technological University Library

-40°C			
5.6 x10^{-4}	51	58.4	67.9
5.6 x10^{-3}	57	68.7	76.6
5.6 x10^{-2}	63	76.5	83.3

4.1.2 99.3Sn-0.7Cu solder alloy results

The mechanical properties of Sn-0.7Cu lead-free solder alloy show similar trend but with low magnitude compared to Sn-3.8Ag-0.7Cu solder alloy. The elastic modulus, yield stress and UTS increases with strain rate and decreases with temperature. Sn-0.7Cu solder has lower mechanical properties than Sn-3.8Ag-0.7Cu solder alloy, but higher than Sn-37Pb solder.

The temperature and strain rate dependent elastic modulus, yield stress and UTS for the bulk 99.3Sn-0.7Cu solder tensile test results are given in Table 4.1-2. The variance range of test data was also shown to evaluate the repeatability of test results.

Table 4.1-2: Summary of Tensile Test Results for Sn-Cu Solder

	E (GPa)	Yield (MPa)	UTS (MPa)
25°C			
5.6 x10^{-4}	20.2 ± 3.7	31.1 ± 1.7	35.8 ± 2.6
5.6 x10^{-3}	25.6 ± 1.2	36.5 ± 2.4	45.0 ± 1.5
5.6 x10^{-2}	32.0 ± 2.1	47.8 ± 2.8	52.0 ± 1.6
75°C			
5.6 x10^{-4}	15.6 ± 1.6	22.8 ± 1.1	26.1 ± 0.6
5.6 x10^{-3}	18.9 ± 2.1	30.4 ± 1.8	34.2 ± 2.1
5.6 x10^{-2}	23.3 ± 2.4	35.8 ± 1.4	42.0 ± 0.8
125°C			
5.6 x10^{-4}	11.6 ± 2.6	16.5 ± 2.6	18.2 ± 1.5
5.6 x10^{-3}	15.0 ± 1.8	21.4 ± 4.4	26.1 ± 2.8
5.6 x10^{-2}	18.9 ± 1.7	29.5 ± 3.8	38.2 ± 4.1

ATTENTION: The Singapore Copyright Act applies to the use of this document. Nanyang Technological University Library

4.1.3 Comparison with other reported results

4.1.3.1 Comparison with tin-lead solder

Shi [68] reported the mechanical properties for 63Sn-37Pb solder at different temperatures and strain rates. The comparison of elastic modulus, yield stress and UTS for Sn-3.8Ag-0.7Cu, Sn-0.7Cu and 63Sn-37Pb [68] at room temperature and high temperature are shown in Figs 4.1-10, 4.1-11 and 4.1-12, respectively. It can be noted that Sn-Ag-Cu has the highest mechanical properties of the three solders. While Sn-Cu solder has similar mechanical properties with Sn-37Pb solder. The differences in elastic modulus are significant for three solders. At room temperature, the Sn-Ag-Cu has a modulus of 50GPa, compared with about 30GPa for Sn-Cu and Sn-Pb solders. However, the difference in yield stress and UTS is not as large as elastic modulus.

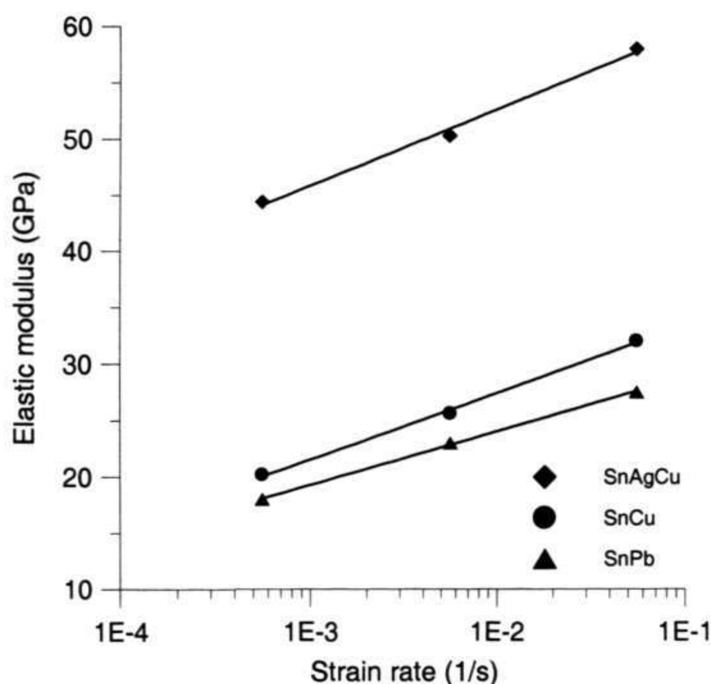

Fig. 4.1-10(a) Comparison of Elastic modulus at room temperature

ATTENTION: The Singapore Copyright Act applies to the use of this document. Nanyang Technological University Library

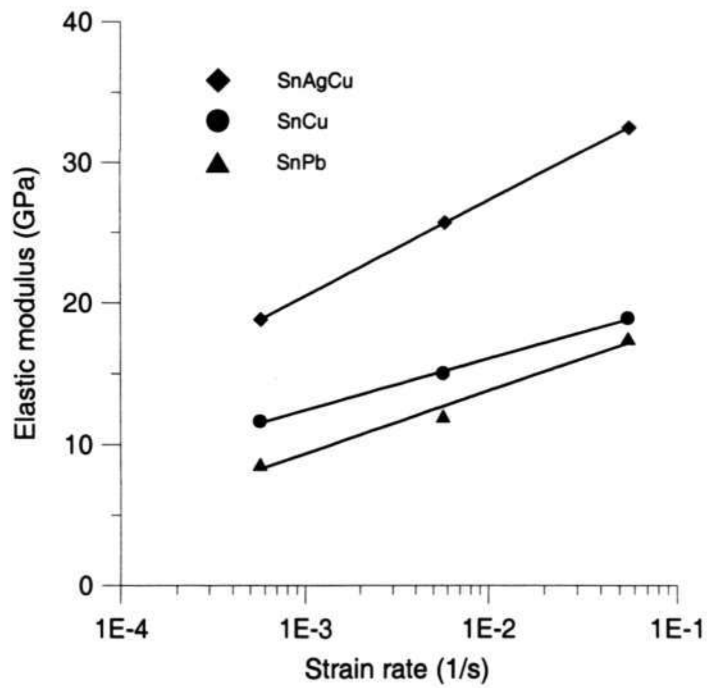

Fig. 4.1-10(b) Comparison of Elastic modulus at high temperature (125°C)

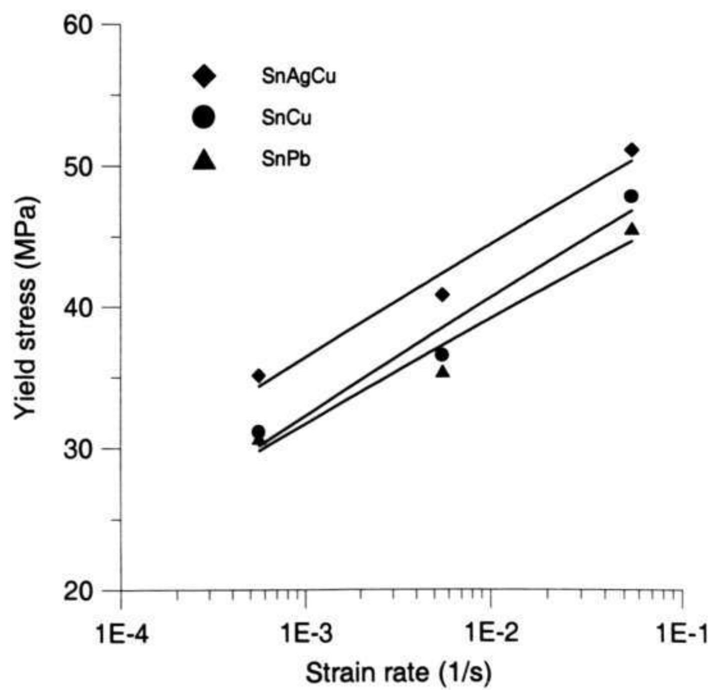

Fig. 4.1-11(a) Comparison of yield stress at room temperature

ATTENTION: The Singapore Copyright Act applies to the use of this document. Nanyang Technological University Library

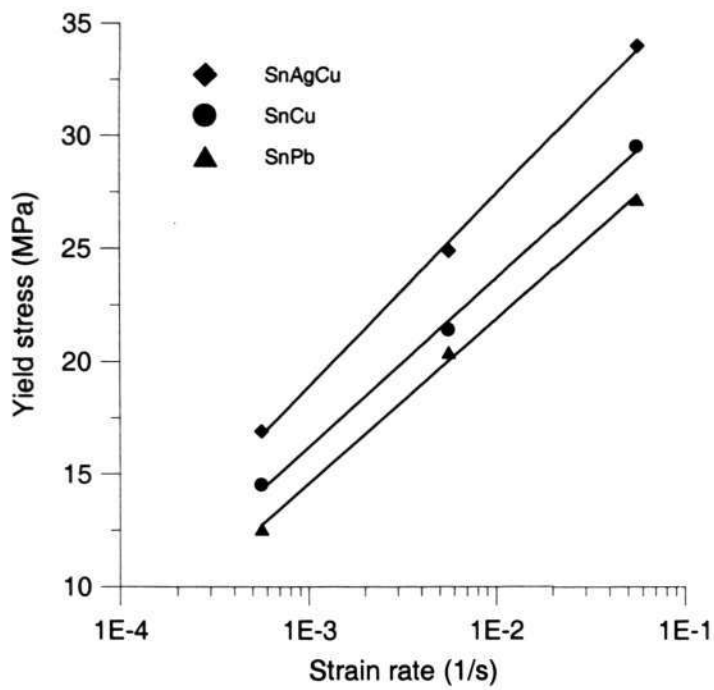

Fig. 4.1-11(b) Comparison of yield stress at high temperature (125°C)

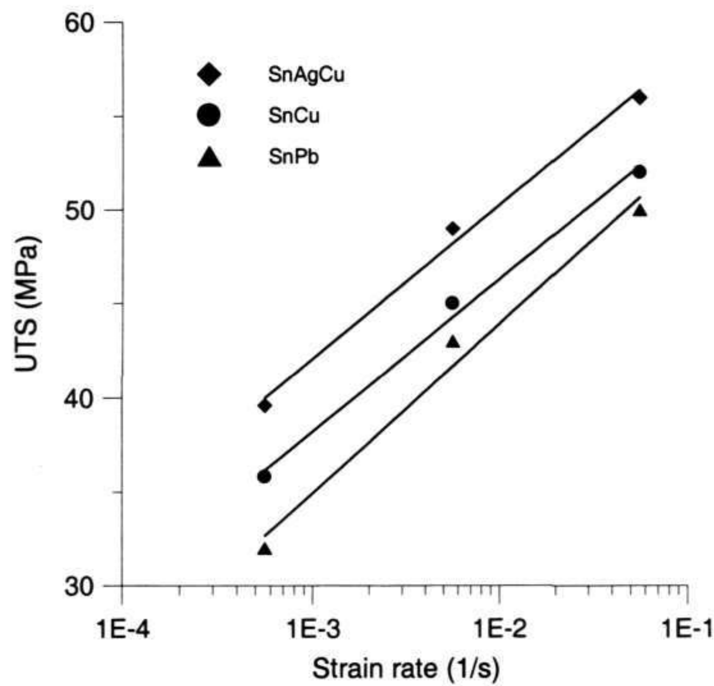

Fig. 4.1-12(a) Comparison of UTS at room temperature

ATTENTION: The Singapore Copyright Act applies to the use of this document. Nanyang Technological University Library

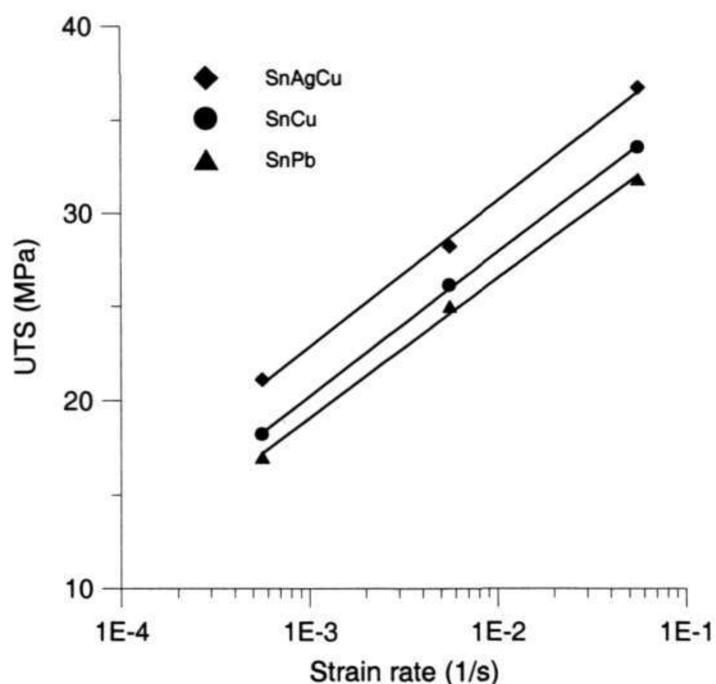

Fig. 4.1-12(b) Comparison of UTS at high temperature (125°C)

4.1.3.2 Comparison with other lead-free solders data

The reported mechanical properties for other lead-free solder data will be summarized and compared with the author's data.

Some reported test data [69-81] were reviewed for Sn-Ag-Cu and Sn-Cu lead-free solders. Harrison et al [73] and Kanchanomai et al [35] reported elastic modulus of Sn-Ag-Cu at different temperatures, data comparison with author's result is shown in Fig. 4.1-13. Tensile strength for Sn-Ag-Cu and Sn-Cu lead-free solders at different temperatures were also reported (NCMS, 1998 [69]; Lin, 2001 [72]; Kim, 2002 [77]; Kanchanomai, 2002 [37]; Plumbridge, 2001 [74]), the comparison is shown in Fig. 4.1-14 and 15. Temperature and strain effect on tensile strength reported by author and other researchers (Foley, 2000 [70]; Amagai, 2002 [76]; Hirose, 2004 [80];

ATTENTION: The Singapore Copyright Act applies to the use of this document. Nanyang Technological University Library

Shohji, 2004 [81]) for Sn-Ag-Cu solder is shown in Fig. 4.1-16, it was found that the author's test results were compared well with other researchers' results.

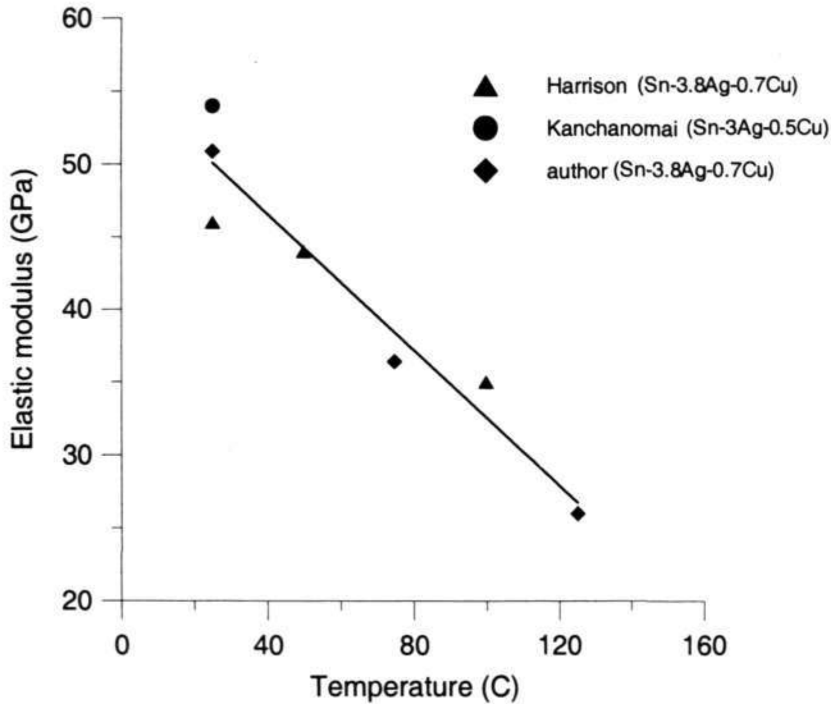

Fig. 4.1-13 Comparison of elastic modulus at different temperatures for Sn-Ag-Cu

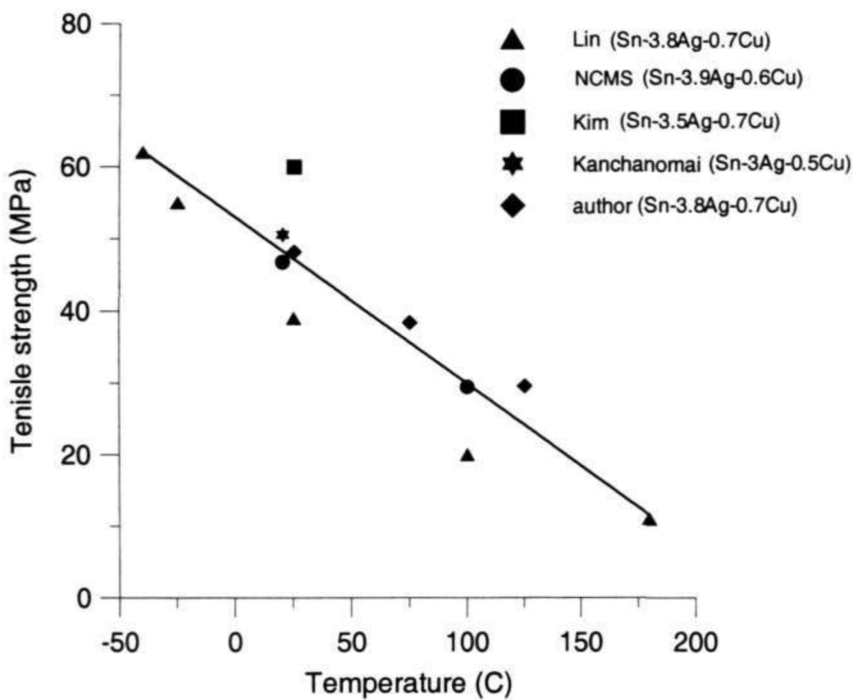

Fig. 4.1-14 Comparison of tensile strength at different temperatures for Sn-Ag-Cu

ATTENTION: The Singapore Copyright Act applies to the use of this document. Nanyang Technological University Library

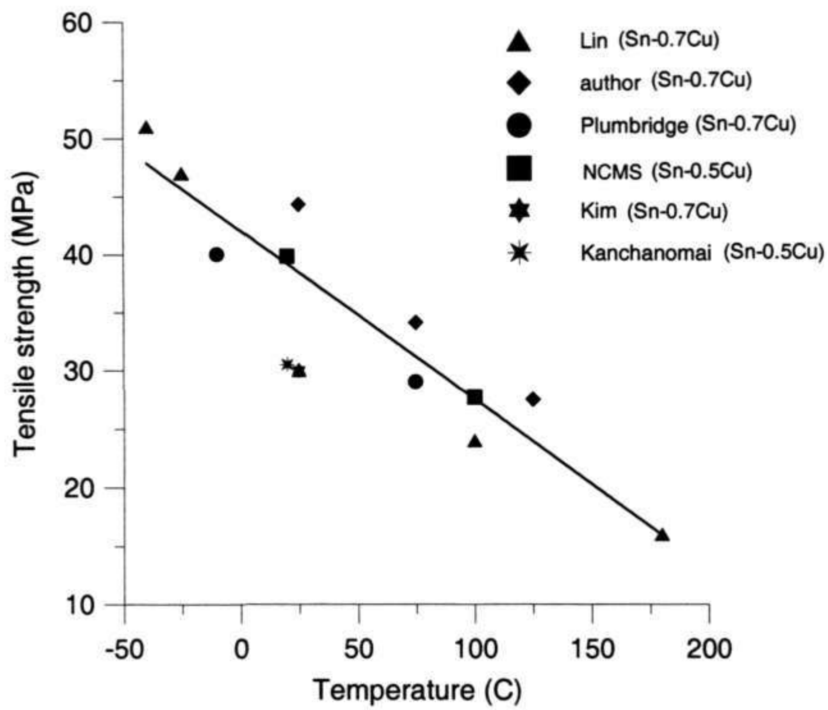

Fig. 4.1-15 Comparison of tensile strength at different temperatures for Sn-Cu

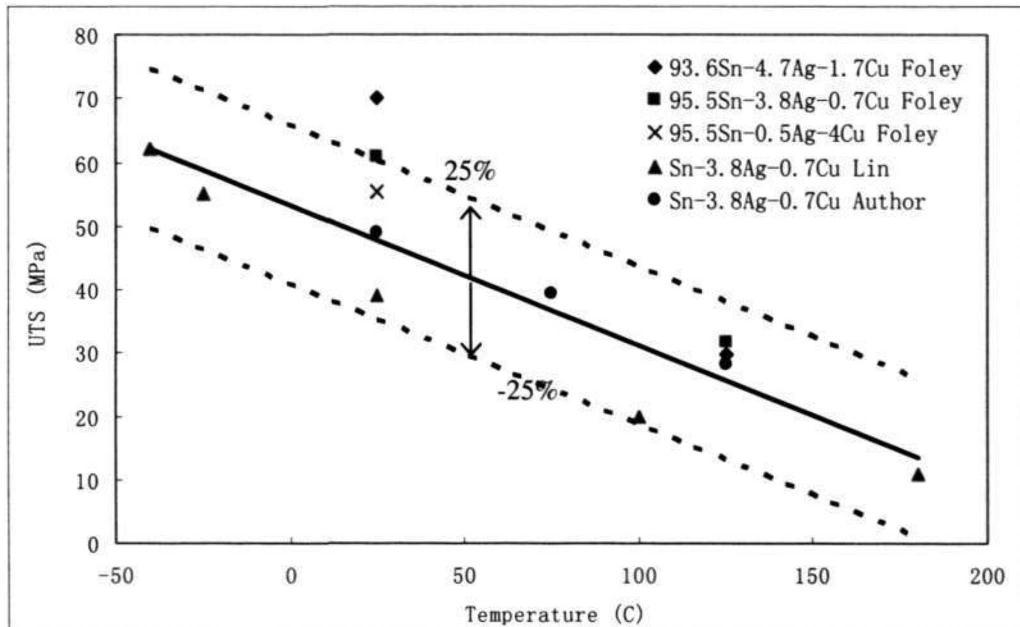

Fig. 4.1-16 (a) Temperature effects of UTS for Sn-Ag-Cu at strain rate of 1E-3 s^{-1}

ATTENTION: The Singapore Copyright Act applies to the use of this document. Nanyang Technological University Library

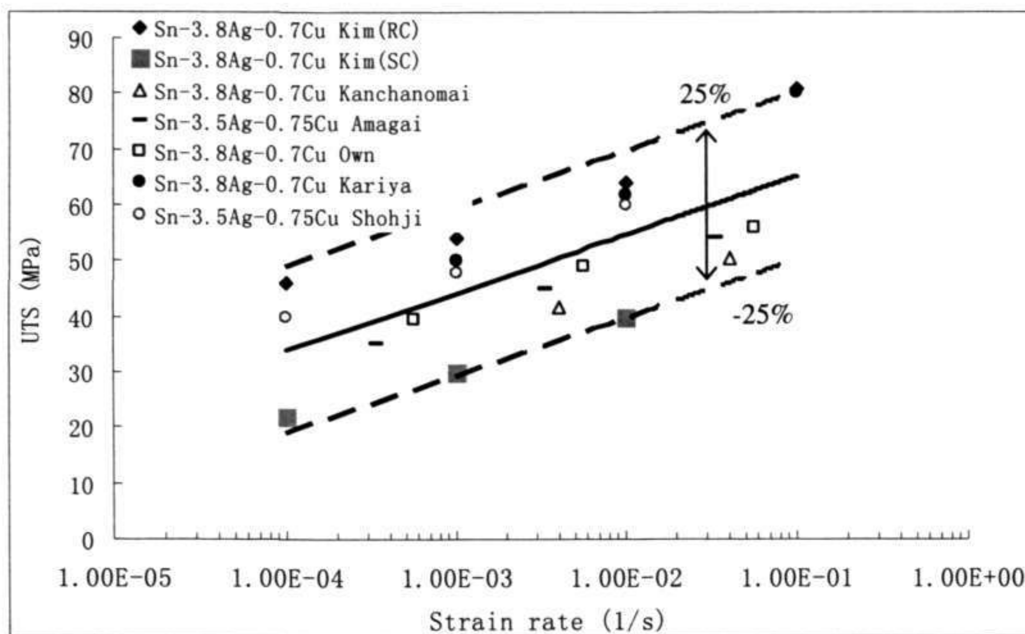

Fig. 4.1-16 (b) Strain rate effect of UTS for Sn-Ag-Cu at room temperature

4.2 Analysis of tensile test result

4.2.1 Strain rate and temperature dependent tensile properties

In section 4.1, it had been found that the mechanical properties of Sn-3.8Ag-0.7Cu and Sn-0.7Cu are dependent on temperature and strain rate. Hence, a statistical method incorporating linear regression was employed to quantify the temperature and strain rate dependent mechanical properties of 95.5Sn-3.8Ag-0.7Cu and 99.3Sn-0.7Cu lead-free solders.

The elastic modulus of 95.5Sn-3.8Ag-0.7Cu and 99.3Sn-0.7Cu is as follows:

$$E(T,\dot{\varepsilon})_{SnAgCu} = (0.00074T + 6.44)\log(\dot{\varepsilon}) + (-0.1932T + 65.935) \quad (4.2.1)$$

$$E(T,\dot{\varepsilon})_{SnCu} = (-0.0235T + 6.396)\log(\dot{\varepsilon}) + (-0.157T + 42.1) \quad (4.2.2)$$

ATTENTION: The Singapore Copyright Act applies to the use of this document. Nanyang Technological University Library

The yield stress and UTS were established and expressed individually as follows:

$$\sigma_y(T,\dot{\varepsilon})_{SnAgCu} = (-0.2053T + 76.61)(\dot{\varepsilon})^{(6.54\times10^{-4}T+0.074)} \quad (4.2.3)$$

$$\sigma_y(T,\dot{\varepsilon})_{SnCu} = (-0.199T + 65.1)(\dot{\varepsilon})^{(2.87\times10^{-4}T+0.08254)} \quad (4.2.4)$$

$$UTS(T,\dot{\varepsilon})_{SnAgCu} = (-0.2161T + 81.32)(\dot{\varepsilon})^{(6.27\times10^{-4}T+0.0619)} \quad (4.2.5)$$

$$UTS(T,\dot{\varepsilon})_{SnCu} = (-0.062T + 65.8)(\dot{\varepsilon})^{(7.9\times10^{-4}T+0.0545)} \quad (4.2.6)$$

The calculated values and percentage error of the predicted elastic modulus, yield stress and UTS compared to the test results for Sn-3.8Ag-0.7Cu and Sn-0.7Cu lead-free solders are given in Table 4.2-1 and 4.2-2, respectively. The equations of elastic modulus, yield stress and UTS are within 5% of the test results. That means the curve-fitted equations (4.2.1) to (4.2.6) gave satisfactory estimation of the temperature and strain rate dependant mechanical properties compared to the tensile test result of 95.5Sn-3.8Ag-0.7Cu and 99.3Sn-0.7Cu lead-free solders.

ATTENTION: The Singapore Copyright Act applies to the use of this document. Nanyang Technological University Library

Table 4.2-1: Calculated Values From Equations and Percentage Error for Sn-Ag-Cu

Test Conditions	Elastic Modulus (% error)	Yield Stress (% error)	UTS (% error)
25°C			
5.6 x10^{-4}	40.1(4)	36.3(3.5)	42.5(4.7)
5.6 x10^{-3}	46.6(3.5)	44.7(4.2)	50.8(3.6)
5.6 x10^{-2}	53(3.8)	55.1(2.5)	60.7(4.7)
75°C			
5.6 x10^{-4}	30.3(1.3)	24.4(4.7)	28.8(0.63)
5.6 x10^{-3}	36.8(2.3)	32.3(3.5)	37(4.6)
5.6 x10^{-2}	43.3(2.1)	42.9(3.4)	47.6(1.2)
125°C			
5.6 x10^{-4}	20.5(0.6)	15.9(3.7)	19(3.6)
5.6 x10^{-3}	27.1(4.1)	22.7(5.0)	26.3(3.3)
5.6 x10^{-2}	33.6(3.4)	32.5(4.4)	36.3(1.2)
-40°C			
5.6 x10^{-4}	52.8(3.5)	59.3(1.5)	68.3(0.58)
5.6 x10^{-3}	59.2(3.9)	66.2(3.7)	74.3(2.9)
5.6 x10^{-2}	65.6(4.2)	73.9(3.4)	80.9(2.9)

Table 4.2-2: Calculated Values From Equations and Percentage Error for Sn-Cu

Test Conditions	Elastic Modulus (% error)	Yield Stress (% error)	UTS (% error)
25°C			
5.6 x10^{-4}	19.2(4.8)	30.7(1.3)	36.8(2.7)
5.6 x10^{-3}	25.0(2.3)	37.7(3.4)	43.6(3.1)
5.6 x10^{-2}	30.9(3.6)	46.4(2.9)	51.8(0.46)
75°C			
5.6 x10^{-4}	15.2(2.7)	22.9(0.7)	26.0(0.33)
5.6 x10^{-3}	19.8(4.8)	29.2(3.9)	33.8(1.1)
5.6 x10^{-2}	24.4(4.7)	37.1(3.6)	43.9(4.6)
125°C			
5.6 x10^{-4}	11.1(4.2)	16.5(0.09)	18.4(0.86)
5.6 x10^{-3}	14.6(3.3)	21.7(1.4)	26.1(0.13)
5.6 x10^{-2}	18.0(4.6)	28.5(3.4)	37.2(2.6)

ATTENTION: The Singapore Copyright Act applies to the use of this document. Nanyang Technological University Library

Apparent elastic modulus, yield stress and UTS can be calculated from equations (4.2.1) to (4.2.6) for different temperatures and strain rates. By using these properties, bi-linear stress-strain curves can be generated for Finite Element Analysis (FEA) application, as shown in Fig. 4.2-1. However, bi-linear curve is only an approximate analysis; actual stress strain curves (See Fig. 4.2-2) should be modeled for more accurate application. Hence, curve-fitting of Anand model will be discussed next.

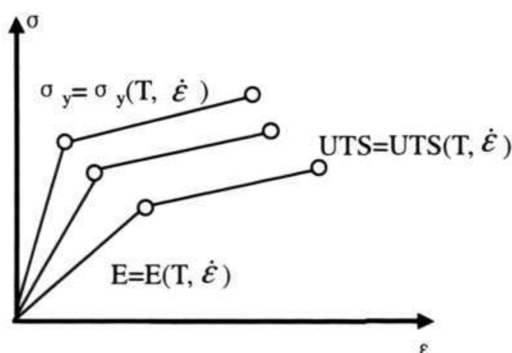

Fig. 4.2-1 Schematic illustration of bi-linear strain curves

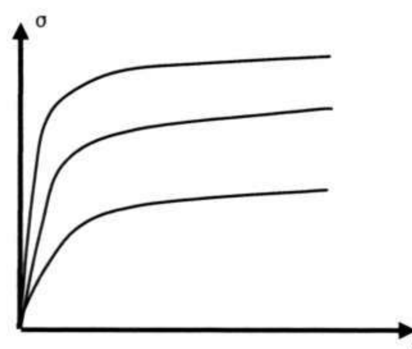

Fig. 4.2-2 Schematic illustration of actual stress strain curves

4.2.2 Application to Anand visco-plastic model

The Anand visco-plastic model is widely used in thermo-mechanical analysis of solder joint reliability. It includes two kinds of equations, the first one deal with relationship between saturation stress and strain rate under certain temperature, while the second one deal with the relationship between strain and stress under certain strain rate and temperature. They are given in Eqs. (4.2.7) and (4.2.8):

ATTENTION: The Singapore Copyright Act applies to the use of this document. Nanyang Technological University Library

$$\sigma^* = \frac{\hat{s}}{\xi}\left(\frac{\dot{\varepsilon}_p}{A}e^{Q/RT}\right)^n \sinh^{-1}\left[\left(\frac{\dot{\varepsilon}_p}{A}e^{Q/RT}\right)^m\right] \tag{4.2.7}$$

where variables $\dot{\varepsilon}_p$ and T denote strain rate and temperature respectively. And parameters *Q/R*, *A*, $\hat{s}/\xi$, *m* and *n* can be determined by a nonlinear fitting method.

$$\sigma = \sigma^* - [(\sigma^* - cs_0)^{(1-a)} + (a-1)ch_0\sigma^{*(-a)}\,\varepsilon_p]^{1/(1-a)} \tag{4.2.8}$$

where variable ε_p denote the nonlinear strain, and *a*, s_0 and h_0 are parameters to be determined. And *c* is a function of strain rate and temperature:

$$c \equiv \frac{1}{\xi}\sinh^{-1}\left[\left(\frac{\dot{\varepsilon}_p}{A}e^{Q/RT}\right)^m\right] \qquad c < 1 \tag{4.2.9}$$

All variables and parameters involved in Eq. (4.2.9) have been used in Eq. (4.2.7). Even though, ξ in Eq. (4.2.9) is used independently and it is used as a part of parameter $\hat{s}/\xi$. If ξ is regarded as an independent parameter, there will be 9 parameters involved in Anand model. But ξ and $\hat{s}$ could not be determined by curve fitting of Eq. (4.2.7) and Eq. (4.2.8). However, the Anand model has been implemented with nine parameters in the ANSYS Finite Element software. Hence, the user needs to "guess" the value of ξ by the condition of $c<1$. The procedure to determine all nine parameters is as follows:

1) Determination of the saturation stress σ^* under a series of strain rate and temperature by creep test.
2) Curve fitting of parameters *Q/R*, *A*, $\hat{s}/\xi$, *m* and *n* in Eq. (4.2.7).

ATTENTION: The Singapore Copyright Act applies to the use of this document. Nanyang Technological University Library

3) Determination of ξ and $\hat{s}$. For value of $\hat{s}/\xi$ has been determined in step (2), value of ξ should be "guessed" such that the value of c will match condition: c<1. And then value of $\hat{s}$ can be derived from $\hat{s}/\xi$ and guessed ξ.

4) Curve fitting of a, s_0 and h_0 by Eq. (4.2.8).

Based on the tensile and creep test of Sn-3.8Ag-0.7Cu and Sn-0.7Cu solder at different temperatures, strain rates or stress levels, nine constants in Anand model can be determined, as shown in Table 4.2-3. Commercial curve-fitting software Datafit 8.0 from Oakdale Engineering was used in curve-fitting of Anand model.

Table 4.2-3 Parameters in Anand model for Sn-3.8Ag-0.7Cu and Sn-0.7Cu

	A	Q/R	ξ	m	$\hat{s}$	n	h_0	a	s_0
Sn-3.8Ag-0.7Cu	65.92	6656	8	0.346	80.8	n1	h1	1.29	37.1
Sn-0.7Cu	9875	5276	2	0.176	65.2	n2	h2	1.03	33.8

The comparison of model prediction and the raw test data for Sn-3.8Ag-0.7Cu lead-free solder is shown in Fig. 4.2-3, 4.2-4 and 4.2-5. The separated points in the figures express the experimental results obtained in this study; the solid lines in the figures denote the calculated stress-strain curves with the values of parameters obtained in Anand model curve-fitting. It is recognized that calculated results can predict the tensile stress-strain curves very well. The curve-fit result for Sn-0.7Cu also gave good agreement with test data.

ATTENTION: The Singapore Copyright Act applies to the use of this document. Nanyang Technological University Library

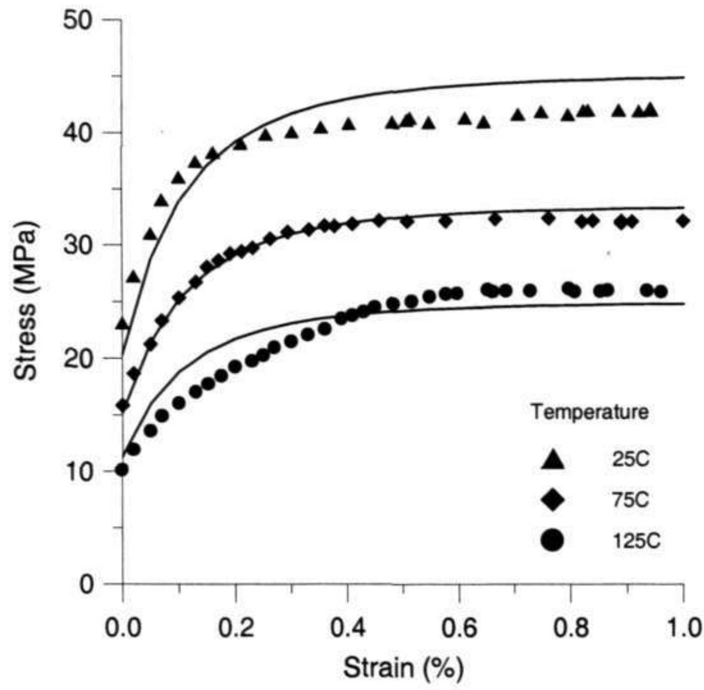

Fig. 4.2-3 Anand model curvefitting at strain rate of $5.6\times10^{-4}\ s^{-1}$

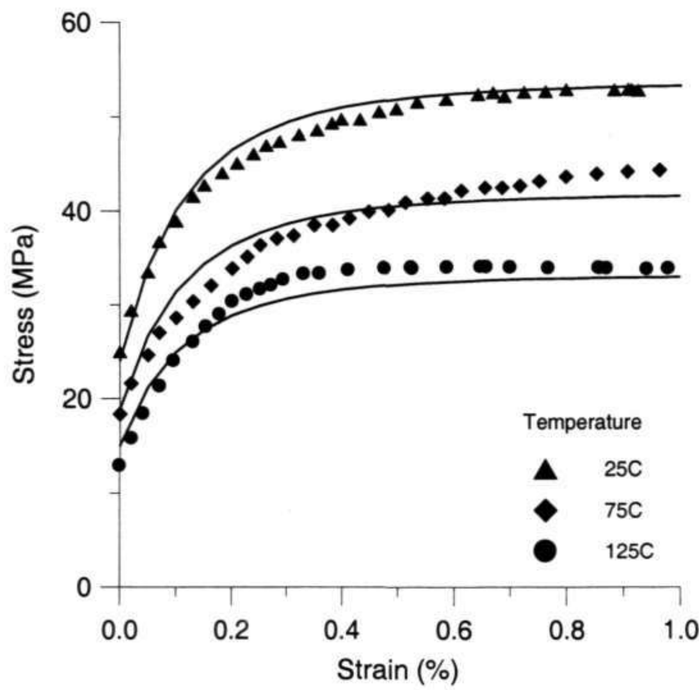

Fig. 4.2-4 Anand model curvefitting at strain rate of $5.6\times10^{-3}\ s^{-1}$

ATTENTION: The Singapore Copyright Act applies to the use of this document. Nanyang Technological University Library

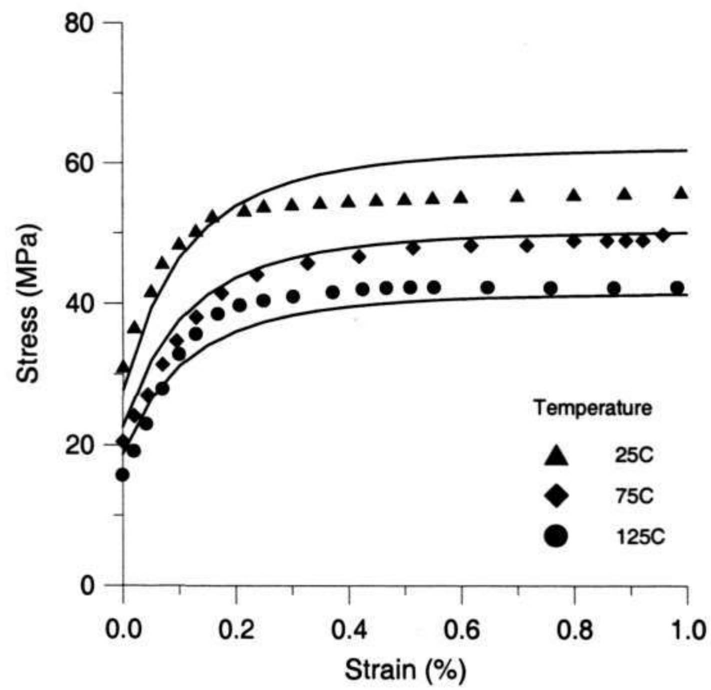

Fig. 4.2-5 Anand model curvefitting at strain rate of $5.6\times10^{-2}\,s^{-1}$

ATTENTION: The Singapore Copyright Act applies to the use of this document. Nanyang Technological University Library

Chapter 5. Creep Test Data & Analysis

In this chapter, the creep behavior for different temperatures and stress levels for the two lead-free solders were investigated. The steady state creep strain rate results were characterized by a hyperbolic sine creep constitutive model.

5.1 Creep test result

5.1.1 Creep behavior of lead-free solders

Creep tests of Sn-3.8Ag-0.7Cu and Sn-0.7Cu lead-free solders were carried out at several different temperatures with constant load set at several different stress levels. In all creep tests, the creep-time displays three stages, namely primary, secondary and tertiary creep. A typical curve is shown in Fig. 5.1-1. A typical strain rate versus time curve is shown in Fig. 5.1-2. Attention was focused on steady-state (secondary) creep since it dominates the creep rupture life of solder. Based on the curve, the creep rate can be determined for any given time by taking the derivative of the creep strain time. The minimum rate was taken as the creep stain rate of the steady-state stage.

ATTENTION: The Singapore Copyright Act applies to the use of this document. Nanyang Technological University Library

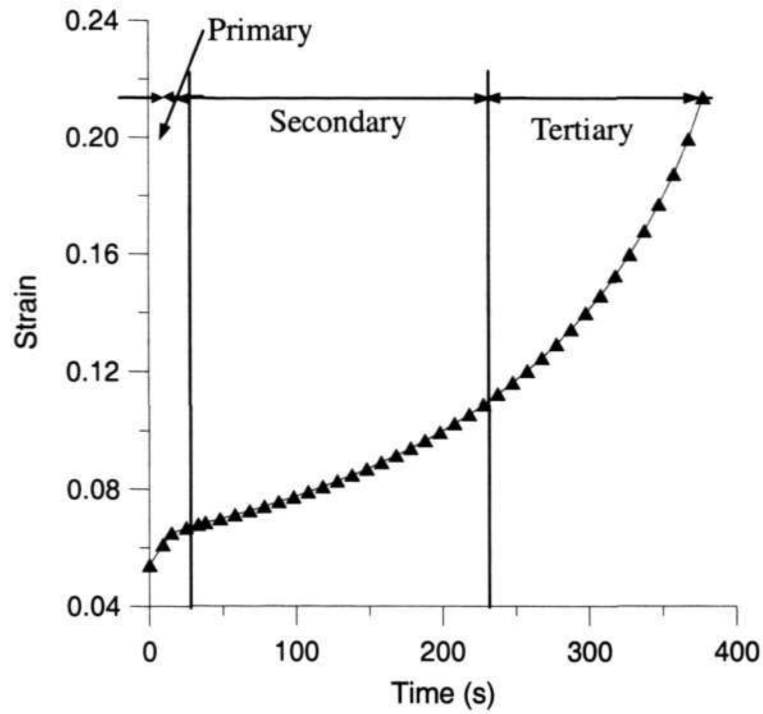

Fig.5.1-1 Creep-time curve obtained at 25MPa, 25°C (Sn-0.7Cu)

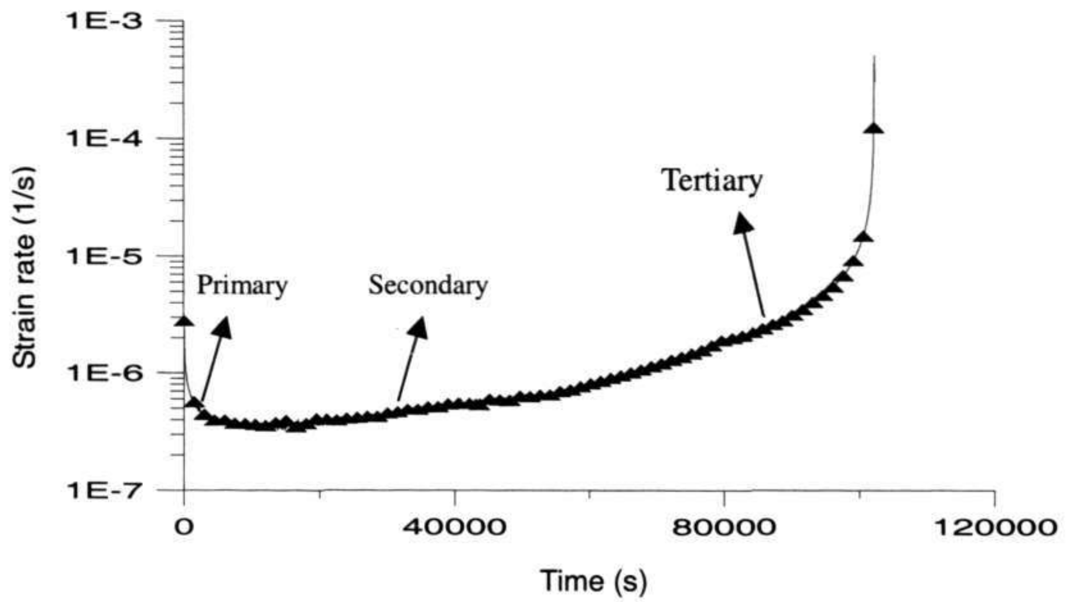

Fig.5.1-2 Strain rate- time curve obtained at 5MPa, 25°C (Sn-0.7Cu)

ATTENTION: The Singapore Copyright Act applies to the use of this document. Nanyang Technological University Library

By plotting all the strain-time curves under each condition into one graph, the effect of stress and temperature on the steady strain rate of lead-free solder alloy could be evaluated. The typical strain-time curves for Sn-0.7Cu solder, at a constant temperature of 125°C is shown in Fig. 5.1-3, and at a constant stress level of 7MPa is given in Fig. 5.1-4. It is noted that the steady strain rate of Sn-0.7Cu lead-free solders is strongly dependent on the test temperature and stress level. For Sn-3.8Ag-0.7Cu, the same trend can be found.

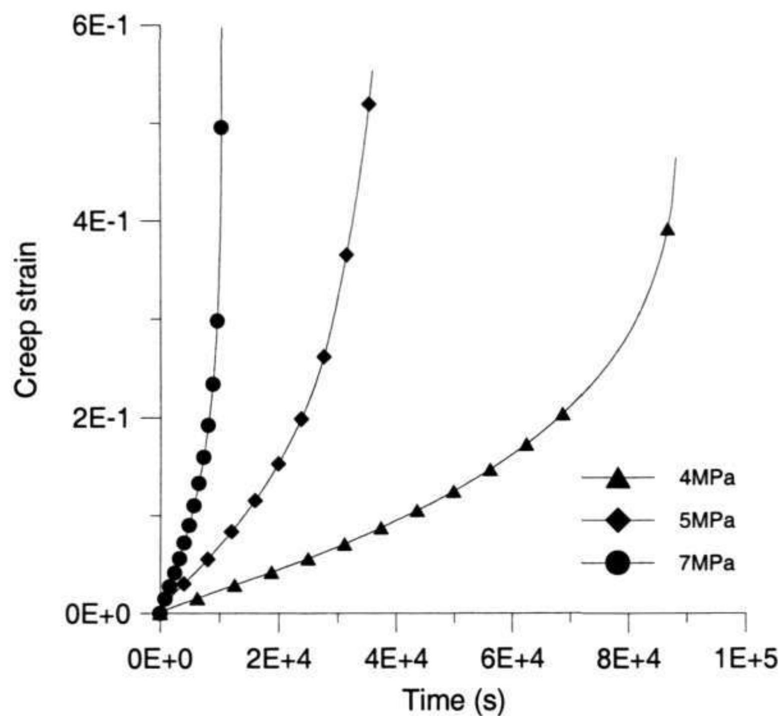

Fig.5.1-3 Creep-time curve at constant temperature of 125°C (Sn-0.7Cu)

ATTENTION: The Singapore Copyright Act applies to the use of this document. Nanyang Technological University Library

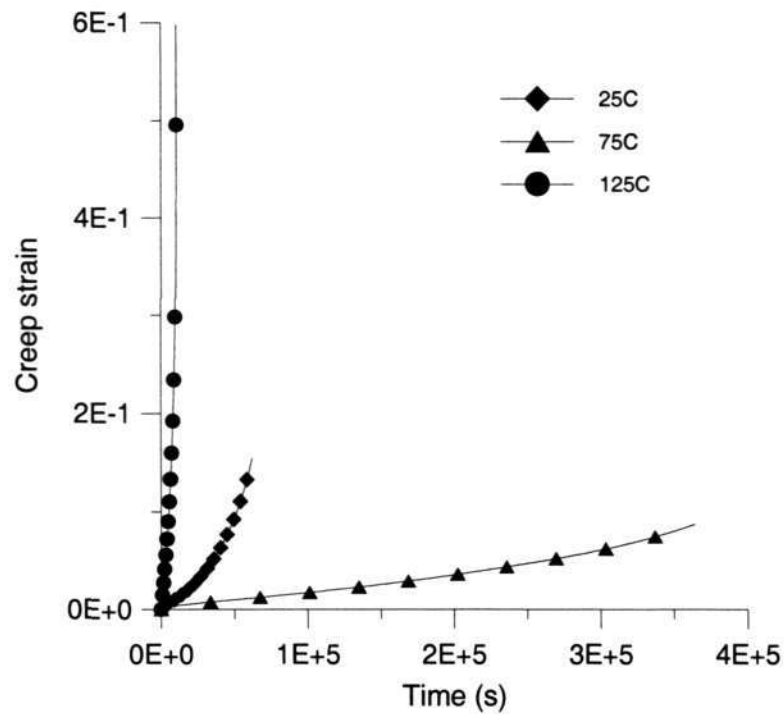

Fig.5.1-4 Creep-time curve at constant stress level of 7MPa (Sn-0.7Cu)

5.1.2 95.5Sn-3.8Ag-0.7Cu solder alloy results

Table 5.1-1 summarizes the steady state creep test result which has been reported by Pang and Xiong et al [82-85]. The steady state creep strain rate against its applied normal stress data is plotted in Fig. 5.1-5. For Sn-3.8Ag-0.7Cu solder, it can be seen that when the temperature and applied normal stress increases, the steady state creep strain rate also increases.

ATTENTION: The Singapore Copyright Act applies to the use of this document. Nanyang Technological University Library

Table 5.1-1 Summary of 95.5Sn-3.8Ag-0.7Cu creep test result

Stress	-40°C	25°C	75°C	125°C
2MPa	-	-	-	6.58E-8
3MPa	-	-	-	2.14E-7
5MPa	-	1.15E-9	3.2E-8	1.83E-6
7MPa	-	-	1.0E-7	1.07E-5
10MPa	-	1.0E-8	2.4E-7	3.37E-5
15MPa	-	8.91E-8	6.4E-6	1.57E-4
20MPa	-	1.4E-6	3.8E-5	3.2E-3
25MPa	1.92E-8	4.1E-6	1.58E-4	-
30MPa	1.74E-7	3.2E-5	-	-
35MPa	-	9.1E-5	1.04E-3	-
40MPa	5.5E-7	3.4E-4	-	-
50MPa	3.24E-6	-	-	-
60MPa	1.3E-5	-	-	-
70MPa	1.3E-4	-	-	-

ATTENTION: The Singapore Copyright Act applies to the use of this document. Nanyang Technological University Library

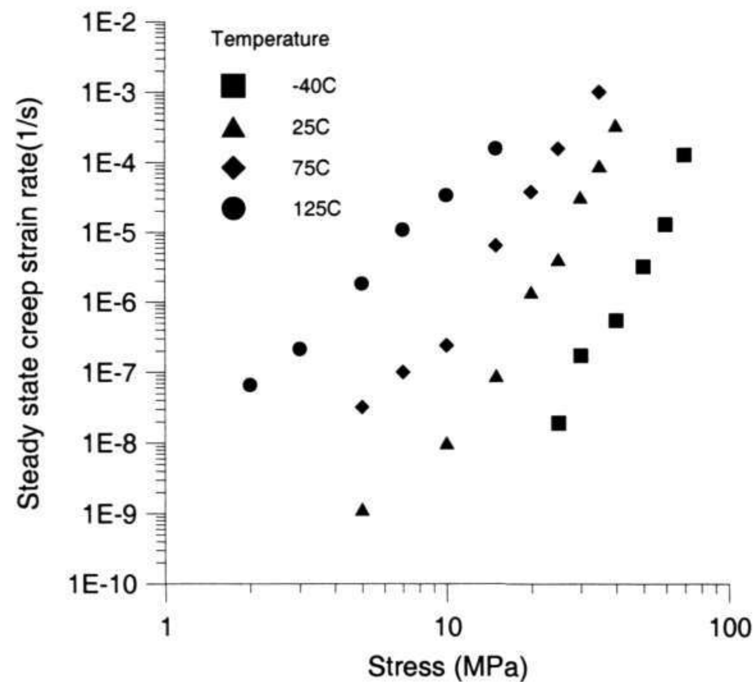

Fig. 5.1-5 Steady-state creep behavior of 95.5Sn-3.8Ag-0.7Cu solder alloy

5.1.3 99.3Sn-0.7Cu solder alloy results

Creep properties of Sn-0.7Cu solder alloy has similar trend with Sn-3.8Ag-0.7Cu solder. The steady state creep strain rate increases with increase in temperature and stress level. The creep properties of Sn-0.7Cu solder is lower than those of the Sn-3.8Ag-0.7Cu solder alloy. The steady state creep strain rates of Sn-0.7Cu solder at different temperatures and stress levels are plotted in Fig. 5.1-6, and the results were summarized in Table 5.1-2.

ATTENTION: The Singapore Copyright Act applies to the use of this document. Nanyang Technological University Library

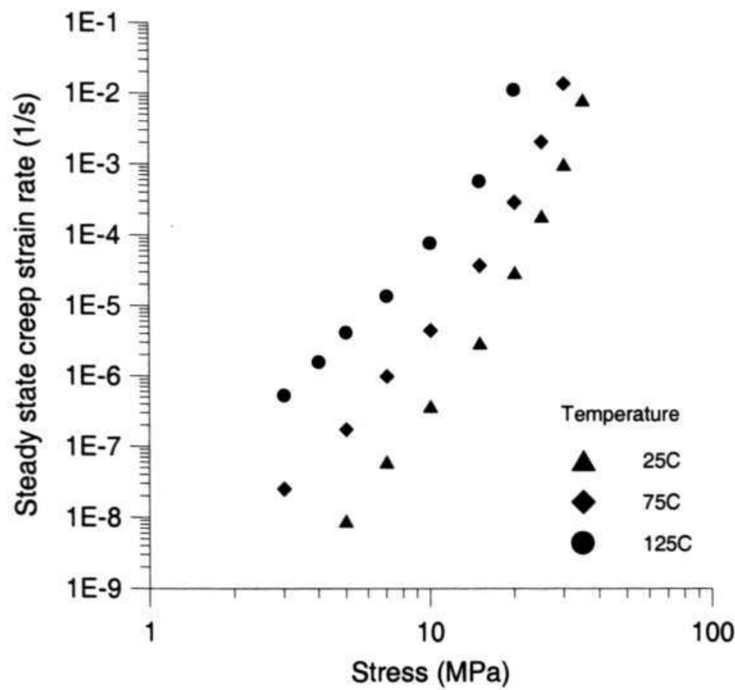

Fig. 5.1-6 Steady-state creep behavior of 99.3Sn-0.7Cu solder alloy

Table 5.1-2 Summary of 99.3Sn-0.7Cu creep test result

Strain Rate / Stress	25°C	75°C	125°C
3MPa	-	2.5E-8	5.21E-7
4MPa	-	-	1.56E-6
5MPa	8.91E-9	1.74E-7	4.07E-6
7MPa	6.03E-8	9.88E-7	1.35E-5
10MPa	3.27E-7	4.47E-6	7.59E-5
15MPa	2.95E-6	3.72E-5	5.6E-4
20MPa	2.96E-5	2.88E-4	1.09E-2
25MPa	1.86E-4	2.04E-3	-
30MPa	9.8E-4	1.35E-2	-
35MPa	7.94E-3	-	-

ATTENTION: The Singapore Copyright Act applies to the use of this document. Nanyang Technological University Library

5.1.4 Comparison with other reported results

5.1.4.1 Comparison with tin-lead solder

Shi [11] reported the creep properties of 63Sn-37Pb solder at different temperatures and stress levels. The comparison of steady state creep strain rate for Sn-3.8Ag-0.7Cu, Sn-0.7Cu and 63Sn-37Pb [11] at room temperature and high temperature are shown in Fig. 5.1-7, and 5.1-8, respectively. It can be noticed that lead-free solder has the better creep resistance than tin-lead solder, while the creep property of Sn-Ag-Cu is better than Sn-Cu solder.

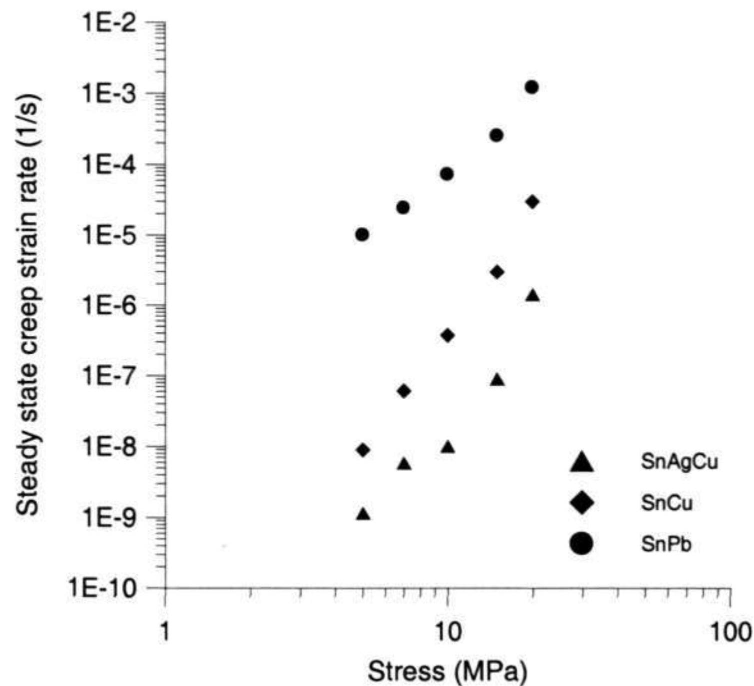

Fig. 5.1-7 Comparison of creep resistance at room temperature (25°C)

ATTENTION: The Singapore Copyright Act applies to the use of this document. Nanyang Technological University Library

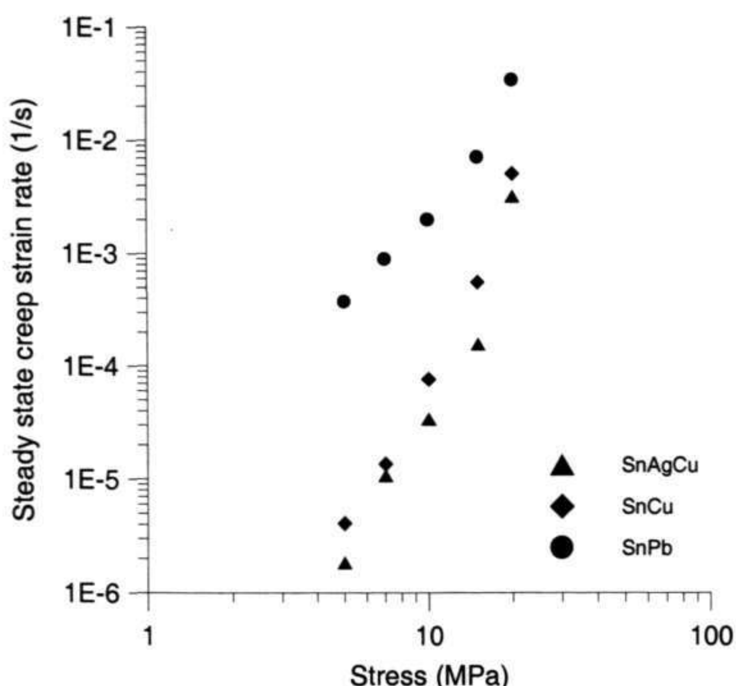

Fig. 5.1-8 Comparison of creep resistance at high temperature (125°C)

5.1.4.2. Comparison with other lead-free data

Some reported creep data [86-100] for Sn-3.8Ag-0.7Cu and other lead-free solder alloys were reviewed. Fig. 5.1-9 and 5.1-10 summarized creep data for Sn-Ag-Cu at room temperature (25°C) and high temperature (125°C). It was found that there is a order variances (1X) for different reported results (Morris, 2003 [96]; Lau, 2003 [101]; Schubert, 2001 [91]; Wiese. 2003 [97]; Pang and Xiong, 2004 [101-102]). Fig. 5.1-11 shows the comparison between the author's creep data with Morris's creep data [96]. The solder joint specimens were used in Morris's tests. The solder thickness is 160 microns and the samples were cooled at two cooling rates of 2.7°C/s and 3.5°C/s, respectively. It was found that the steady state creep strain rates for the

ATTENTION: The Singapore Copyright Act applies to the use of this document. Nanyang Technological University Library

author's bulk solder data were comparable to the solder joint data of Morris [96] at 125-130°C [101-102]. Fig. 5.1-12 shows the author's Sn-Ag-Cu bulk creep data comparison with the NPL [98] solder joint creep data at room temperature and it was noted the result is also acceptable. The creep properties obtained from bulk specimens compares satisfactory with the solder joint creep results for Sn-Ag-Cu solder. However, few creep data for Sn-Cu solder was reported, the author's Sn-Cu data was compared with the data from Plumbridge [93] at 75°C in Fig. 5.1-13 and shows the similar trend.

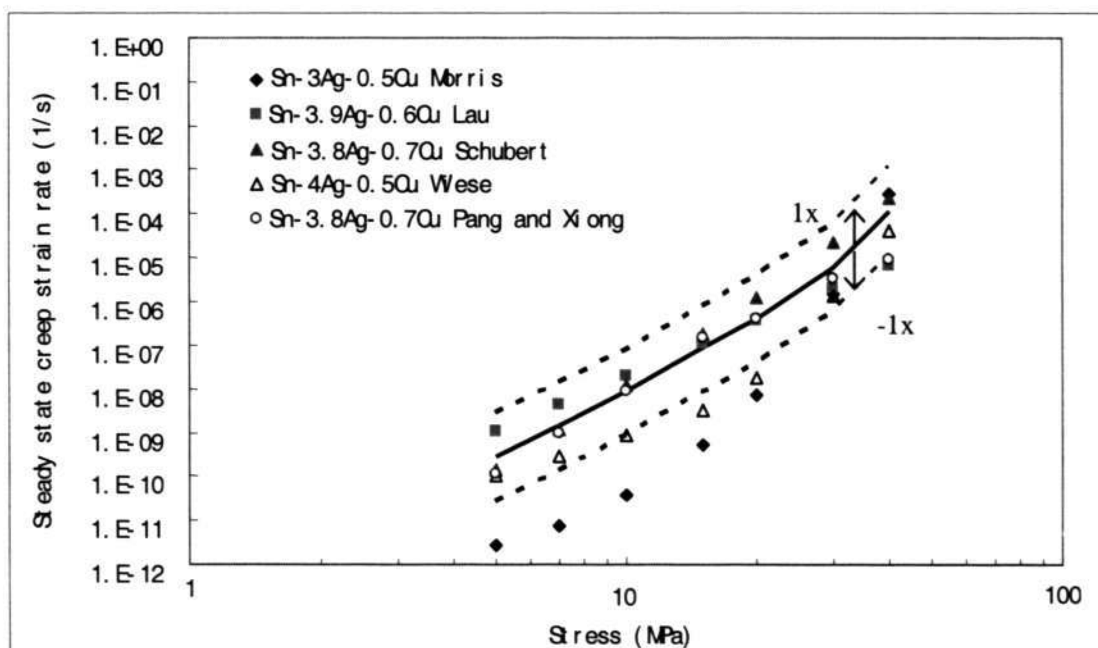

Fig. 5.1-9 Sn-Ag-Cu steady state creep strain rate at 25°C

ATTENTION: The Singapore Copyright Act applies to the use of this document. Nanyang Technological University Library

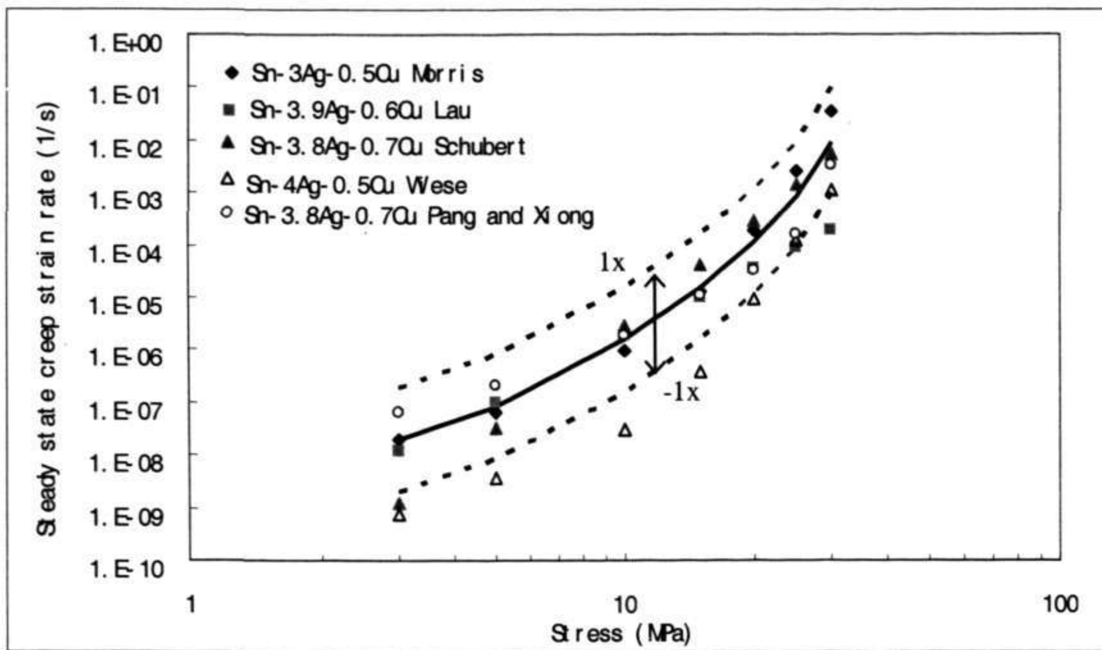

Fig. 5.1-10 Sn-Ag-Cu steady state creep strain rate at 125°C

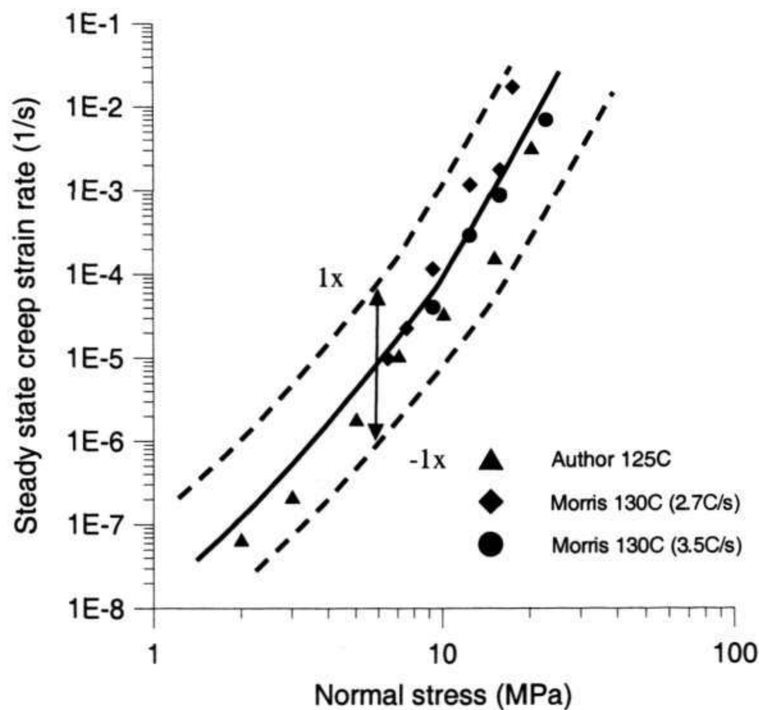

Fig.5.1-11 Comparison of creep properties between author and Morris for Sn-Ag-Cu

ATTENTION: The Singapore Copyright Act applies to the use of this document. Nanyang Technological University Library

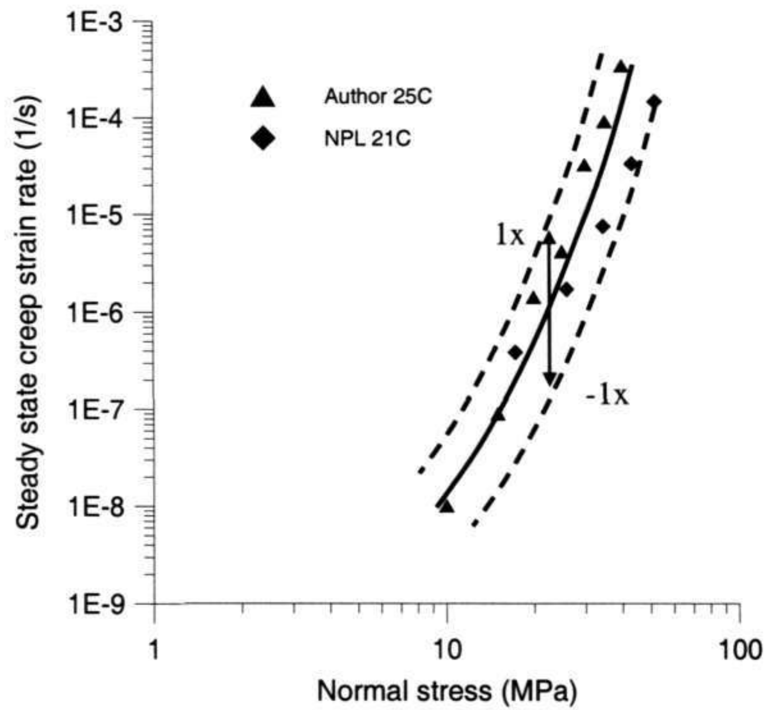

Fig.5.1-12 Comparison of creep properties between author and NPL for Sn-Ag-Cu

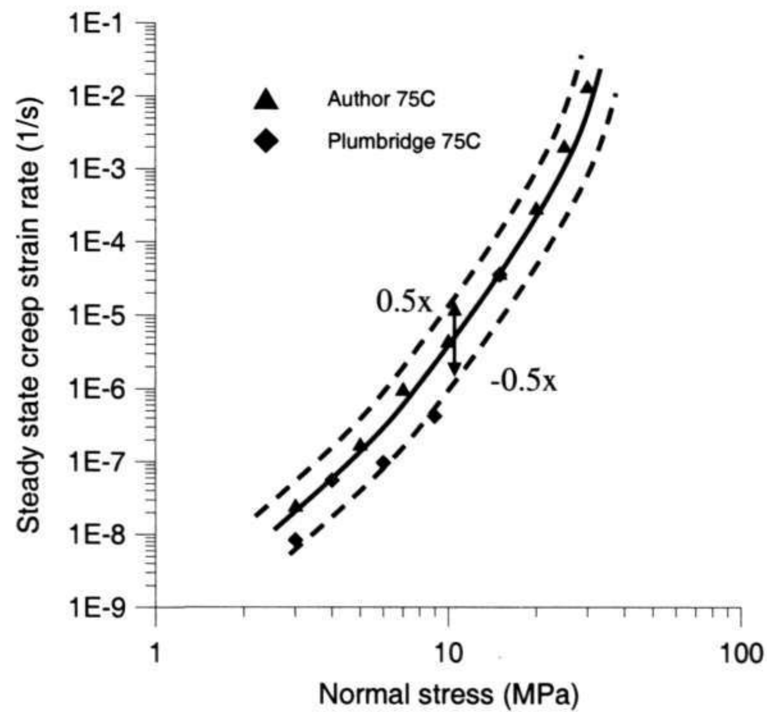

Fig.5.1-13 Comparison of creep properties between author and Plumbridge for Sn-Cu

ATTENTION: The Singapore Copyright Act applies to the use of this document. Nanyang Technological University Library

5.2 Creep models

Creep behavior is often characterized by its steady state creep strain rate, $\dot{\varepsilon}_{ss}$, which can be simply expressed as power law relationship,

$$\dot{\varepsilon} = A\sigma^n e^{\frac{-Q}{kT}} \tag{5.2.1}$$

where A is material constant, σ is applied stress, n is stress exponent, Q is creep activation energy, k is Boltzmann's constant, and T is absolute temperature. The activation energy, Q, and the stress exponent, n, changes with the dominant creep mechanism, and may have different values at different regimes of the applied stress. To describe the steady state creep strain rate at different regimes of stress and temperature, the hyperbolic-sine model is often used. The expressions of the models is,

$$\dot{\varepsilon} = C[\sinh(\alpha\sigma)]^n \exp\left(-\frac{Q}{kT}\right) \tag{5.2.2}$$

The results of steady state creep strain rate depend on the normal stress and temperature for 95.5Sn-3.8Ag-0.7Cu and 99.3Sn-0.7Cu lead-free solders were used to curve fit to Eq. (5.2.2). Figs. 5.2-1 and 5.2-2 show the comparison of calculated steady state creep strain rates with the experimental data at different temperatures. The separated points in the figures express the experimental results obtained in this study; the solid lines in the figure denote the steady state creep strain rate curves with the values obtained in curve-fitting. It is recognized that calculated results based on Eq. (5.2.2) show fairly good agreement with experimental results.

After curve-fitting, the parameters for Sn-3.8Ag-0.7Cu and Sn-0.7Cu solder can be

ATTENTION: The Singapore Copyright Act applies to the use of this document. Nanyang Technological University Library

determined, and were shown as,

Hyperbolic-sine model:

$$\dot{\varepsilon}_{SnAgCu} = 501.3[\sinh(0.0316\sigma)]^{4.96} \exp\left(-\frac{5433.5}{T}\right) \quad (5.2.3)$$

$$\dot{\varepsilon}_{SnCu} = 4.35[\sinh(0.096\sigma)]^{3.7} \exp\left(-\frac{4835.2}{T}\right) \quad (5.2.4)$$

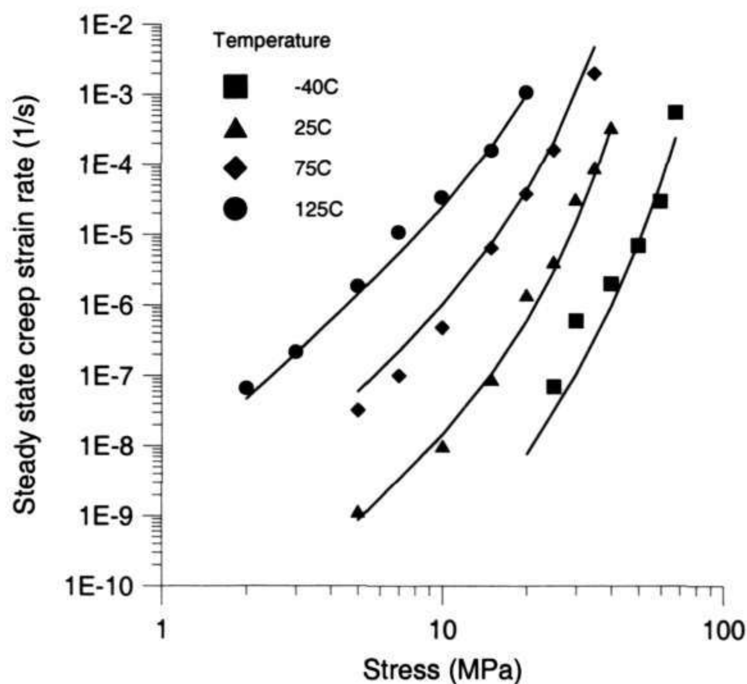

Fig. 5.2-1Hyperbolic-sine model of 95.5Sn-3.8Ag-0.7Cu solder alloy

ATTENTION: The Singapore Copyright Act applies to the use of this document. Nanyang Technological University Library

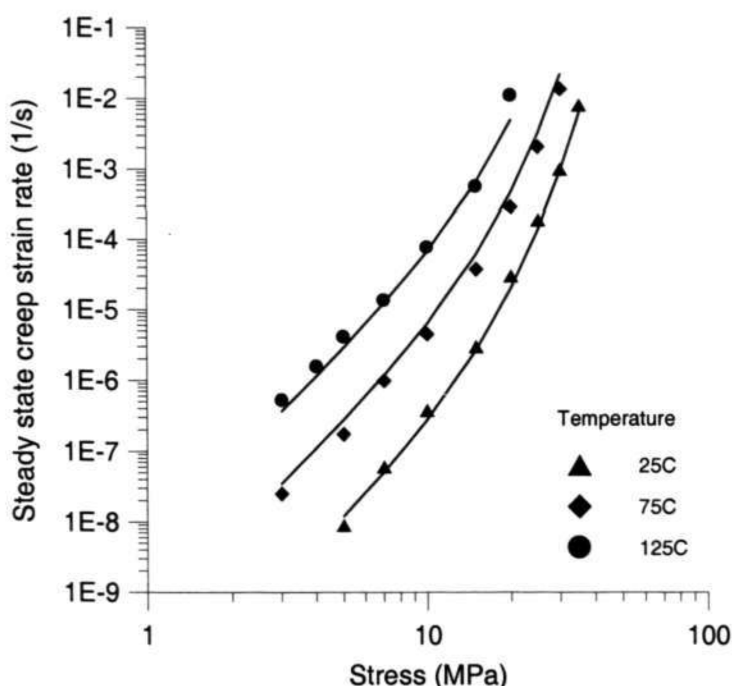

Fig. 5.2-2 Hyperbolic-sine model of 99.3Sn-0.7Cu solder alloy

Lau [99], Schubert and Pang [100] also reported their creep test data for Sn-Ag-Cu solder. Their curve-fitted results for the hyperbolic-sine creep model is shown below [83],

Lau (95.5Sn-3.9Ag-0.6Cu) $\dot{\varepsilon} = 4.41\times10^{5}[\sinh(0.005\sigma)]^{4.2}\exp(-5412/T)$ (5.2.5)

Schubert (95.5Sn-3.8Ag-0.7Cu) $\dot{\varepsilon} = 2.78\times10^{5}[\sinh(0.02447\sigma)]^{6.41}\exp(-6496/T)$ (5.2.6)

A comparison of the Sn-Ag-Cu solder material, specimen type, stress exponent and activation energy from Lau, Schubert and the author' s creep test result is given in Table 5.2-1. It is noted that the stress exponent n varies from 4.2 to 6.4, while the activation energy, Q, varies from 45KJ/mol - 54KJ/mol. A comparison of the steady state creep model using the equations (5.2.3), (5.2.5) and (5.2.6) are shown in Fig.

ATTENTION: The Singapore Copyright Act applies to the use of this document. Nanyang Technological University Library

5.2-3. From the figure, it can be seen that the author's creep data agree well with data reported by Lau. Satisfactory agreement with Schubert's data was seen at low stresses, but some difference is noted at higher stresses above 10 MPa.

Table 5.2-1 Comparison of different reported creep test data for Sn-Ag-Cu

	Material	Specimen	Stress exponent n	Active energy Q (KJ/mol)
Author	95.5Sn3.8Ag0.7Cu	Cylindrical bulk specimen with gauge diameter of 3mm and gauge length of 15mm	4.96	45.2
Lau	95.5Sn3.9Ag0.6Cu	Compression specimen with diameter of 10mm and length of 19mm	4.2	45
Schubert	95.5Sn3.8Ag0.7Cu	Flat bulk specimen with 3×3mm cross section and gauge length of 30mm	6.4	54

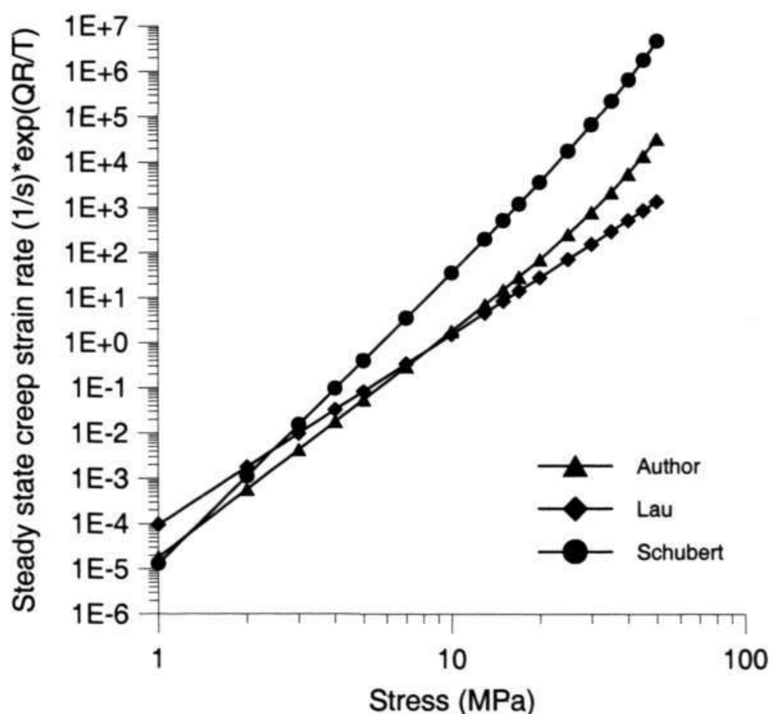

Fig. 5.2-3 Comparison of steady-state creep behavior of different researchers for Sn-Ag-Cu

ATTENTION: The Singapore Copyright Act applies to the use of this document. Nanyang Technological University Library

Chapter 6. Low Cycle Fatigue Test Data & Analysis

In this chapter, low cycle fatigue behaviors for the two lead-free solders tested over the range of temperatures, frequencies and strain levels were analyzed. Coffin-Manson and Morrow's models were used to characterize the low cycle fatigue behavior of the Sn-3.8Ag-0.7Cu and Sn-0.7Cu solder alloys.

6.1 Low Cycle Fatigue test result

6.1.1 Cyclic stress-strain behavior

After calculating cyclic stress and strain in each cycle, stress-strain hysteresis loop of Sn-0.7Cu and Sn-3.8Ag-0.7Cu solders at the tenth cycle for 2% total strain range at temperature of 125°C and frequency of 1Hz are shown in Fig. 6.1-1.

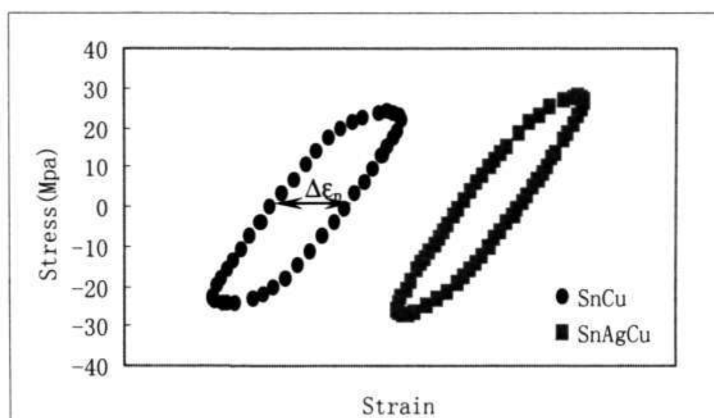

Fig. 6.1-1 Cyclic stress-strain hysteresis loops at the tenth cycle of fatigue test

For the same total strain range, Sn-0.7Cu solder has larger plastic range and smaller stress range than Sn-3.8Ag-0.7Cu solder. The results correspond to a greater tensile strength for Sn-3.8Ag-0.7Cu solder alloy as shown in Chapter 4. The plastic range

ATTENTION: The Singapore Copyright Act applies to the use of this document. Nanyang Technological University Library

increased with the applied total strain range, and will increase slightly with the number of cycles, as shown in Fig. 6.1-2.

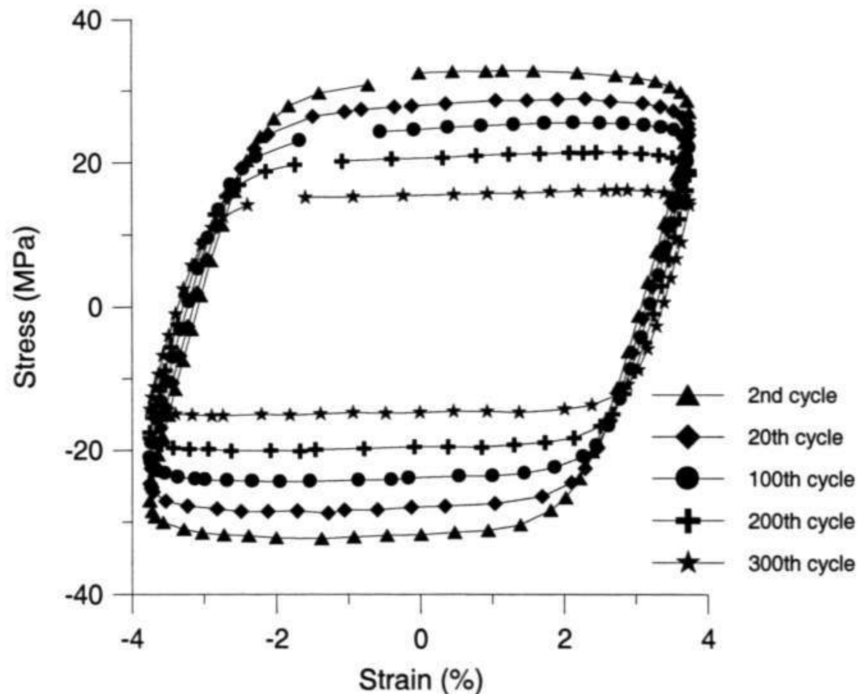

Fig. 6.1-2 Hysteresis loop at various cycles at 25°C, 7.5% and 0.01Hz of Sn-0.7Cu solder

The relationship between stress amplitude (one-half of the stress range) and number of cycles for Sn-0.7Cu and Sn-3.8Ag-0.7Cu solders for different total strain ranges at 125°C and 1Hz are shown in Fig. 6.1-3. Cyclic softening was observed for both lead-free solders. At the beginning of the fatigue test, stress amplitude reduces rapidly; after the first stage, stress amplitude shows slower reduction, which was defined as the second stage of the fatigue test; and finally, at the third stage, the stress reduction rate increases again and leads to final fracture. It is also can be noticed that the decrease rate of stress amplitude at secondary stage increases with the total strain range increases, which can be compared between Figs. 6.1-3 (a) and (b).

ATTENTION: The Singapore Copyright Act applies to the use of this document. Nanyang Technological University Library

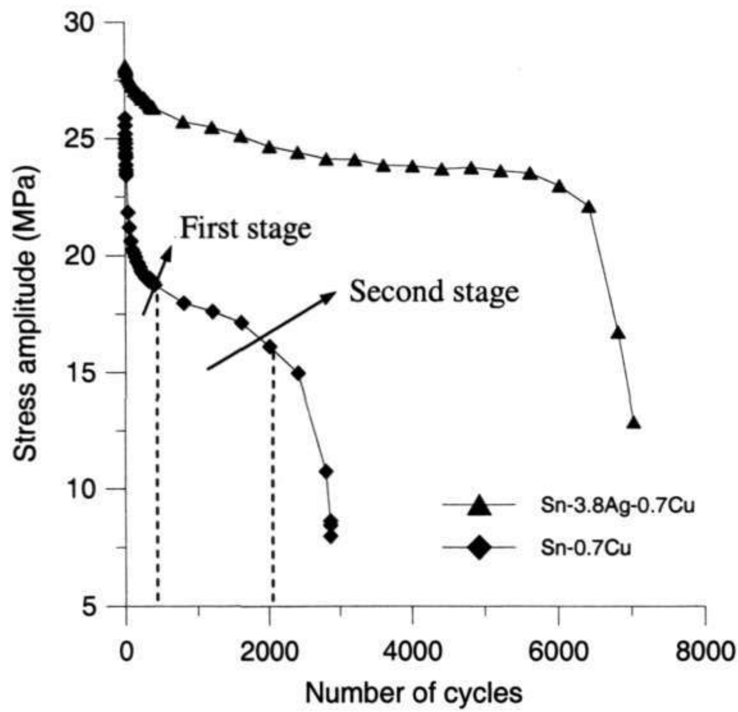

Fig. 6.1-3(a) Relationship between stress amplitude and number of cycles at 2% total strain range, 125°C and 1Hz

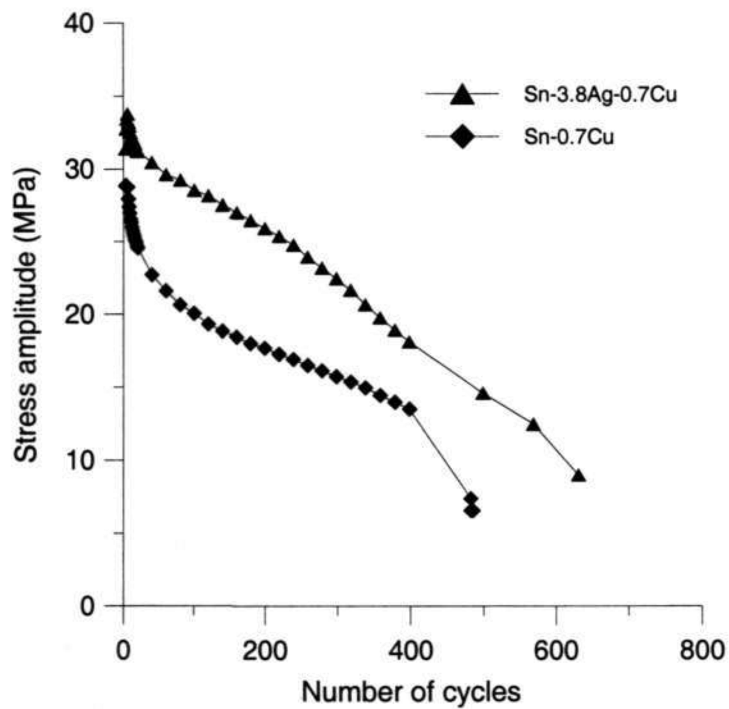

Fig. 6.1-3(b) Relationship between stress amplitude and number of cycles at 7.5% total strain range, 125°C and 1Hz

ATTENTION: The Singapore Copyright Act applies to the use of this document. Nanyang Technological University Library

6.1.2 *Effect of temperature on low cycle fatigue behavior*

Test result of Sn-0.7Cu solder at different temperatures will show the effect of temperature on low cycle fatigue. Hysteresis loops at beginning of the second stage were selected to plot at different temperatures at strain range of 3.5% and frequency of 1Hz. The material response at different temperature can be evaluated and compared as shown in Fig.6.1-4. While the Sn-3.8Ag-0.7Cu solder has the similar trends with Sn-0.7Cu solder [103-104].

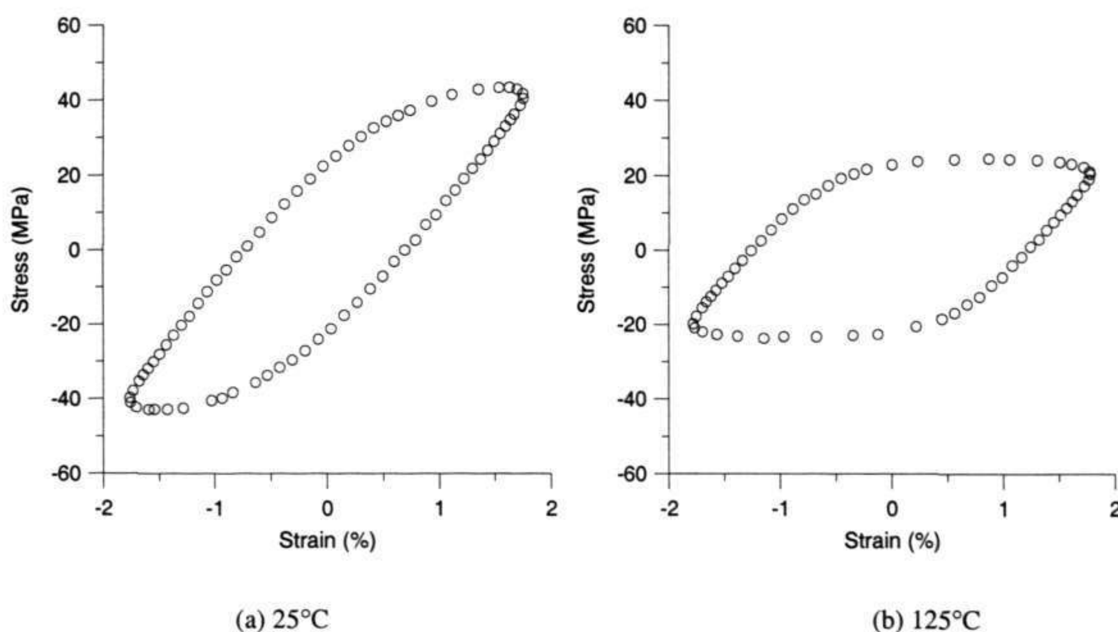

Fig. 6.1-4 Hysteresis loop at 1Hz and strain range of 3.5% for Sn-0.7Cu

The relationship between the fatigue life and plastic strain obtained from tests of 0.01Hz at three different temperatures (25, 75 and 125°C) is presented in Fig. 6.1-5. The fatigue life versus inelastic strain energy density plot is given in Fig. 6.1-6.

ATTENTION: The Singapore Copyright Act applies to the use of this document. Nanyang Technological University Library

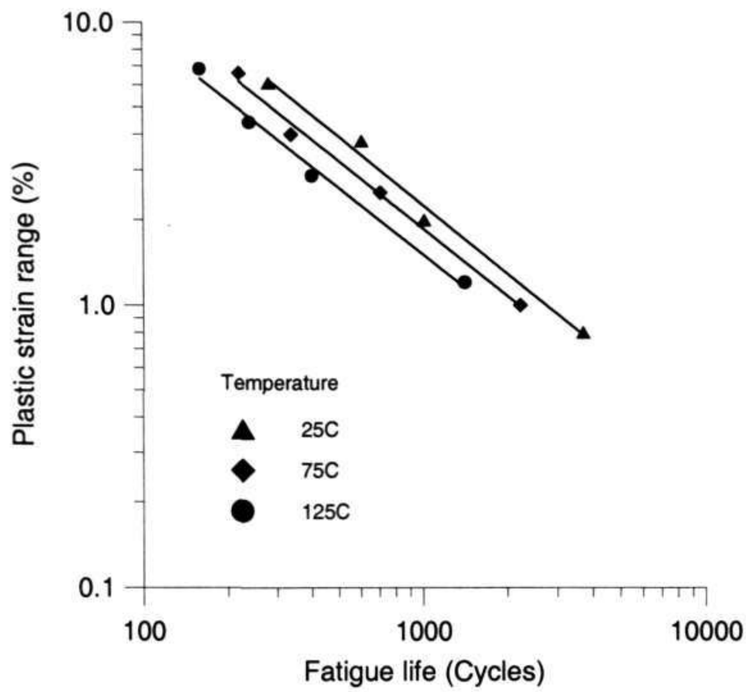

Fig. 6.1-5 Plastic strain versus fatigue life at 0.01Hz for different temperatures

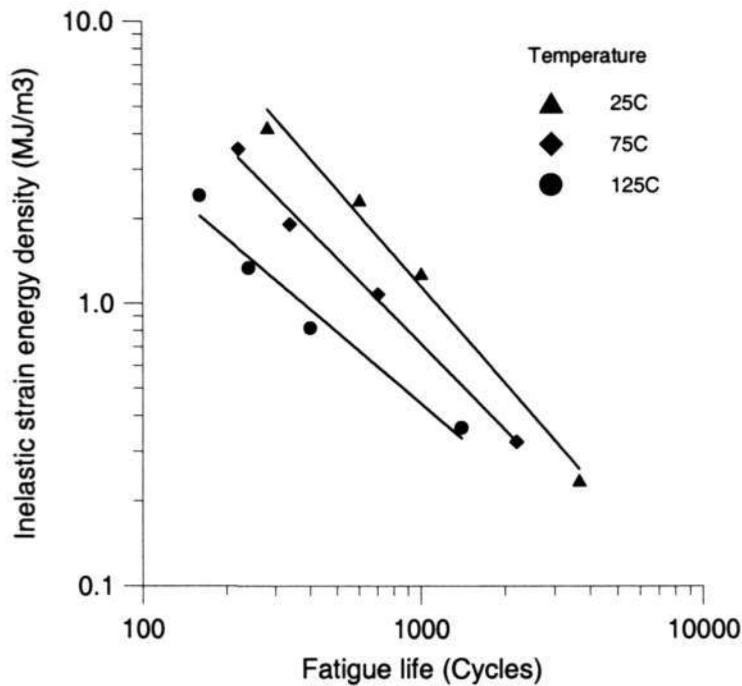

Fig. 6.1-6 Inelastic strain energy density versus fatigue life at 0.01Hz for different temperatures

ATTENTION: The Singapore Copyright Act applies to the use of this document. Nanyang Technological University Library

From Fig. 6.1-5 and 6.1-6, the values of constants for Coffin-Manson model and Morrow's energy-based model can be determined for different temperatures by taking the slope and the interception the plastic strain (inelastic strain energy density) axis. It was found that the value of m and C in Coffin-Manson model decreases with increasing temperature. For energy-based model, the same trend can be found.

6.1.3 Effect of Frequency on low cycle fatigue behavior

The fatigue test result of Sn-0.7Cu solder will show the frequency on low cycle fatigue. By plotting the hysteresis loop of different frequency at 125°C and strain range of 7.5%, the material response at different temperature can be evaluated and compared (Fig. 6.1-7). Sn-3.8Ag-0.7Cu solder has the similar trend.

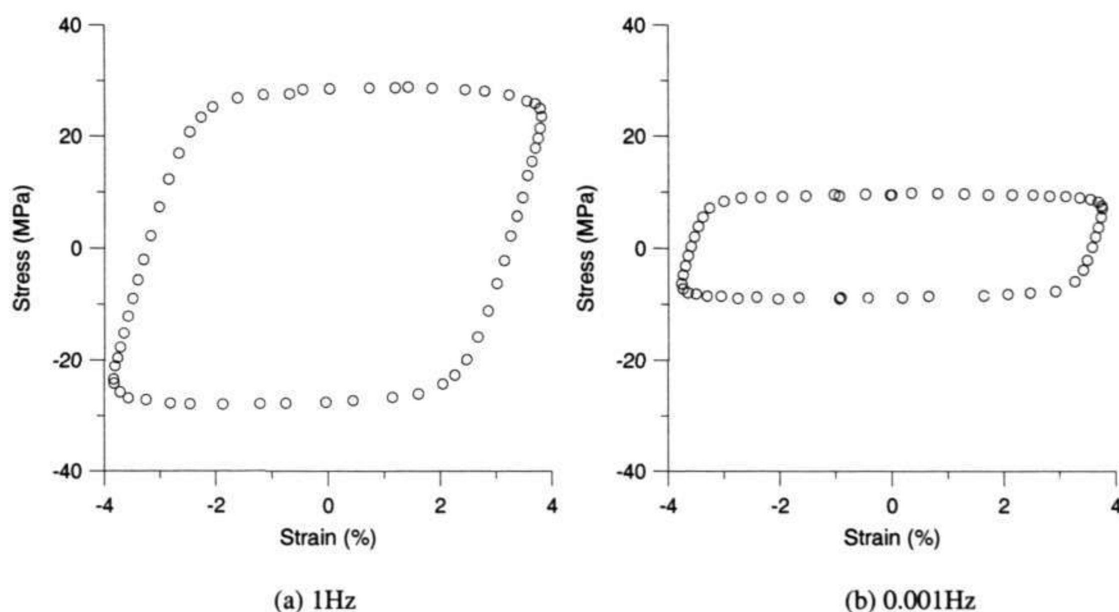

Fig. 6.1-7 Hysteresis loop at 125°C and strain range of 7.5% for Sn-0.7Cu

ATTENTION: The Singapore Copyright Act applies to the use of this document. Nanyang Technological University Library

After conducting the tests at the same temperature and total strain but at different frequencies, the fatigue life of lead-free solder was found to decrease with decreasing frequency. This characteristic of fatigue life can be attributed to accumulate creep damage during fatigue testing. As the frequency decreases, the time for each cycle increases, and this allow more time for creep to develop and thus leads to lower fatigue life in terms of cycles to failure.

As can be seen from Fig. 6.1-8 and 6.1-9, the Coffin-Manson model and energy-based model can be used to describe the fatigue behavior of lead-free solder for any given frequency. However, the fatigue results have some difference at different frequencies, the value of fatigue exponent m and ductility coefficient C changes as frequency changes. It was found that, for both models, the m value decrease with frequency, but the frequency dependent is small. However, the C value decreases significantly as the frequency decreases, and is strongly frequency dependent.

ATTENTION: The Singapore Copyright Act applies to the use of this document. Nanyang Technological University Library

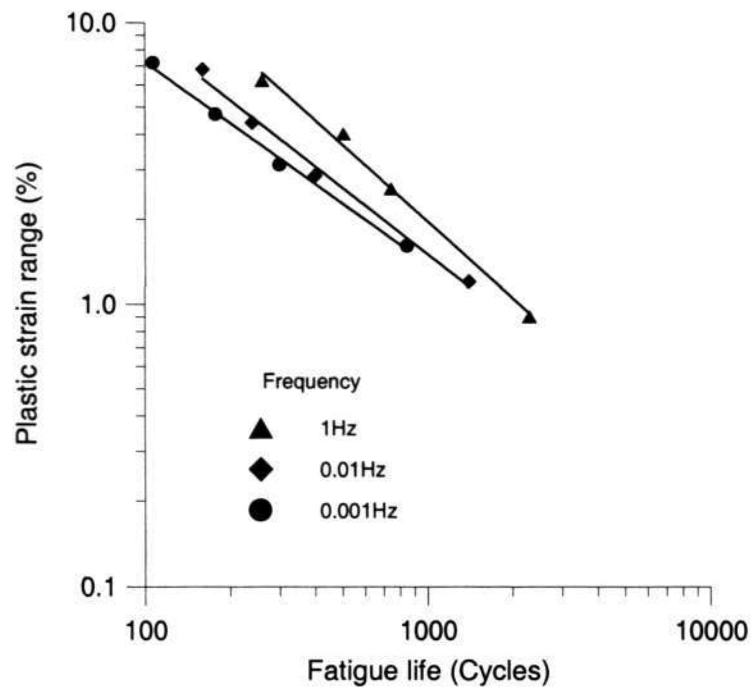

Fig. 6.1-8 Plastic strain versus fatigue life at 125°C for different frequencies

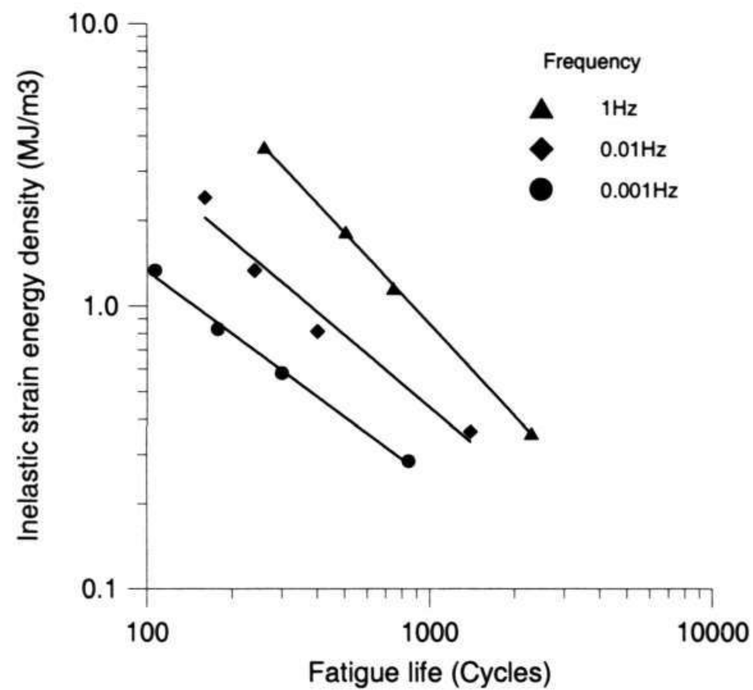

Fig.6.1-9 Inelastic strain energy density versus fatigue life at 125°C for different frequencies

ATTENTION: The Singapore Copyright Act applies to the use of this document. Nanyang Technological University Library

6.1.4 Comparison with other reported results

6.1.4.1 Comparison with tin-lead solder

Shi [51-52] reported the fatigue properties for 63Sn-37Pb solder at different temperatures and frequencies. The comparison of fatigue resistance for Sn-3.8Ag-0.7Cu, Sn-0.7Cu and 63Sn-37Pb [51-52] at room temperature & high frequency and high temperature & low frequency are shown in Fig 6.1-10, and 6.1-11, respectively. It can be noticed that lead-free solder has the better fatigue resistance than tin-lead solder, while the fatigue property of Sn-Ag-Cu is better than Sn-Cu solder.

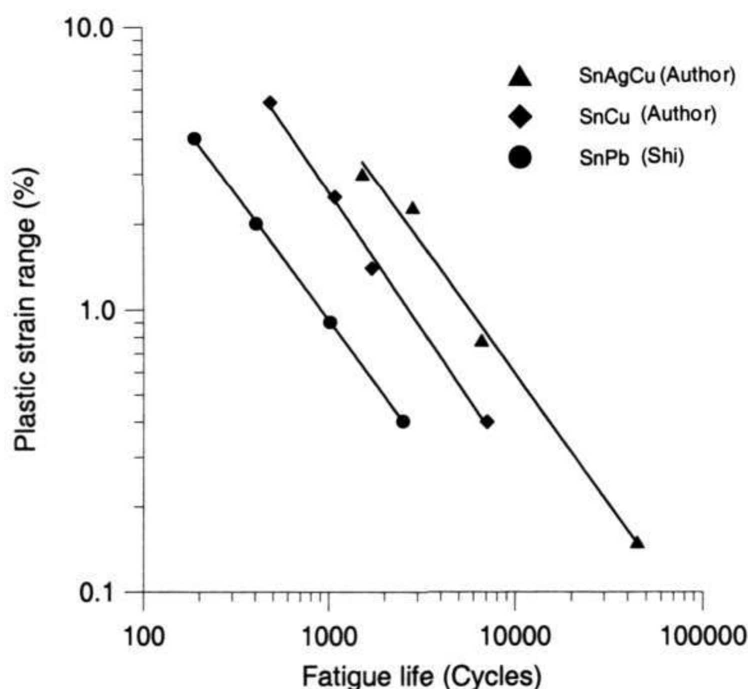

Fig. 6.1-10 Comparison of fatigue resistance at room temperature and 1Hz

ATTENTION: The Singapore Copyright Act applies to the use of this document. Nanyang Technological University Library

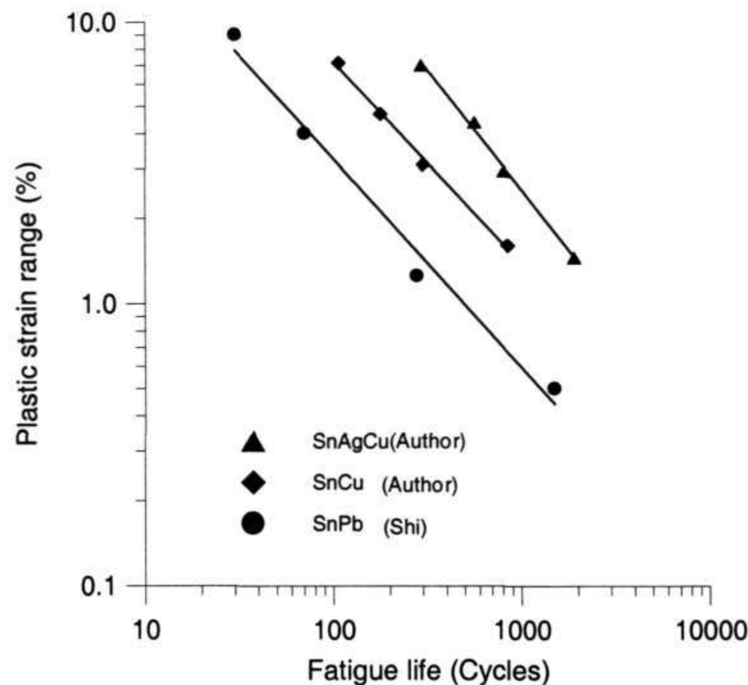

Fig. 6.1-11 Comparison of fatigue resistance at high temperature (125°C) and 10^{-3}Hz

6.1.4.2 Comparison with other lead-free data

Reported studies (Mavoori, 1994 [26]; Kariya, 1998 [28]; Kanchanomai, 2002 [33-35]) have studied that the low cycle fatigue behavior of lead-free and lead-bearing solder alloys. Fig. 6.1-12 shows the fatigue test result at room temperature and 1Hz of different reported data of lead-free and lead-bearing solder alloys. The fatigue failure was defined as 50% reduction of maximum tensile load. From Fig. 6.1-12, it can be noticed that the conventional tin-lead solder has the lowest fatigue life at the same test condition, three types of lead-free solder: 99.3Sn-0.7Cu, 97Sn-3Ag and 95.5Sn-3.8Ag-0.7Cu solder all have better fatigue property than 63Sn-37Pb solder at room temperature and 1Hz. However, for lead-free solder alloys, the fatigue life of 99.3Sn-0.7Cu is lower than the other two lead-free solder alloys,

ATTENTION: The Singapore Copyright Act applies to the use of this document. Nanyang Technological University Library

while 97Sn-3Ag and 95.5Sn-3.8Ag-0.7Cu solder have similar fatigue life [103-104].

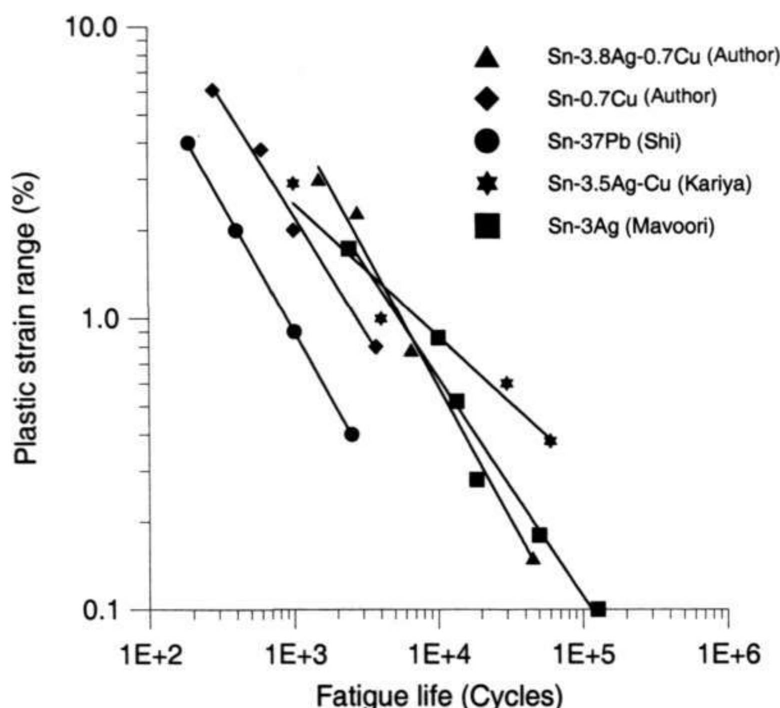

Fig. 6.1-12 Comparison of LCF data for solder alloys at room temperature and 1Hz

Isothermal LCF test data for Sn-Ag, Sn-Ag-Cu lead-free solders at 0.1Hz and room temperature were reported by Kanchanomai et al [33-35]. Their failure criteria were defined at the 25% load drop of the stress amplitude. Comparison with other LCF data by Mavoori, and Kariya, at 1Hz and room temperature, is shown in Fig. 6.1-13. It can be seen that at the same test condition, Sn-Ag and Sn-Ag-Cu have comparable fatigue life. However, the fatigue life data from Kanchanomai [35], at 0.1Hz and with a failure definition of 25% load drop, is lower than the result by Mavoori [26] and Kariya [28] and the author's data. Fatigue ductility exponent (m) and fatigue ductility coefficient (C) in the Coffin-Manson model for these solder alloys at room temperature are summarized in Table 6-1.

ATTENTION: The Singapore Copyright Act applies to the use of this document. Nanyang Technological University Library

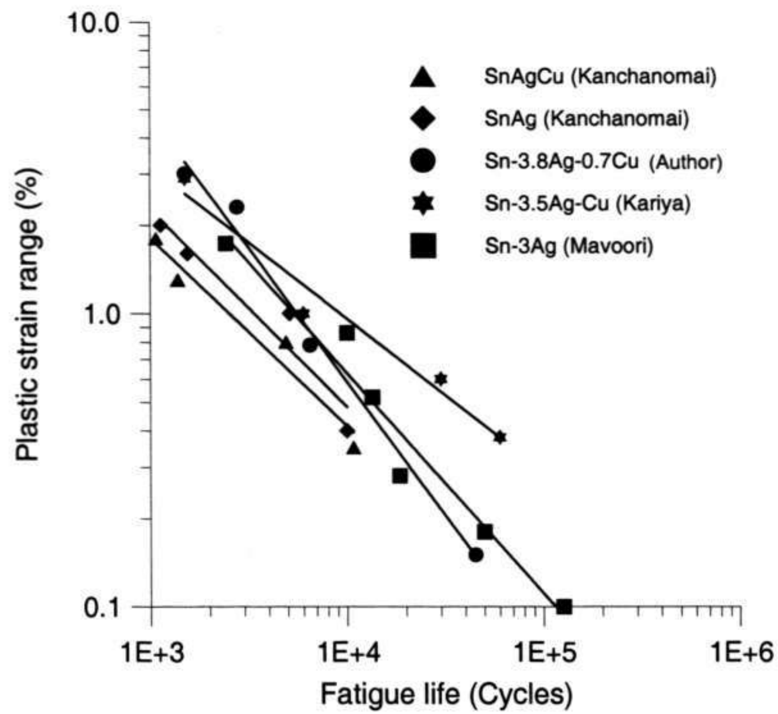

Fig. 6.1-13 Comparison of LCF data for lead-free solders for different fatigue criterions

Table 6-1 Coffin-Manson parameters of lead-free solders at room temperature

	m	C
SnAg [Kanchanomai] (25°C and 0.1Hz)	0.93	21.9
SnAgCu [Kanchanomai] (25°C and 0.1Hz)	0.73	3.7
SnAgCu [Kariya] (25°C and 1Hz)	0.75	6.4
SnAg [Mavoori] (25°C and 1Hz)	0.45	0.57

ATTENTION: The Singapore Copyright Act applies to the use of this document. Nanyang Technological University Library

In recent years, some researchers also conducted the isothermal fatigue tests for real solder joints (Kariya, 2004 [106]; Lau, 2004 [107] ; Lin, 2004 [108]). Kariya et al [106] conducted shear fatigue tests of Sn-1Ag-0.5Cu, Sn-3Ag-0.5Cu and Sn-1.2Ag-0.5Cu-0.05Ni lead-free solder for flip chip interconnections. The coffin-Manson relations for each alloy are,

For Sn-1Ag-0.5Cu: $$\Delta\varepsilon_{in} N_f^{0.62} = 1.4 \tag{6.1.1}$$

For Sn-3Ag-0.5Cu: $$\Delta\varepsilon_{in} N_f^{0.45} = 0.78 \tag{6.1.2}$$

Fro Sn-1.2Ag-0.5Cu-0.05Ni: $$\Delta\varepsilon_{in} N_f^{0.44} = 0.78 \tag{6.1.3}$$

Lin et al [108] also investigated Sn-3.5Ag, Sn-0.7Cu and Sn-3.8Ag-0.7Cu solder for flip chip applications. It was found that the fatigue life is dependent on failure mode. The life is longer when the failure was through the bulk of solder; however, fatigue life will be very short if failure occurred in the interface.

Lau et al [107] studied 95.5Sn-3.9Ag-0.5Cu lead-free solder for a solder-bumped WLCSP, load control was used in isothermal fatigue tests. The relationship between the fatigue life and strain energy density is shown as,

$$N_f = 18.15(\Delta W)^{-1.96} \tag{6.1.4}$$

Fig. 6.1-14 shows the strain control fatigue behavior comparison of author's bulk specimen and other solder joint specimens (Kariya, 2004 [106]; Lin, 2004 [108]). It was found that author's bulk data has fairy good comparison with other solder joints data from real packaging assembly.

ATTENTION: The Singapore Copyright Act applies to the use of this document. Nanyang Technological University Library

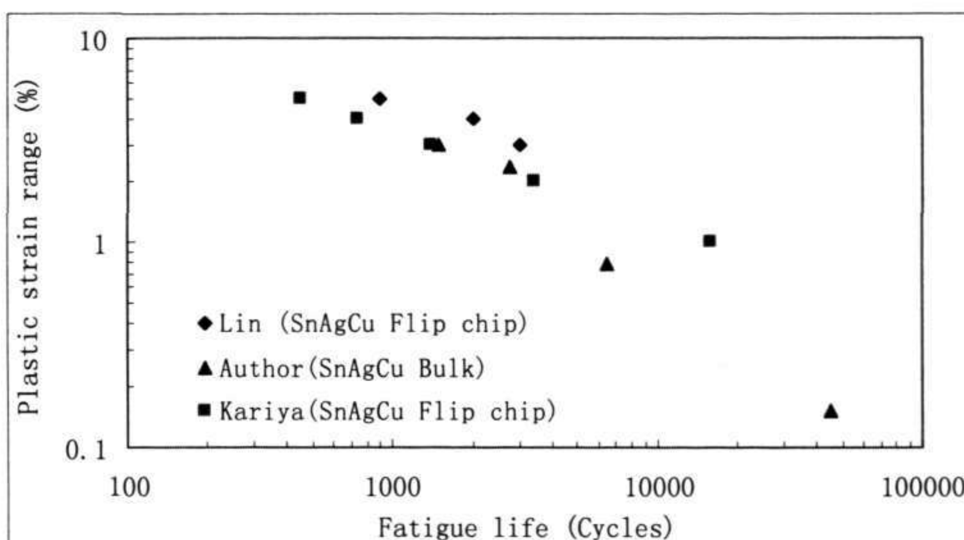

Fig. 6.1-14 Fatigue behavior comparison of bulk solder and solder joint

6.2 Low cycle fatigue models

The Coffin-Manson model [38-39] has been widely used to relate low cycle fatigue life (N_f) of metallic materials with the plastic strain range ($\Delta\varepsilon_p$), as shown below:

$$N_f^m \Delta\varepsilon_p = C \tag{6.2.1}$$

where m and C are material constants.

The Morrow's energy-based model [105] was also used to predict low cycle fatigue lives. The model predicts fatigue life in terms of inelastic strain energy density (W_p), given below:

$$N_f^n W_p = A \tag{6.2.2}$$

where n is fatigue exponent, and A is material ductility coefficient. The inelastic strain energy density was determined from the area surrounded by a stable hysteresis loop.

Based on the low cycle fatigue test result at different temperatures and frequencies,

ATTENTION: The Singapore Copyright Act applies to the use of this document. Nanyang Technological University Library

the m, C, n and A at different conditions can be determined for 95.5Sn-3.8Ag-0.7Cu and 99.3Sn-0.7Cu lead-free solders. The results are summarized in Table 6.2-1 and 6.2-2.

Table 6.2-1(a) m and C for Coffin-Manson model of Sn-3.8Ag-0.7Cu

	m			C		
	25°C	75°C	125°C	25°C	75°C	125°C
1Hz	0.913	0.896	0.889	26.3	19.8	16.0
0.01Hz	0.904	0.889	0.871	20.7	16.0	12.1
0.001Hz	0.891	0.876	0.853	13.9	11.5	9.2

Table 6.2-1(b) n and A for Morrow's model of Sn-3.8Ag-0.7Cu

	n			A		
	25°C	75°C	125°C	25°C	75°C	125°C
1Hz	1.103	1.079	0.953	14865	6208.3	1492.8
0.01Hz	0.973	0.944	0.926	1426.2	1144.3	578.9
0.001Hz	0.935	0.914	0.897	1144.4	666.9	311.7

ATTENTION: The Singapore Copyright Act applies to the use of this document. Nanyang Technological University Library

Table 6.2-2(a) m and C for Coffin-Manson model of Sn-0.7Cu

	m			C		
	25°C	75°C	125°C	25°C	75°C	125°C
1Hz	0.9734	0.9227	0.9022	21.27	12.51	9.98
0.01Hz	0.8067	0.7938	0.7825	5.89	4.46	3.33
0.001Hz	–	–	0.7192	–	–	1.98

Table 6.2-2(b) n and A for Morrow's model of Sn-0.7Cu

	n			A		
	25°C	75°C	125°C	25°C	75°C	125°C
1Hz	1.2157	1.1406	1.1064	9542.9	2864.8	1387.8
0.01Hz	1.1396	1.0084	0.8379	1524.8	559.46	143.71
0.001Hz	–	–	0.7328	–	–	38.64

To model frequency dependent low cycle fatigue behavior of Sn-3.8Ag-0.7Cu and Sn-0.7Cu lead-free solders, the frequency-modified Coffin-Manson relationship [51] can be introduced to describe the low cycle fatigue behavior of Sn-0.7Cu solder, given below.

$$\left[N_f \nu^{(k-1)}\right]^m \Delta\varepsilon_p = C \tag{6.2.3}$$

ATTENTION: The Singapore Copyright Act applies to the use of this document. Nanyang Technological University Library

where ν is frequency, k, is frequency exponent. Based on the fatigue test results at different frequencies at 125°C, the frequency exponent, k, can be determined to be 0.95 and 0.91 for Sn-3.8Ag-0.7Cu and Sn-0.7Cu solder, respectively. Then the frequency modified fatigue life $N_f \nu^{(k-1)}$ can be calculated. When the plastic strain was plotted against the frequency-modified fatigue life, all the fatigue life data obtained at different frequencies were found to fit well into a single line, as shown in Fig. 6.2-1 and 6.2-2. This means that the frequency-modified Coffin-Manson model can be used to model the effect of frequency for the low cycle fatigue behavior of Sn-3.8Ag-0.7Cu and Sn-0.7Cu solder.

Similarly, the frequency-modified Morrow model can be used to model the frequency effect, as given below:

$$\left[N_f \nu^{(h-1)}\right]^n W_p = A \qquad (6.2.4)$$

where ν is the frequency, h is frequency exponent. Based on fatigue test of Sn-3.8Ag-0.7Cu and Sn-0.7Cu solder at different frequencies, the frequency exponent, h, can be determined to be 0.82 and 0.762, respectively. Figures 6.2-3 and 6.2-4 show the inelastic strain energy density plotted against the frequency-modified fatigue life at 125°C. It can be seen that all fatigue life data at different frequencies falls on a single line. Hence, the frequency-modified Morrow model can be used to model the effect of frequency for the low cycle fatigue behavior of lead-free Sn-3.8Ag-07Cu and Sn-0.7Cu solder.

ATTENTION: The Singapore Copyright Act applies to the use of this document. Nanyang Technological University Library

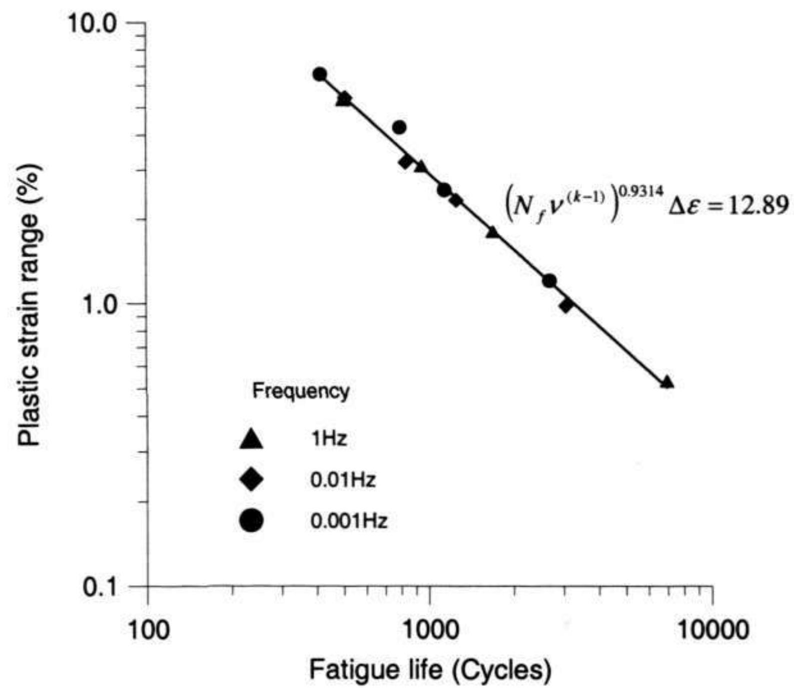

Fig. 6.2-1 Plastic strain versus frequency-modified fatigue life at 125°C for Sn-Ag-Cu (k=0.95)

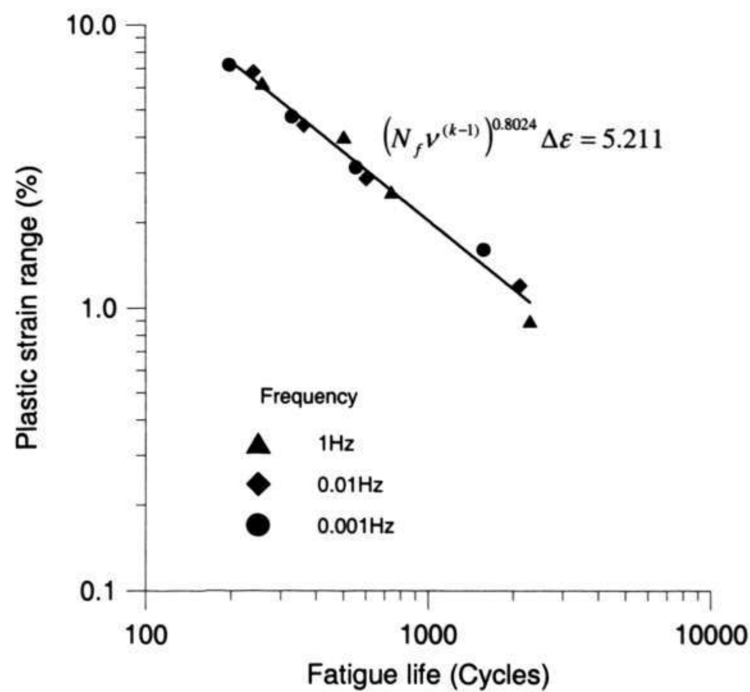

Fig. 6.2-2 Plastic strain versus frequency-modified fatigue life at 125°C for Sn-Cu (k=0.91)

ATTENTION: The Singapore Copyright Act applies to the use of this document. Nanyang Technological University Library

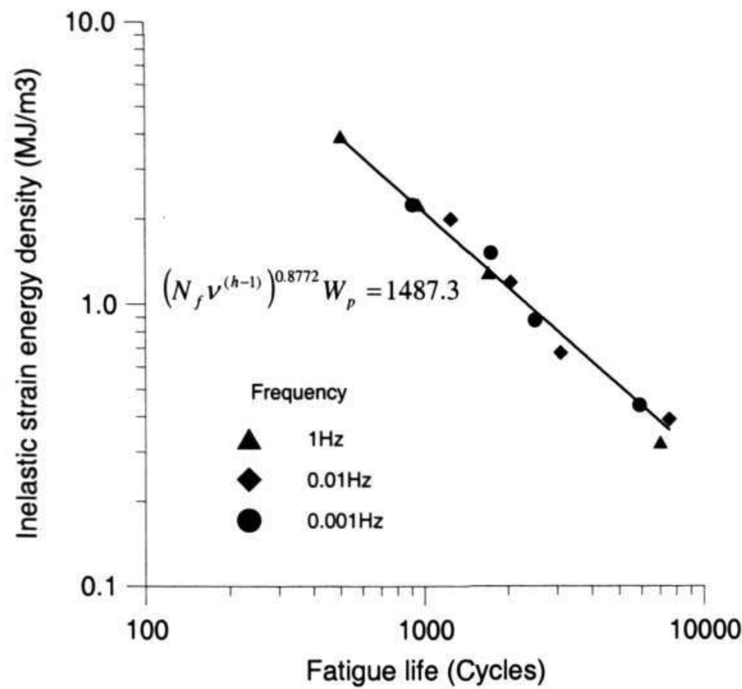

6.2-3 Inelastic strain energy density versus frequency-modified fatigue life at 125°C for Sn-Ag-Cu (h=0.82)

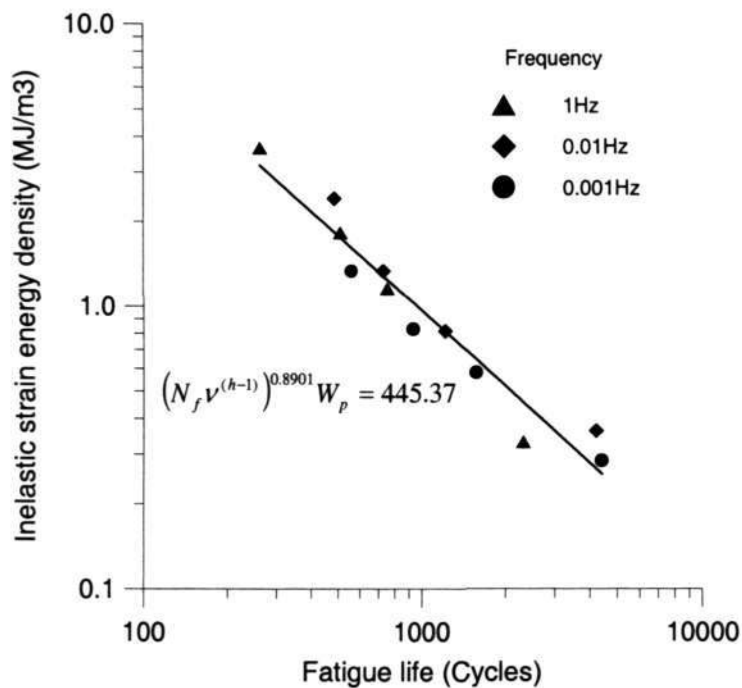

Fig. 6.2-4 Inelastic strain energy density versus frequency-modified fatigue life at 125°C for Sn-Cu (h=0.762)

ATTENTION: The Singapore Copyright Act applies to the use of this document. Nanyang Technological University Library

Chapter 7. Research on New Visco-plastic Model, Fatigue Model and Impact Yield Stress for 95.5Sn-3.8Ag-0.7Cu Solder

This chapter reports on new developments in (i) A visco-plastic constitutive model, which deals with the hardening-softening behavior; (ii) A fatigue model based on a damage parameter (load drop rate, $\frac{d\Phi}{dN}$), which compensates for temperature and frequency effects; (iii) Yield stress equation combining impact and tensile test results, covering a wide range of strain rate from 10^{-4} to 10^{3} s^{-1}.

7.1 New visco-plastic model for 95.5Sn-3.8Ag-0.7Cu solder

A new visco-plastic constitutive model has been developed in this study, and applied to predict the visco-plastic behavior of Sn-3.8Ag-0.7Cu lead-free solder. This model can deal with both hardening and softening effect.

7.1.1 Model Formulation

Based on the theory of plasticity [109-110], under isothermal, constant strain rate condition, for fully developed flows where $\dot{\varepsilon} \approx \dot{\varepsilon}_p$, the expression of incremental plastic flow hardening (or softening) form can be expressed as,

$$\frac{d\sigma}{d\varepsilon} = H \tag{7.1.1}$$

ATTENTION: The Singapore Copyright Act applies to the use of this document. Nanyang Technological University Library

where H consists all the physical mechanisms that affect the hardening (or softening) of the plastic flow, such as strain hardening, dynamic recovery, static recovery and internal damage, etc. However, for solder materials, the most two important mechanisms are dynamic recovery and strain hardening [12-13], then Eq. (7.1.1) can be represented as,

$$\frac{d\sigma}{d\varepsilon} = H(\sigma_{dr}, \varepsilon) \tag{7.1.2}$$

where σ_{dr} is an internal variable, with dimension of stress to represent the dynamic recovery stress; and ε is the effect of strain hardening.

Though the strain hardening and dynamic recovery can be modeled by a combined dynamic hardening term, it will be more appropriate to study the visco-plastic behavior of solder material if these two effects can be studied separately. Then the hardening formulation in this model can be expressed as,

$$\frac{d\left(\frac{\sigma}{\sigma_{dr}}\right)}{d\varepsilon} = h(\varepsilon) \tag{7.1.3}$$

In Eq. (7.1.3), $h(\varepsilon)$ was associated with strain hardening only, because the dynamic recovery effect in former function H has been described by σ_{dr} and moved to the left side of the formula. It is also interesting to find that, σ_{dr} has the dimension of stress, and then $\frac{\sigma}{\sigma_{dr}}$ is dimensionless. It is reasonable to consider h as the function of ε, which is also dimensionless, at the right of the expression.

ATTENTION: The Singapore Copyright Act applies to the use of this document. Nanyang Technological University Library

7.1.1.1 Evaluation of dynamic recovery stress σ_{dr}

Dynamic recovery can be viewed as creep occurring at the high strain rates. The true stress-strain behavior of a material experiencing only dynamic recovery is illustrated in Fig. 7.1-1. It can be seen that the overall level of the flow stress curve increases with increase in strain rate and decrease with increase in temperature. The stress increases with further strain, eventually obtaining a steady-state value (σ_{ss}). During the transient period, a steady-state microstructure is developing in much the same way it does during steady-state creep [111]. This means the flow stress equation can be used to describe the saturation stress, σ_{ss}. The flow stress equation can be expressed from the steady state creep strain rate expression,

$$\dot{\varepsilon} = Ae^{-Q/RT}[\sinh(\frac{\sigma}{B})]^{1/m} \tag{7.1.4}$$

The static stress is taken as the saturation stress, σ_{ss}, which is the function of strain rate and absolute temperature,

$$\sigma_{ss} = B\sinh^{-1}[(\frac{\dot{\varepsilon}}{A}e^{Q/RT})^{m}] \tag{7.1.5}$$

The dynamics recovery stress is assumed to be equal to the saturation stress,

$$\sigma_{dr} = \sigma_{ss} = B\sinh^{-1}[(\frac{\dot{\varepsilon}}{A}e^{Q/RT})^{m}] \tag{7.1.6}$$

where A, B are material constants, Q is activation energy, m is creep exponent.

ATTENTION: The Singapore Copyright Act applies to the use of this document. Nanyang Technological University Library

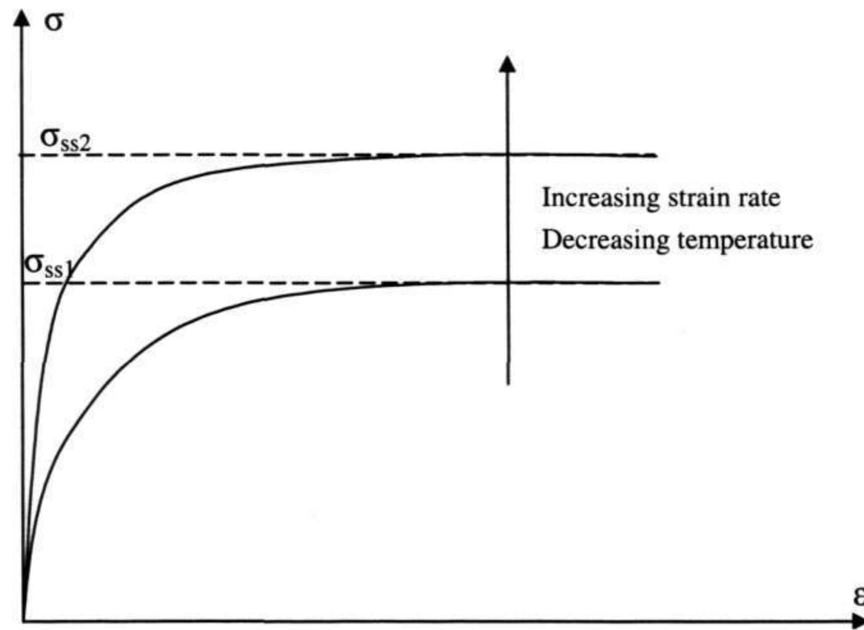

Fig.7.1-1 Schematic of the stress-strain behavior under dynamic recovery

7.1.1.2 Evaluation of hardening-softening parameter σ_{h-s}

In section 7.1.1.1, the dynamic recovery stress, σ_{dr}, was assumed to be equal to the creep constant stress or saturation stress, σ_{ss}. It is true only if the ultimate tensile strength (UTS) is not reached and no softening behavior is noted. That means the constitutive model only can predict the small strain part of the stress-strain curves. As we know, though the stress will increase with strain in hardening part, it will reach its maximum limit at ultimate tensile strength (UTS). After that, the stress-strain behavior goes into the softening part as it curves downwards. In order to represent the complete hardening-softening behavior, the dynamic recovery stress, σ_{dr} should be extended to model both hardening and softening effects, denoted by the parameter, σ_{h-s}, and expressed as,

ATTENTION: The Singapore Copyright Act applies to the use of this document. Nanyang Technological University Library

$$\sigma_{h-s} = \sigma_{h-s}(\sigma_{ss}, \varepsilon) \tag{7.1.7}$$

Eq. (7.1.7) shows that the hardening-softening parameter is not only dependent on saturation stress, but the strain as well. The formation of $\sigma_{h-s}(\sigma_{ss}, \varepsilon)$ which is adopted to represent the hardening-softening behavior is,

$$\sigma_{h-s} = \sigma_{ss} - \sigma_{ss} \frac{|\varepsilon - b|}{\varepsilon + c} \tag{7.1.8}$$

In physical terms, the hardening-softening parameter σ_{h-s} denotes the maximum stress the material can bear at a given strain rate, temperature and strain. In the hardening part, it will increase with strain and go to the maximum value till $\varepsilon = b$. When $\varepsilon > b$, it goes into the softening part, σ_{h-s} will decrease with strain.

7.1.1.3 Evaluation of strain hardening function $h(\varepsilon)$

The increase in the stress because of previous deformation is known as strain hardening, or work hardening. A power law relationship was used to describe the strain hardening, as shown in Eq. (7.1.9),

$$\sigma = K\varepsilon^n \tag{7.1.9}$$

where n is the strain-hardening exponent and K is the strength coefficient. While in this study, a new relationship that considers the initial strain is proposed. The form of $h(\varepsilon)$ which is adopted to represent the strain hardening behavior with the initial strain effect is,

ATTENTION: The Singapore Copyright Act applies to the use of this document. Nanyang Technological University Library

$$h(\varepsilon)=\frac{a}{(a+\varepsilon-\varepsilon_i)^2} \tag{7.1.10}$$

where a is the strain hardening parameter, ε_i is the initial strain, which describe the strain history of the material.

7.1.1.4. Summary of model formulation

Combining Eqs. (7.1.3), (7.1.6), (7.1.8) and (7.1.10), the new model can be summarized as:

Hardening-softening equation:

$$\frac{d\left(\dfrac{\sigma}{\sigma_{h-s}}\right)}{d\varepsilon}=\frac{a}{(a+\varepsilon-\varepsilon_i)^2} \tag{7.1.11}$$

Hardening-softening parameter:

$$\sigma_{h-s}=\sigma_{ss}-\sigma_{ss}\frac{|\varepsilon-b|}{\varepsilon+c} \tag{7.1.12}$$

where $\sigma_{dr}=\sigma_{ss}=B\sinh^{-1}[(\frac{\dot{\varepsilon}}{A}e^{Q/RT})^m]$

Integrated form of Eq. (7.1.11) is:

$$\sigma=\sigma_{ss}\left(1-\frac{|\varepsilon-b|}{\varepsilon+c}\right)\frac{\varepsilon-\varepsilon_i}{a+\varepsilon-\varepsilon_i} \tag{7.1.13}$$

where ε_i is the initial strain at the point $\sigma=0$.

If only hardening effect was considered, Eq. (7.1.13) can be simplified to the form as,

$$\sigma=\sigma_{dr}\frac{\varepsilon-\varepsilon_i}{a+\varepsilon-\varepsilon_i} \tag{7.1.14}$$

ATTENTION: The Singapore Copyright Act applies to the use of this document. Nanyang Technological University Library

7.1.2 Parameter determination

There are four parameters involved in formulation of saturation stress and three parameters involved in strain-stress formulation. Therefore, there are seven material parameters, *A*, *B*, *Q/R*, *m*, a, b and c to be determined for this model.

Stress-strain curves can be built from tensile test data with zero initialized stress state. However, if only tensile data is used for curve fitting, loading-unloading behavior could not be represented by the model. Therefore, some load-unload-reload test results were used to show the stress-strain behavior where initial strain need not be zero($\varepsilon_i \neq 0$). The normal step to determine the seven parameters of this model is as follows,

1) Determination of saturation stress from steady state creep relation.

2) Nonlinear curve fitting of *A*, *B*, *Q/R*, *m* in Eq. 7.1.6.

3) Nonlinear curve fitting of *a, b* and *c* in Eq. 7.1.13. At least one non-zero initialized strain curve must be used. In step 3), parameters determined in step 1) will be used. Similarly, if only hardening effect was considered, parameter *a* can be fitted from nonlinear fitting of Eq. 7.1.14.

Based on the test result of Sn-3.8Ag-0.7Cu, seven material constants for hardening-softening model and five material constants for hardening model were determined, shown in Table 7.1-1.

Table 7.1-1: Material constants for Sn-3.8Ag-0.7Cu

	A	*Q/R*	*B*	*m*	*a*	*b*	*c*
Hardening-softening	18.59	5645	13.1	0.3	a1	7.4×10^{-3}	0.778
Hardening	18.59	5645	13.1	0.3	a2	-	-

ATTENTION: The Singapore Copyright Act applies to the use of this document. Nanyang Technological University Library

The comparison of model prediction and the raw data for Sn-3.8Ag-0.7Cu is shown in Fig. 7.1-2 and 7.1-3. Fig. 7.1-2 shows the results of simple tensile tests, while Fig. 7.1-3 shows load-unload test results. The separated points in the figures express the experimental results obtained in this study; the solid lines in the figures denote the calculated stress-strain curves with the values obtained in curve-fitting. From Fig. 7.1-2, it is recognized that calculated results show fairly good agreement with experimental results in both hardening and softening parts; however, from Fig. 7.1-3, it can be seen that new developed model can predict not only the simple tensile stress-strain curves, but also the load-unload curves.

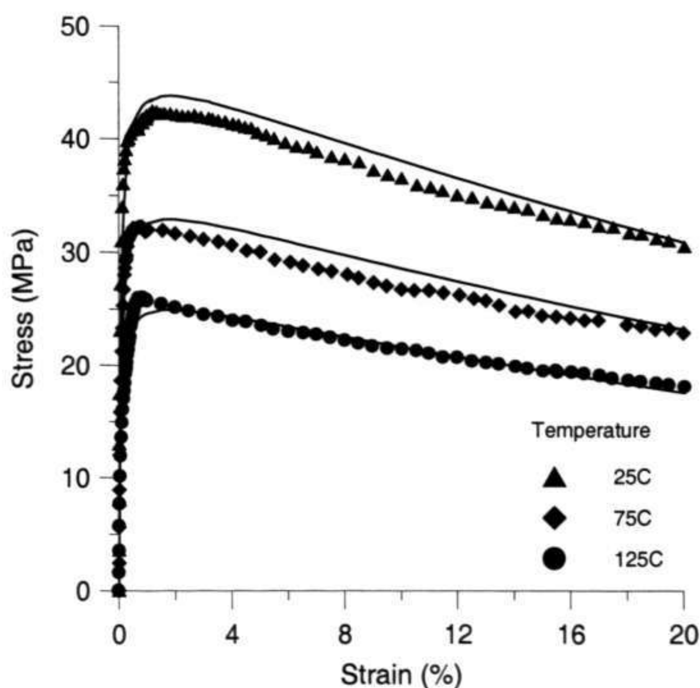

Fig. 7.1-2(a) Hardening-softening stress-strain behavior at strain rate of 5.6×10^{-4} s^{-1}

ATTENTION: The Singapore Copyright Act applies to the use of this document. Nanyang Technological University Library

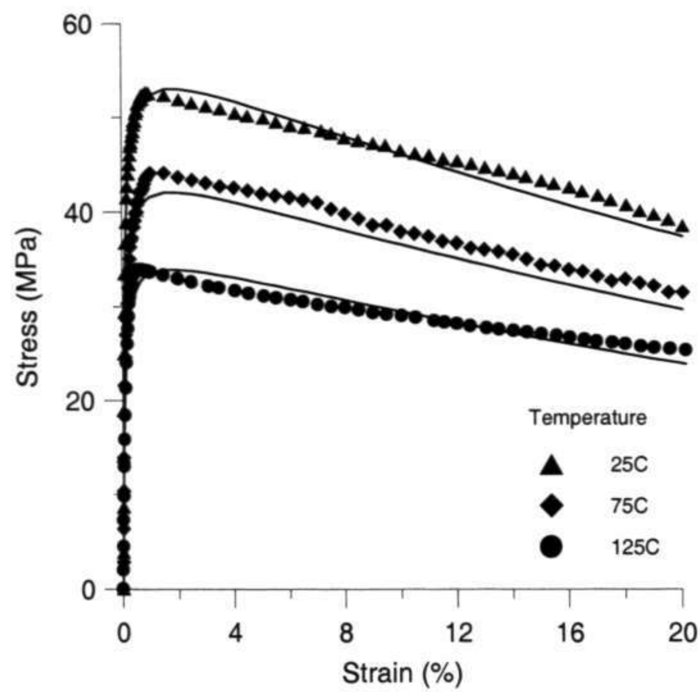

Fig. 7.1-2(b) Hardening-softening stress-strain behavior at strain rate of 5.6×10^{-3} s^{-1}

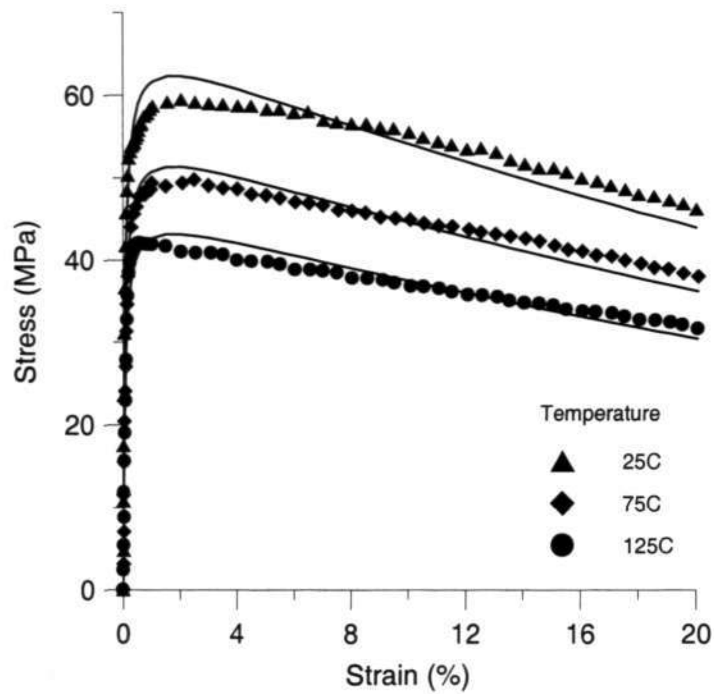

Fig. 7.1-2(c) Hardening-softening stress-strain behavior at strain rate of 5.6×10^{-2} s^{-1}

ATTENTION: The Singapore Copyright Act applies to the use of this document. Nanyang Technological University Library

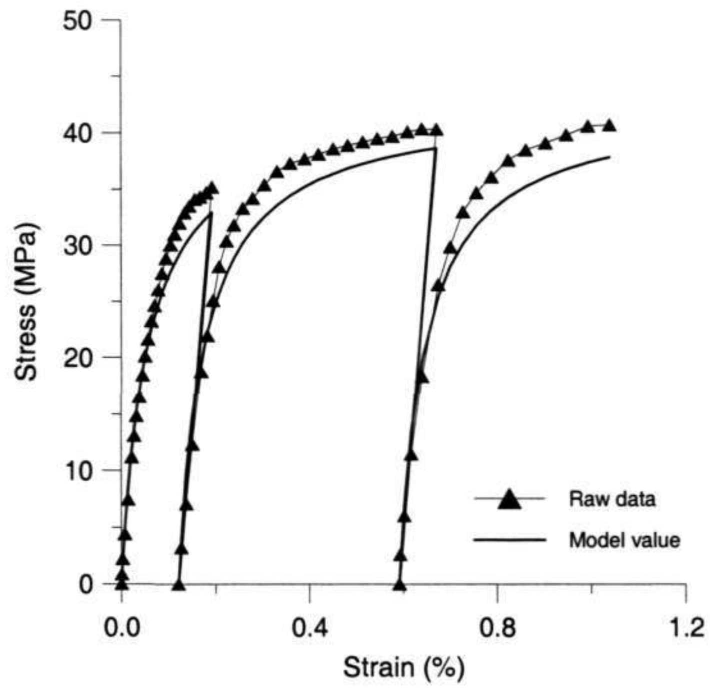

Fig. 7.1-3(a) Load-unload test at 25°C and 5.6×10^{-4} s^{-1}

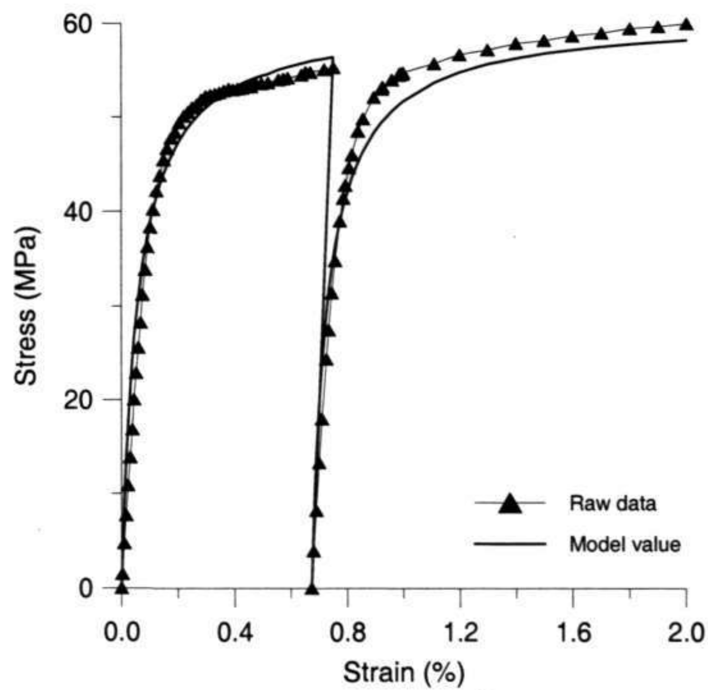

Fig. 7.1-3(b) Load-unload test at 25°C and 5.6×10^{-2} s^{-1}

ATTENTION: The Singapore Copyright Act applies to the use of this document. Nanyang Technological University Library

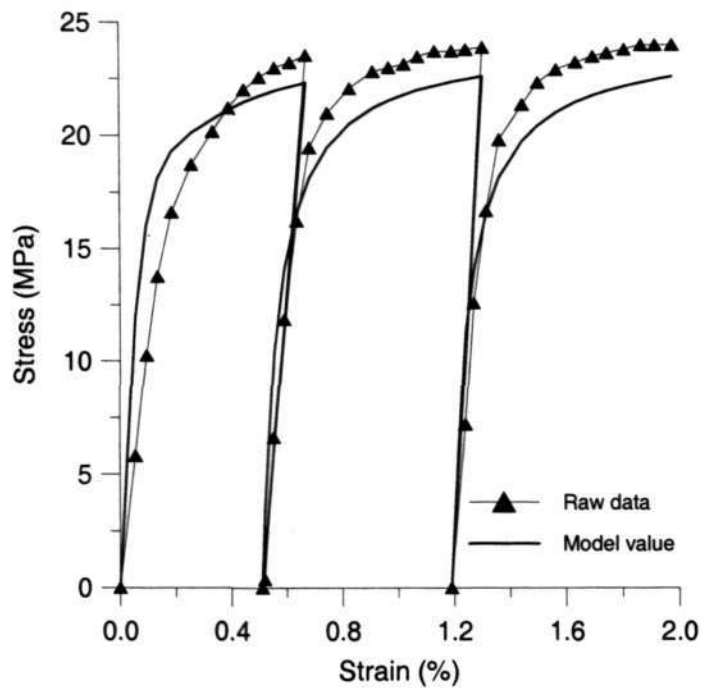

Fig. 7.1-3(c) Load-unload test at 125°C and 5.6×10^{-4} s^{-1}

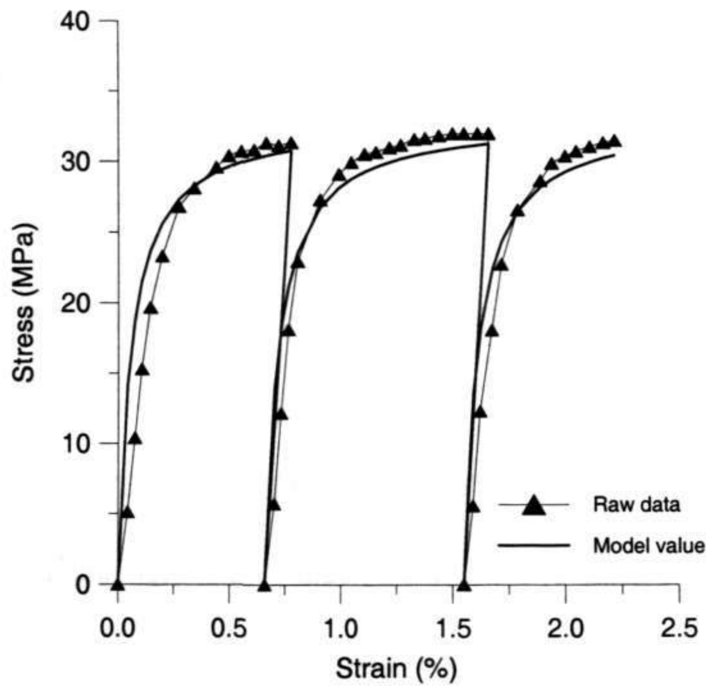

Fig. 7.1-3(d) Load-unload test at 125°C and 5.6×10^{-3} s^{-1}

ATTENTION: The Singapore Copyright Act applies to the use of this document. Nanyang Technological University Library

7.2 New load drop rate fatigue model for 95.5Sn-3.8Ag-0.7Cu solder

From Chapter 6, it was found that the fatigue exponent m (or n) and ductility coefficient C (or A) are dependent on temperature and frequency in the traditional Coffin-Manson or Morrow fatigue models. Although the frequency modified model solves the frequency dependent effect, it is still difficult to characterize the temperature and frequency dependent low cycle fatigue behavior of solder alloys in the thermal-mechanical loading conditions. Furthermore, the plastic strain range or inelastic strain energy density used in Coffin-Manson or Morrow's model is based on an approximated "stable" hysteresis loop. However, from Fig. 6.1-2 and 6.1-3, it is noted that there is no "stable" hysteresis loop during the fatigue test of Pb-free solder alloys. The cyclic properties will change during the fatigue period, it may not be reasonable to use the initial cyclic properties to characterize the long-term fatigue life. In this study, a new fatigue model based on load drop rate was developed to characterize the low cycle fatigue behavior of Sn-3.8Ag-0.7Cu lead-free solder alloy.

7.2.1 Strain range, temperature and frequency dependent load drop rate

During the fatigue test, the amplitude of the stress will decrease as shown in Fig. 7.2-1. It was observed that the total fatigue life could be divided into three stages based on the change of the load drop rate. At the beginning of the fatigue test, stress amplitude reduces rapidly, which may be due to cyclic softening and crack initiation process. After crack initiation, stable cracks propagation will increase with fatigue cycles. This propagation mechanism causes a linear reduction of the stress amplitude,

ATTENTION: The Singapore Copyright Act applies to the use of this document. Nanyang Technological University Library

defined as the second stage of the fatigue failure process. Thirdly, final failure occurs as the load drop rate increases rapidly leading to fatigue fracture. In Fig. 7.2-1, it can be noted that the second stage is the dominated stage during the fatigue life. It was also found that the load drop rate at this stage depends on total strain range, temperature and frequency as shown in Figs. 7.2-2 to 7.2-4. For example, Fig. 7.2-2 shows the Sn-3.8Ag-0.7Cu solder results tested at 25°C and 0.01Hz for different strain ranges (from 2%-7.5%).

The load drop rate at the second stage is defined as $\frac{d\Phi}{dN}$, where $\Phi = \sigma / \sigma_0$, σ_0 is the peak stress at the beginning of the 2nd stage of the fatigue process (See Fig. 7.2-1).

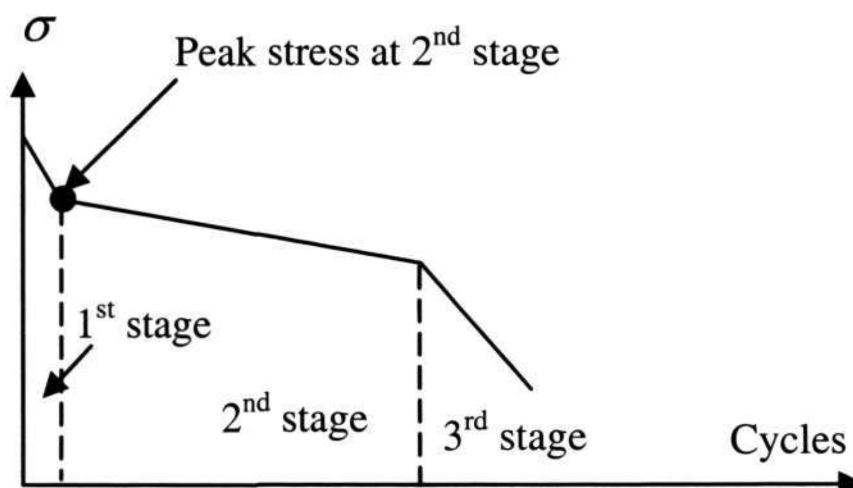

Fig. 7.2-1 Definition of load drop rate

ATTENTION: The Singapore Copyright Act applies to the use of this document. Nanyang Technological University Library

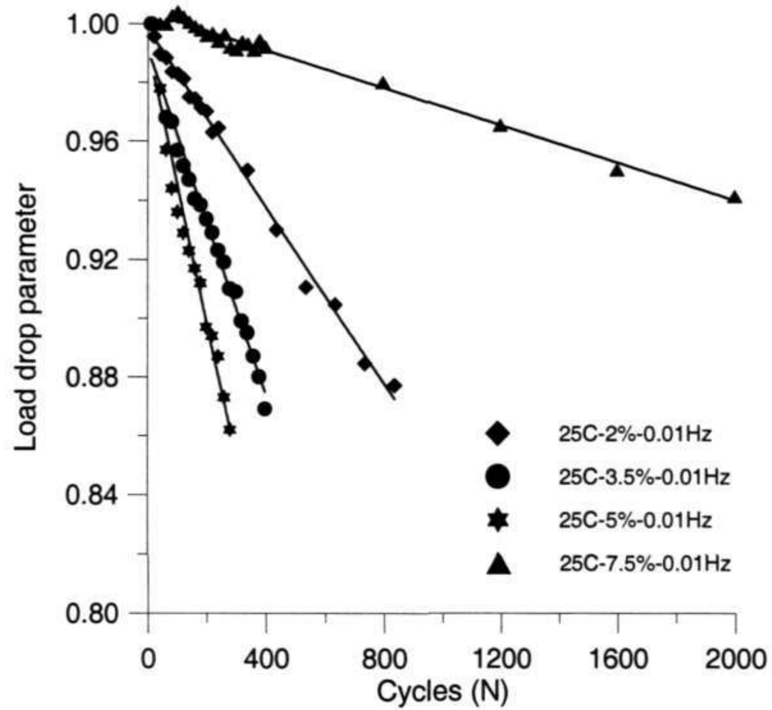

Fig. 7.2-2 Effect of total strain range on load drop rate

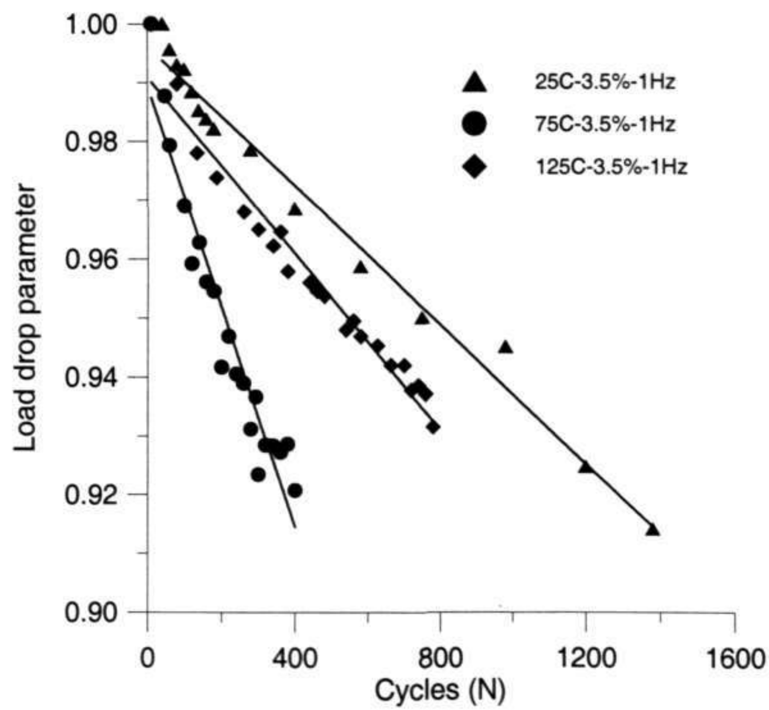

Fig. 7.2-3 Effect of temperature on load drop rate

ATTENTION: The Singapore Copyright Act applies to the use of this document. Nanyang Technological University Library

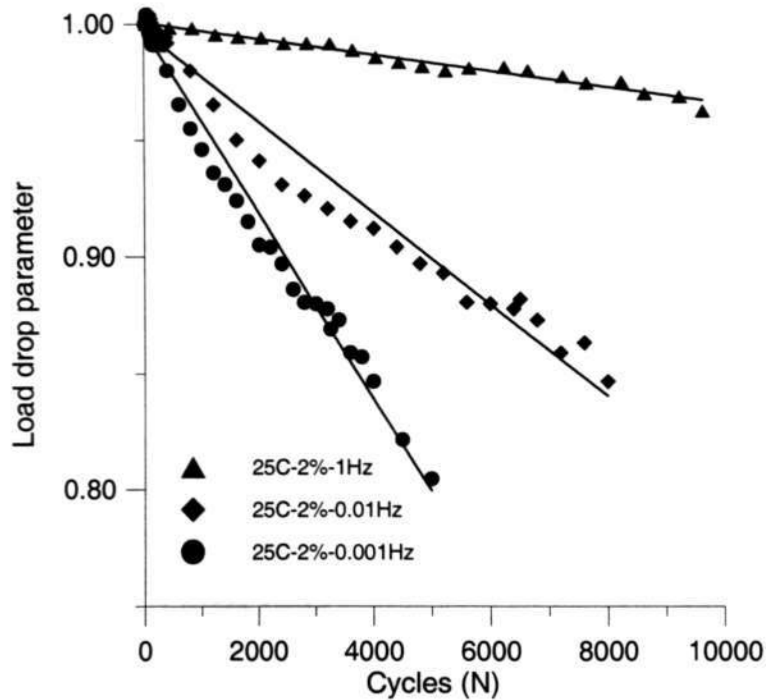

Fig. 7.2-4 Effect of frequency on load drop rate

By plotting the load drop rate $\frac{d\Phi}{dN}$ with the strain range, temperature and frequency, it was found that the load drop rate at the second stage has a power law relationship with total strain range, a linear relationship with temperature and logarithmic relationship with frequency, as seen in Figs. 7.2-5 to 7.2-7.

ATTENTION: The Singapore Copyright Act applies to the use of this document. Nanyang Technological University Library

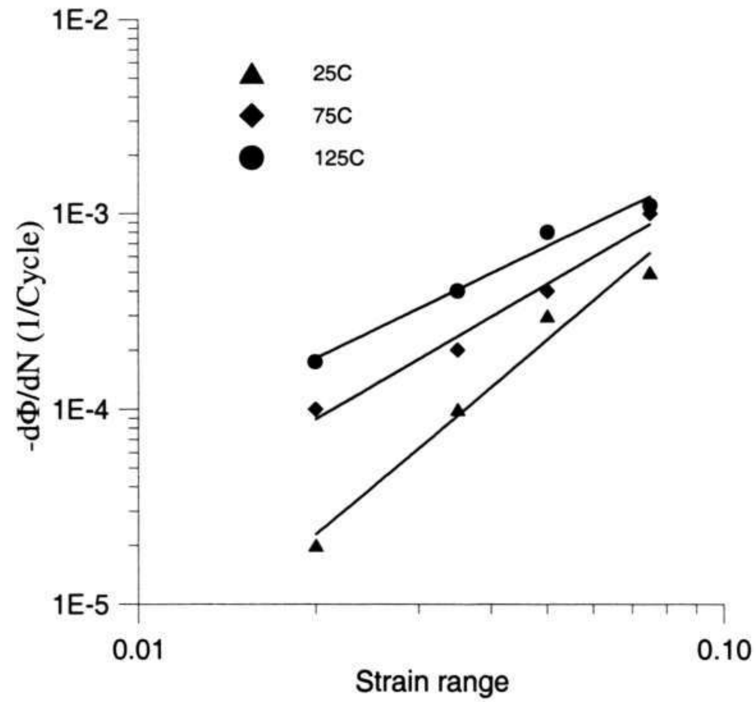

Fig. 7.2-5 Power law relationship of total strain range and load drop rate at 0.01Hz

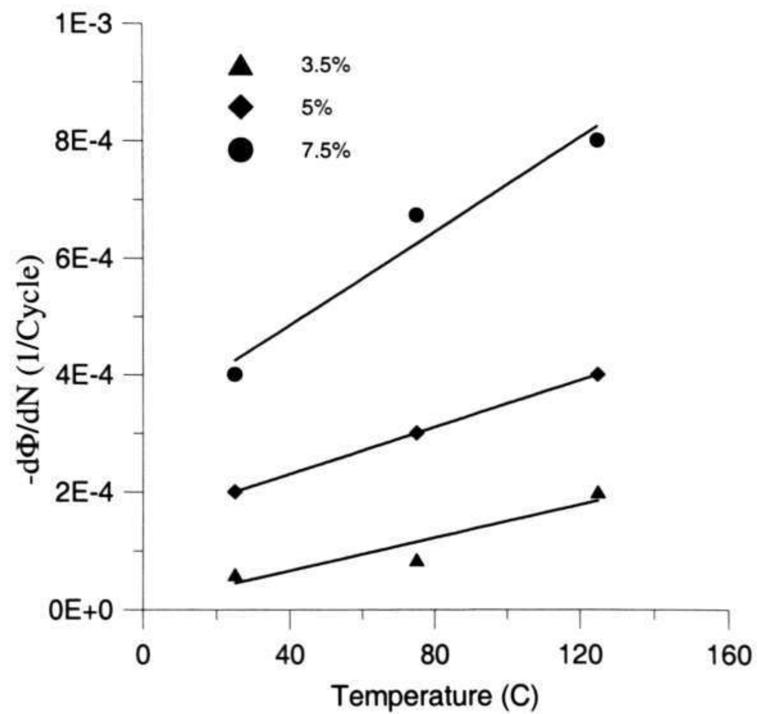

Fig. 7.2-6 Linear relationship of temperature and load drop rate at 1Hz

ATTENTION: The Singapore Copyright Act applies to the use of this document. Nanyang Technological University Library

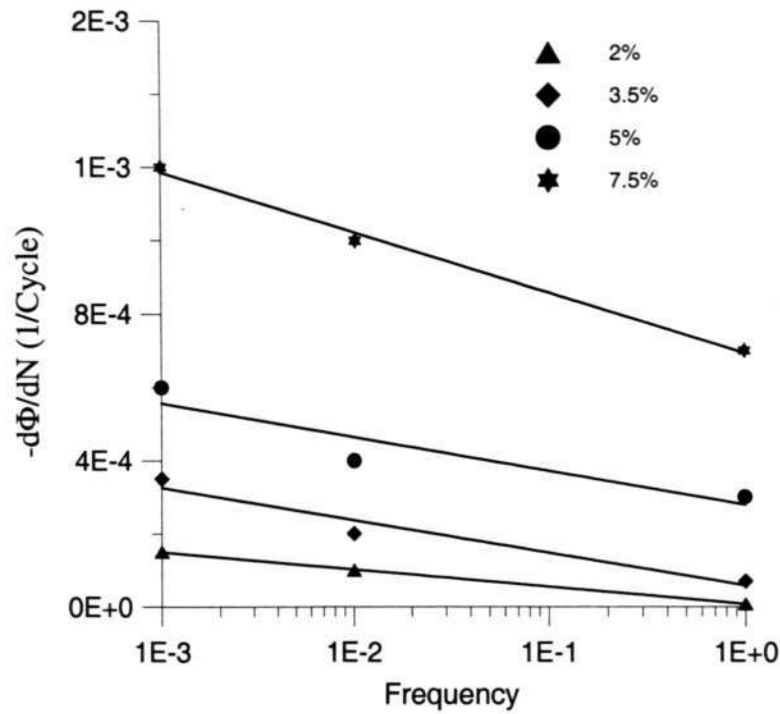

Fig. 7.2-7 Logarithmic relationship of frequency and load drop rate at 75°C

7.2.2 Load drop rate damage model

From the damage mechanics point of view, load drop is due to accumulated damage in the material during the fatigue test duration. The total damage consists of two major parts, fatigue damage and creep damage. The time-dependent creep-fatigue damage model [112-113] can expressed as,

$$\dot{D}_{total} = D_f |\dot{\sigma}| + \dot{D}_c \tag{7.2.1}$$

For fatigue damage, D_f, can be written as

$$D_f = C_f |\sigma|^{m_f} (1 - D)^{-k} \tag{7.2.2}$$

where $D = 1 - \Phi$, C_f and m_f are material constants.

ATTENTION: The Singapore Copyright Act applies to the use of this document. Nanyang Technological University Library

For creep damage rate, $\dot{D}_c$, can be written as

$$\dot{D}_c = C_c|\sigma|^{m_c}(1-D)^{-k} \tag{7.2.3}$$

where C_c and m_c are material constants.

So Eq. (7.2.1) can be rewritten as

$$\dot{D}_{total} = \left(C_f|\sigma|^{m_f}|\dot{\sigma}| + C_c|\sigma|^{m_c}\right)(1-D)^{-k} \tag{7.2.4}$$

where $\dot{D}_{total}$ is the total damage rate.

While the stress-strain relation during the low cycle fatigue test can be assumed as

$$\sigma = (aT+b)\dot{\varepsilon}^{n_1}(\Delta\varepsilon)^{n_2} \tag{7.2.5}$$

where a, b, n_1 and n_2 are material constants, T is temperature in °C, $\dot{\varepsilon}$ is strain rate, $\Delta\varepsilon$ is the strain range.

Integrating Eq. (7.2.4) with respect to time t, for simplification, let k=0,

$$\oint_{cycle} dD_{total} = \oint_{cycle} C_f|\sigma|^{m_f} d|\sigma| + \oint_{cycle} C_c|\sigma|^{m_c} dt \tag{7.2.6}$$

$$\oint_{cycle} C_f|\sigma|^{m_f} d|\sigma| = \frac{4C_f(aT+b)^{m_f+1}}{m_f+1}\dot{\varepsilon}^{n_1(m_f+1)}(\Delta\varepsilon)^{n_2(m_f+1)} \tag{7.2.7}$$

$$\begin{aligned}\oint_{cycle} C_c|\sigma|^{m_c} dt &= 2C_c\int_0^{\frac{\Delta\varepsilon}{\dot{\varepsilon}}}(aT+b)^{m_c}\left[\dot{\varepsilon}^{n_1}(\Delta\varepsilon_{current})^{n_2}\right]^{m_c} dt \\ &= 2C_c(aT+b)^{m_c}\dot{\varepsilon}^{n_1 m_c}\int_0^{\frac{\Delta\varepsilon}{\dot{\varepsilon}}}(\dot{\varepsilon}t)^{n_2 m_c} dt \\ &= \frac{2C_c(aT+b)^{m_c}}{n_2 m_c+1}\dot{\varepsilon}^{n_1 m_c-1}(\Delta\varepsilon)^{n_2 m_c+1}\end{aligned} \tag{7.2.8}$$

ATTENTION: The Singapore Copyright Act applies to the use of this document. Nanyang Technological University Library

$$\oint_{cycle} dD_{total} = \frac{\Delta D_{total}}{\Delta N} \tag{7.2.9}$$

So Eq. (7.2.6) can be rewritten as

$$\begin{aligned}\frac{\Delta D_{total}}{\Delta N} = & \frac{4C_f (aT+b)^{m_f+1}}{m_f+1} \dot{\varepsilon}^{n_1(m_f+1)} (\Delta\varepsilon)^{n_2(m_f+1)} \\ & + \frac{2C_c (aT+b)^{m_c}}{n_2 m_c + 1} \dot{\varepsilon}^{n_1 m_c - 1} (\Delta\varepsilon)^{n_2 m_c + 1}\end{aligned} \tag{7.2.10}$$

In damage mechanics, $D = 1 - \Phi$, which means

$$\frac{\Delta D}{\Delta N} = -\frac{d\Phi}{dN} \tag{7.2.11}$$

Then the simplification of Eq. (7.2.10) can be expressed as

$$-\frac{d\Phi}{dN} = \frac{\Delta D}{\Delta N} = (-a_f T + b_f)\nu^{m_f} (\Delta\varepsilon)^{n_f} + (a_c T + b_c)\nu^{-m_c} (\Delta\varepsilon)^{n_c} \tag{7.2.12}$$

In Eq. (7.2.12), the first term on the right side is the contribution of fatigue damage, the second term is the contribution of the creep damage. It can be found that if frequency decrease, ν^{m_f} in the first term will be smaller, while ν^{-m_c} in the second term will increase. Similarly, when temperature increase, the first term will also decrease because of negative value of $-a_f$, the second term will increase with the increase with temperature. That means the creep damage will be more dominant at the low frequency and high temperature, while the fatigue damage will be more important at high frequency and low temperature.

ATTENTION: The Singapore Copyright Act applies to the use of this document. Nanyang Technological University Library

Based on the decrease rate at different strain range, temperature and frequency, the load drop model for Sn-3.8Ag-0.7Cu solder alloy is,

$$-\left(\frac{d\Phi}{dN}\right)_{SnAgCu} = \left(-2.4\times10^{-4}T + 9.13\right)\nu^{0.179}(\Delta\varepsilon)^{4.14} + \left(8.8\times10^{-5}T + 0.0055\right)\nu^{-0.126}(\Delta\varepsilon)^{1.29} \qquad (7.2.13)$$

Based on the fatigue test result of Sn-3.8Ag-0.7Cu solder alloy, it was found that decrease rate of peak stress, $\frac{d\Phi}{dN}$, has a power law relationship with fatigue life.

$$N_f^m\left(-\frac{d\Phi}{dN}\right) = C \qquad (7.2.14)$$

Fig. 7.2-8 shows the log-log plot of decrease rate of peak stress and fatigue life, it can be found that fatigue lives at different temperatures and frequencies all follow to a master curve, which means the fatigue exponent m and ductility coefficient C in decrease rate model is independent on temperature and frequency. The m and C in load drop model for Sn-3.8Ag-0.7Cu solder alloy is 0.818 and 0.121, respectively.

ATTENTION: The Singapore Copyright Act applies to the use of this document. Nanyang Technological University Library

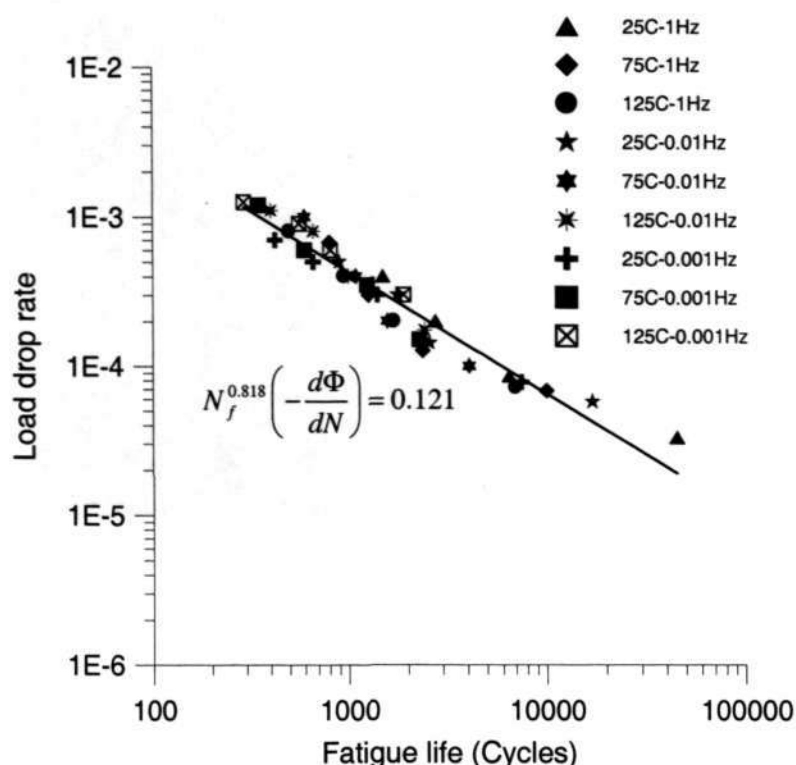

Fig. 7.2-8 Load drop rate model for low fatigue life of Sn-3.8Ag-0.7Cu

7.3 Impact properties and high strain rate model for 95.5Sn-3.8Ag-0.7Cu solder

Impact test were conducted with a Split Hopkinson pressure bar (SHPB) to study the Sn-3.8Ag-0.7Cu lead-free solder behavior under high strain rates. The stress and strain could be measured and calculated based on stress wave theory [114]. Upon the incident pulse hitting the specimen, it is split into reflected and transmitted pulse. Based on the strain gauge readings of incident, reflected and transmitted pulses, stress and strain during the impact tests can be determined. Typical pulse shape and relationship among incident, reflected and transmitted pulses are shown in Fig. 7.3-1 and 7.3-2.

ATTENTION: The Singapore Copyright Act applies to the use of this document. Nanyang Technological University Library

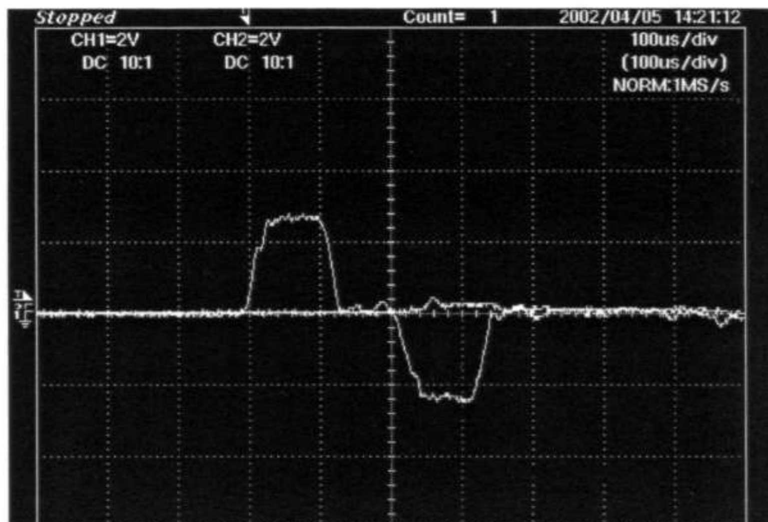

Fig.7.3-1 Typical pulse shape of SHPB test

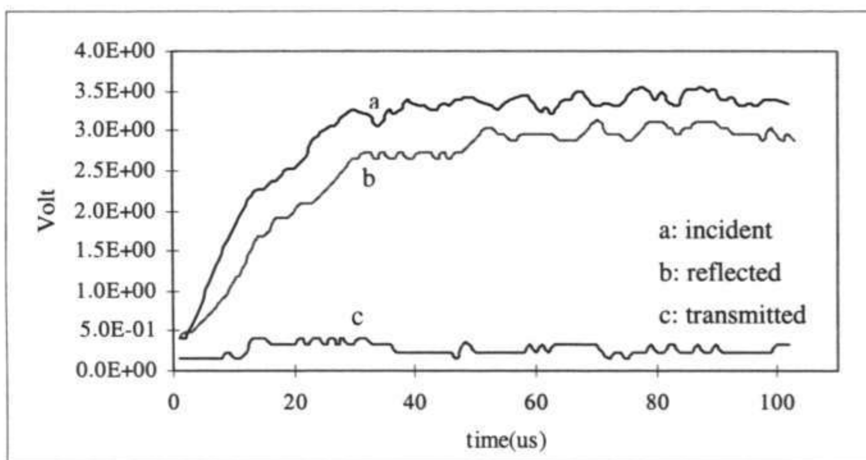

Fig.7.3-2 Typical relationship among incident, reflected and transmitted pulse

By plotting all stress-strain curves into one graph, the effect of strain rate on the Sn-3.8Ag-0.7Cu solders tensile properties of impact tests could be evaluated and compared. The stress-strain curves of Sn-3.8Ag-0.7Cu at room temperature and different strain rates (7×10^{2}, 9×10^{2} and 1.3×10^{3} s^{-1}) are shown at Fig. 7.3-3. The Elastic modulus and Yield stress at different strain rate are summarized in Table 7.3-1.

ATTENTION: The Singapore Copyright Act applies to the use of this document. Nanyang Technological University Library

Table 7.3-1 Impact results of Sn-3.8Ag-0.7Cu lead-free solders

Strain rate	Sn-3.8Ag-0.7Cu	
	E (GPa)	Yield (MPa)
$7 \times 10^2\ s^{-1}$	52.8	129
$9 \times 10^2\ s^{-1}$	53.3	175
$1.3 \times 10^3\ s^{-1}$	54.0	300

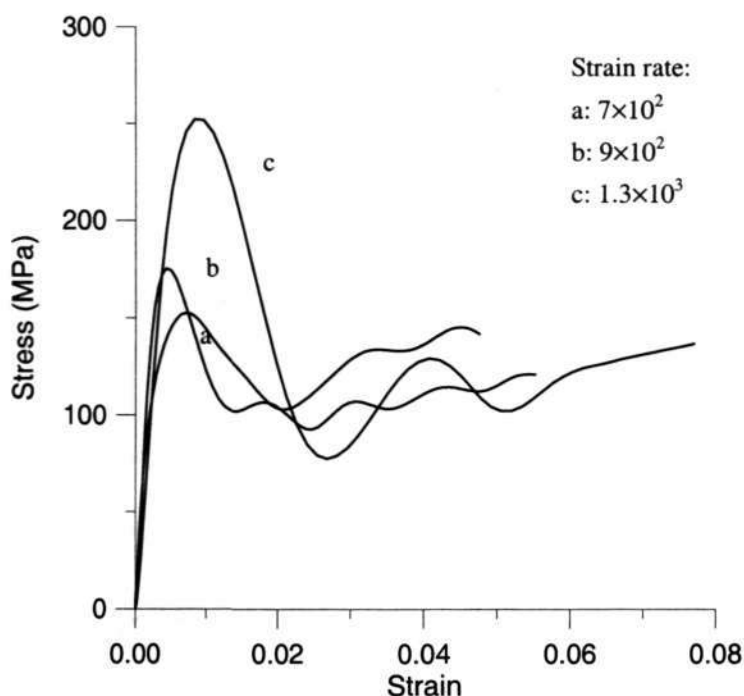

Fig. 7.3-3 Impact stress-strain curves for Sn-3.8Ag-0.7Cu

The temperature and strain rate dependent yield stress equations for Sn-3.8Ag-0.7Cu lead-free solder alloys at normal tensile tests have been described in Eq. (4.2.3). From impact test results, it was also found the mechanical properties of solders at high strain rates (such as impact tests) are dependent on strain rates as well. However, the yield stress equations for normal tensile tests only can predict the yield stress at low

ATTENTION: The Singapore Copyright Act applies to the use of this document. Nanyang Technological University Library

strain rate, if the strain rate is as high as in the impact test (10^2 s^{-1} to 10^3 s^{-1}), the equations are not valid any longer. There is a big difference between the test data and predicted values. The reason is, for most materials, the yield stress will have the dramatic increase at high strain rates (10^2 s^{-1}~10^4 s^{-1}) [115]. The strain rate dependence of yield stress at constant temperature is shown in Fig. 7.3-4.

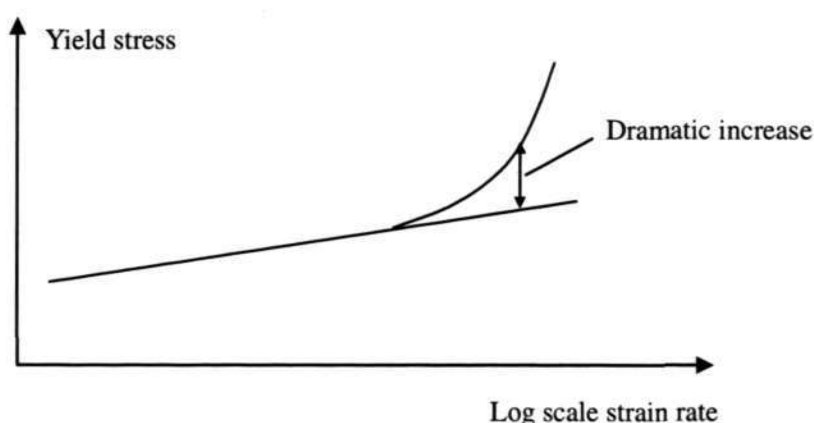

Fig. 7.3-4 Schematic of strain rate dependent yield stress

From Fig. 7.3-4, it can be found that the yield stress have a linear relationship with logarithmic strain rate at low strain rate, so Eqs (4.2.3) can predict the yield stress quite well for normal tensile test. But this linear relationship could not be used to describe the yield stress over the wide range (10^{-4} s^{-1}~10^4 s^{-1}), because the yield stress will increase dramatically when the strain rate reaches the higher level (10^2 s^{-1}~10^4 s^{-1}). The dramatic increase part should be added into the constitutive model to predict the strain rate dependent yield stress over a wide range. The increase part can be described as Eq. (7.3.1),

ATTENTION: The Singapore Copyright Act applies to the use of this document. Nanyang Technological University Library

$$\sigma_{increase} = B\dot{\varepsilon}^m \qquad \dot{\varepsilon} \geq 10^2 \qquad (7.3.1)$$

Based on the impact result at room temperature and three different strain rates, the values of constant B and exponent m can be decided. Combining with the Eqs. (4.2.3), the strain rate dependent yield stress at room temperature over a wide strain rate range (10^{-4} s^{-1}~10^4 s^{-1}) for Sn-3.8Ag-0.7Cu can be described as Eq. (7.3.2).

$$\sigma_y(\dot{\varepsilon})_{SnAgCu} = \begin{cases} 64.1\dot{\varepsilon}^{0.082} & 10^{-4} \leq \dot{\varepsilon} < 10^2 \\ 64.1\dot{\varepsilon}^{0.082} + 1.44\times10^{-5}\dot{\varepsilon}^{2.22} & \dot{\varepsilon} \geq 10^2 \end{cases} \qquad (7.3.2)$$

The experimental value and model value are compared in Figs. 7.3-5.

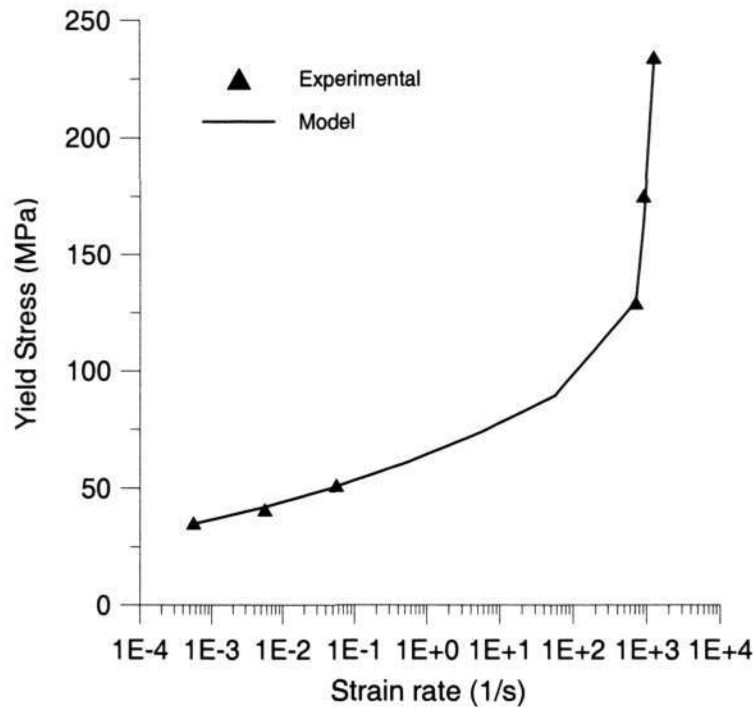

Fig. 7.3-5 Strain rate dependent yield stress for Sn-3.8Ag-0.7Cu

ATTENTION: The Singapore Copyright Act applies to the use of this document. Nanyang Technological University Library

Chapter 8. Application of 95.5Sn-3.8Ag-0.7Cu Visco-plastic Model to Micro-Deformation Analysis of Micro-BGA Assembly

In this chapter, both the in-situ Digital Image Correlation (DIC) measurement and Finite Element Analysis (FEA) of a Micro-BGA assembly under thermal loading were investigated. In FEA, Sn-Ag-Cu solder properties were characterized by the new constitutive model. The FEA simulation is from 25°C to 125°C and the computed deformation is compared to in-situ DIC measurement subject thermal ramp loading.

8.1 In-situ measurements under thermal loading

8.1.1 Test vehicle

The test vehicle used for in-situ measurement is a Micro-BGA assembly that consists of Polyimide, HDI, Silicon (Si), Cu Pads, Sn-3.8Ag-0.7Cu solder joints and a BT board. The package is cross-sectioned and the internal structure was measured. There are 14 by 14 rows, depopulated, 179 solder interconnect I/Os. The die size is 3.49 by 3.49 mm with a height of 0.25 mm. The solder bump height is 0.4 mm, a diameter of 0.54 mm and a pitch of 0.8 mm. The image of the assembly is shown in Fig. 8.1-1. The micro-speckle technique was used to measure the in-situ deformation of Sn-3.8Ag-0.7Cu solder joint under thermal loading. The equipment named Micro-DISC (Digital Image Speckle Correlation) system used for in-situ measurement is described in the next section.

ATTENTION: The Singapore Copyright Act applies to the use of this document. Nanyang Technological University Library

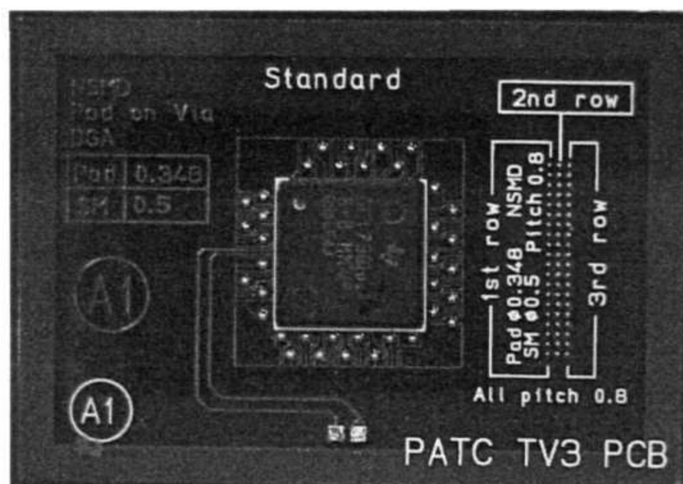

Fig. 8.1-1 Micro-BGA test Vehicle for thermal loading

8.1.2 Micro-DISC system

The Micro-DISC system is shown in Fig. 8.1-2. The system consists of five main parts: a working table; XYZ motorized translation stages; a long-working distance microscope; a miniature thermal cycling chamber; and a computer. The chamber was fixed on the table. Two resistance heaters and three thermoelectric coolers (TECs) were arranged on the walls of the inner chamber to heat and cool the chamber, respectively. A temperature controller was designed to activate the heaters and coolers in order to produce the required temperature in the inner chamber. The microscope was mounted onto the table via the XYZ stages. A positioning controller was provided to drive the stages and further locate the microscope at any desired point in the XY plane and any desired height over the chamber. The microscope included a zoom module, a focus module, a TV tube and an objective lens. The one-time-focus feature made the microscope able to zoom-in and zoom-out the sample without losing

ATTENTION: The Singapore Copyright Act applies to the use of this document. Nanyang Technological University Library

focus for the measurement of macro- and micro-deformation of packages at the same test. A ring-type white light source was mounted to the objective lens to illuminate the sample through the glass window on the top of the inner chamber. A CCD camera was connected to the TV tube to acquire images of the sample under any loading condition. A main software was developed to control all hardware, generate temperature profile, and acquire the images of the specimen. An image correlation software was implemented into the system to correlate a pair of captured images, calculate the displacement fields, then differentiate the displacement fields to get the strain fields, and visualize the results.

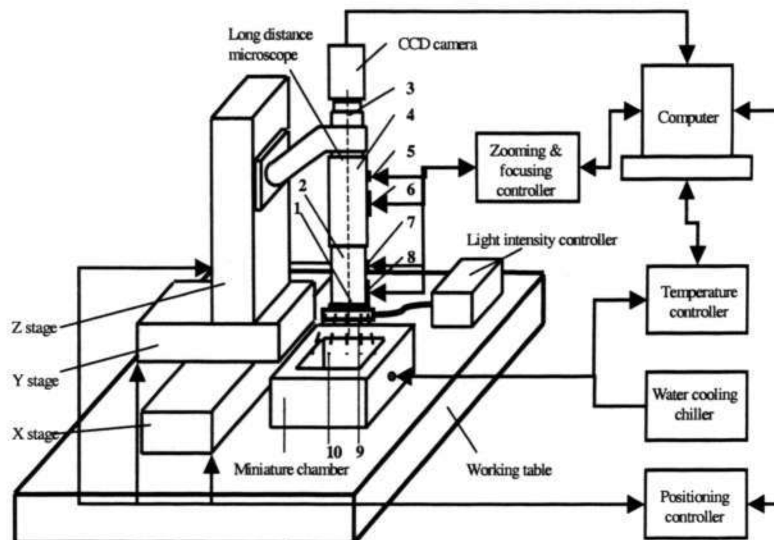

Fig. 8.1-2 Schematic diagram of micro-digital image correlation system (upper left corner: real image of the system): 1 -- objective lens; 2 -- focus module; 3 – TV tube; 4 -- zoom module; 5, 7 -- position sensors; 6, 8 --stepper motors; 9 -- ring light source; 10 -- inner

ATTENTION: The Singapore Copyright Act applies to the use of this document. Nanyang Technological University Library

8.1.3 In-situ thermal deformation measurement

Micro-DISC measurements and digital image correlation (DIC) were carried out on the Micro-BGA assembly subjected to thermal loading. The assembly was sectioned along the symmetric plane. Attention should be paid on the sectioned surface to make sure that the surface has a random speckle pattern for digital image correlation (DIC) analysis. The sectioned plane of the Micro-BGA is shown in Fig. 8.1-3. The outmost solder joint located underneath the corner of the silicon die was chosen for analysis. Measurements were taken at different temperatures of 25°C, 75°C and 125°C. These images for three different temperatures shown in Fig. 8.1-4 were selected for analysis.

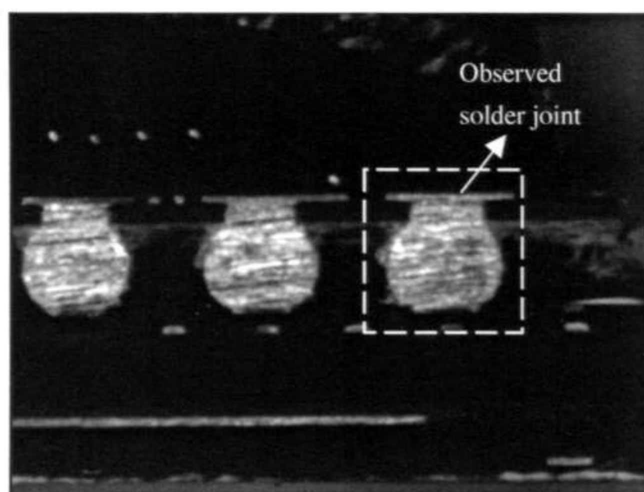

Fig. 8.1-3 Digital images of sectioned surface

ATTENTION: The Singapore Copyright Act applies to the use of this document. Nanyang Technological University Library

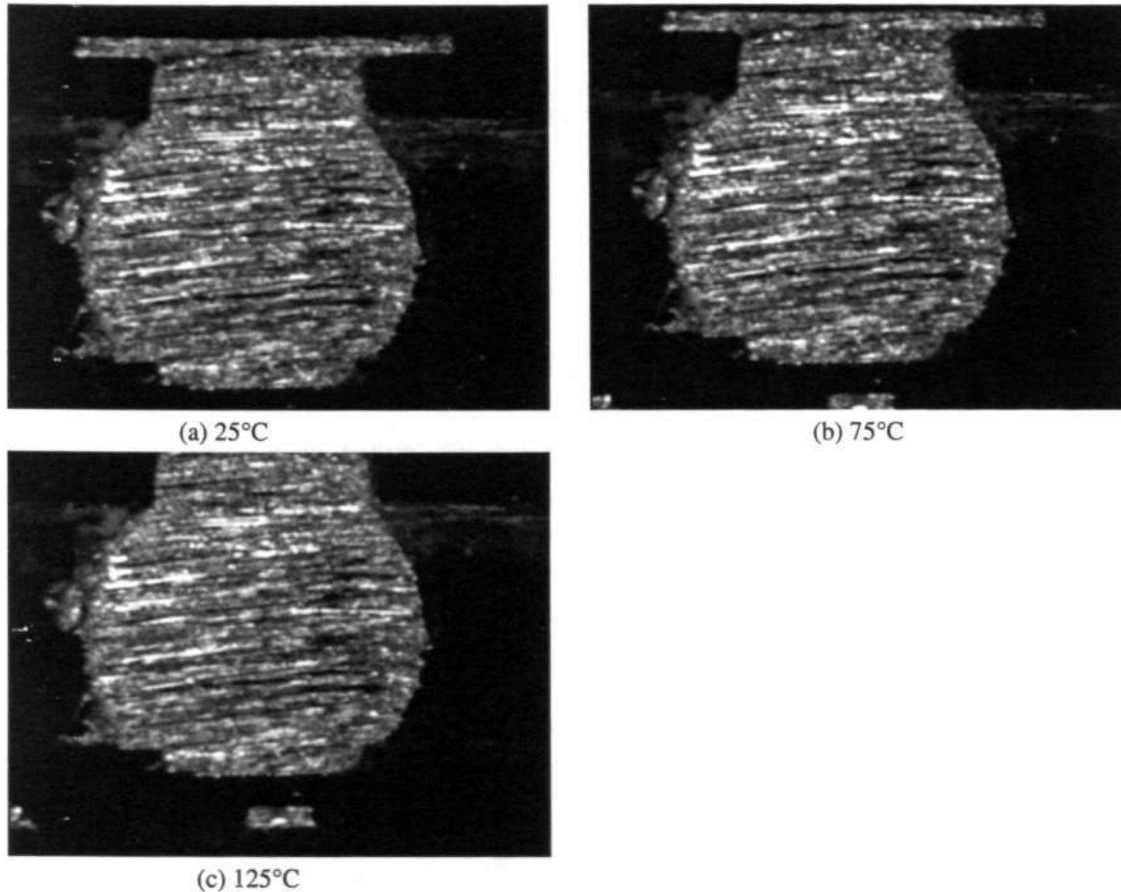

(a) 25°C

(b) 75°C

(c) 125°C

Fig. 8.1-4 Digital images of outmost solder joint during thermal loading

The image at 25°C was at the stress free state and used as the base image. Only the solder joint area was processed for image correlation analysis. The correlated displacement fields in the solder joint at 75°C and 125°C are shown in Fig. 8.1-5 and 8.1-6. The U and V fields are deformations in horizontal (x) and vertical (y) directions respectively. For both temperatures, it is shown that for the largest displacement for U field is located at the bottom right corner of the solder joint. The largest displacement for V field is located at the top right corner of the solder joint. The displacement patterns show that when temperature rise from 25°C to 75°C or 125°C, the deformation of the solder joint has horizontal translation and super-imposed with a

ATTENTION: The Singapore Copyright Act applies to the use of this document. Nanyang Technological University Library

small bending rotation. This observation coincides with the common understanding of the deformation of packaging assembly. Fig. 8.1-7 and 8.1-8 shows the derived shear strain fields from the correlated displacement fields. As indicated in Fig. 8.1-7, the largest shear strain (in absolute value) at 75°C is about –0.63%, and located near the bottom left corner of the solder ball. The overall shear strain is around -0.1%. While for the shear strain at 125°C shown in Fig. 8.1-8, the largest shear strain (in absolute value) is about –1.7%, and the overall strain is around –0.4%. These results agree with those from FEA, which will be described in the following section.

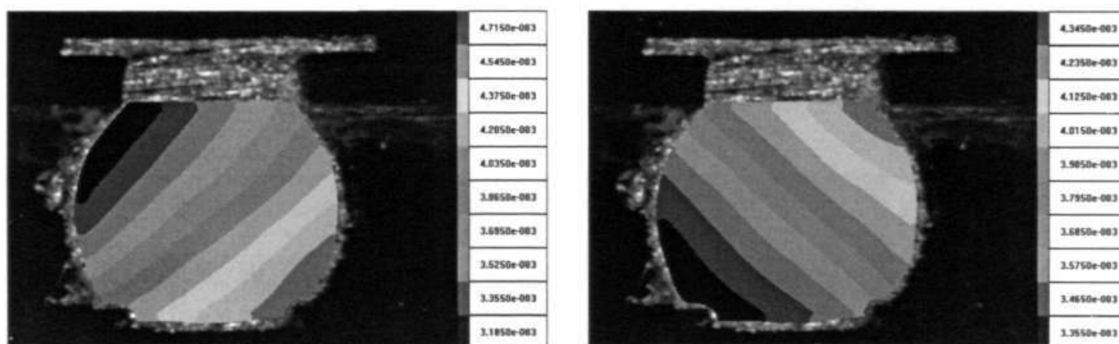

(a) U field (b) V field

Fig.8.1-5 Displacement fields of solder ball at 75°C from correlation (unit: mm)

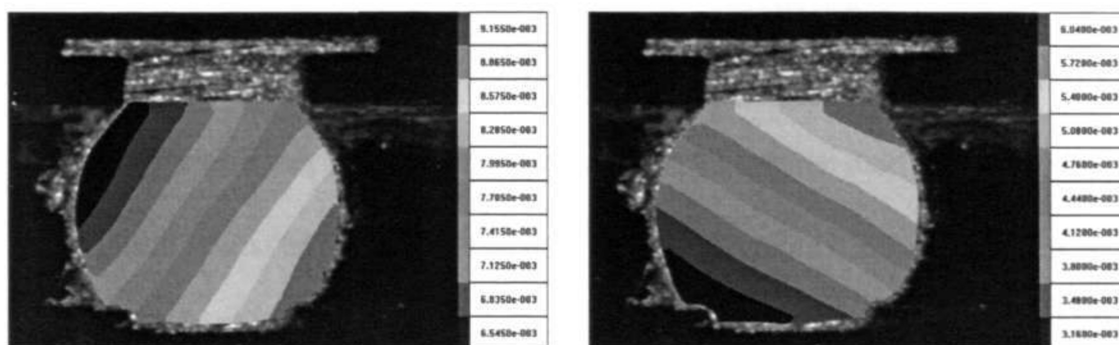

(a) U field (b) V field

Fig.8.1-6 Displacement fields of solder ball at 125°C from correlation (unit: mm)

ATTENTION: The Singapore Copyright Act applies to the use of this document. Nanyang Technological University Library

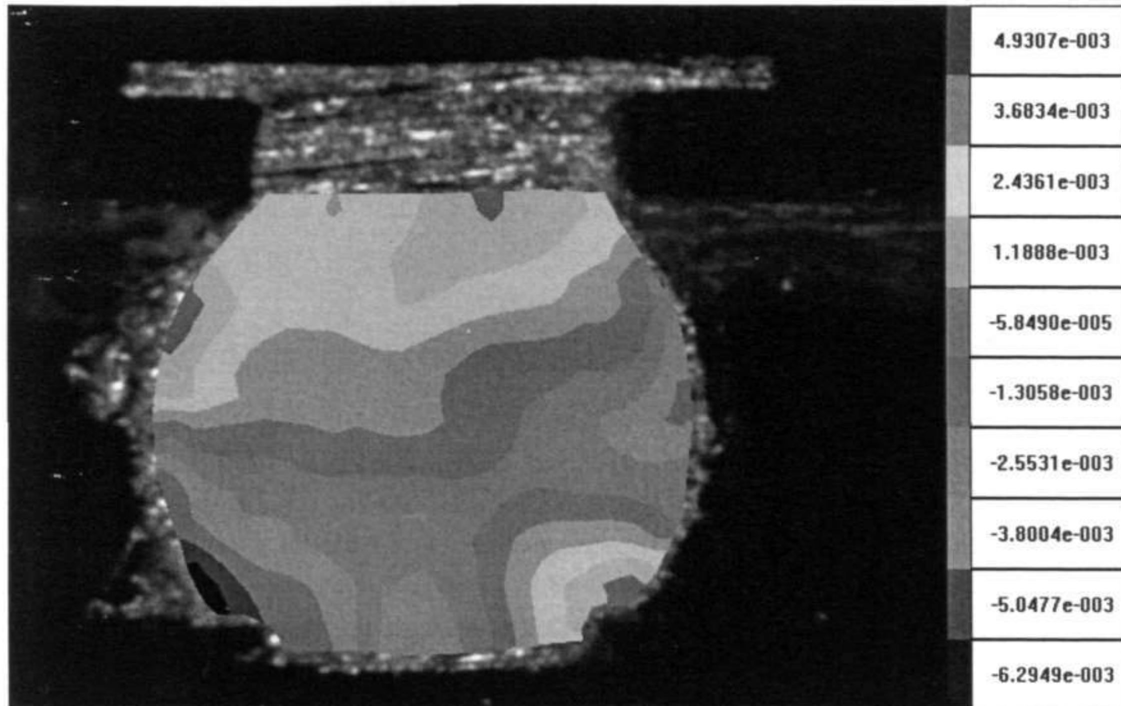

Fig. 8.1-7 Shear strain field of solder ball at 75°C from correlation

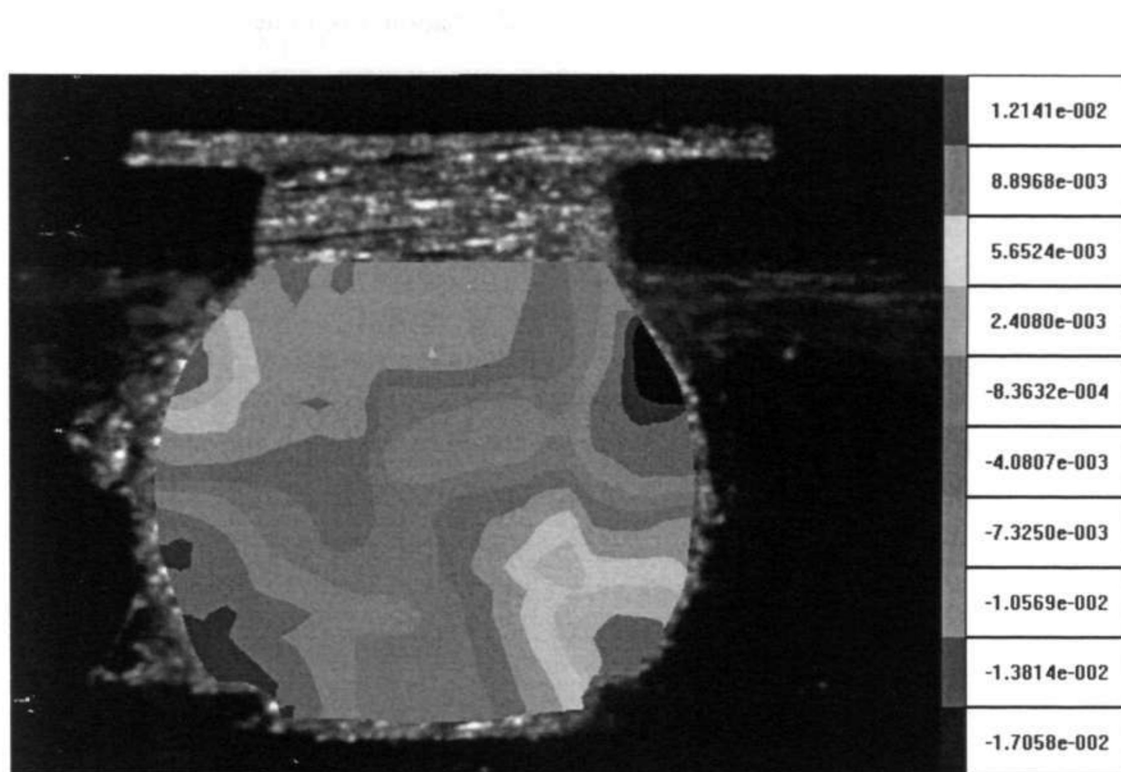

Fig. 8.1-8 Shear strain field of solder ball at 125°C from correlation

ATTENTION: The Singapore Copyright Act applies to the use of this document. Nanyang Technological University Library

8.2 FEA application of new visco-plastic model

Finite Element Analysis (FEA) is a computer-based numerical technique for calculating the strength and behavior of engineering structures. This technique is used extensively in solving thermal-mechanical problems in the electronic package due to the inability to calculate the displacement using close form equations.

In this work, a commercial FEA program, ANSYS 6.1 is used to solve this thermal-mechanical problem. A 2-Dimension plane strain model was used to model the Micro-BGA. Fig. 8.2-1 shows the 2-D model with the materials defined. The elements of the solder ball with the furthest distance from the neutral point (DNP) were refined as it will experience the largest deformation. For nodes along a plane of symmetry, movement perpendicular to its plane must be restricted. A node was restricted in the y-direction to prevent free body translation and rotation in the space during simulation. The finite element modeling employed the visco-plastic equations for solder and the visco-elastic equations for molding compound. The constitutive models used for various materials in the Micro-BGA assembly are summarized in Table 8.2-1.

ATTENTION: The Singapore Copyright Act applies to the use of this document. Nanyang Technological University Library

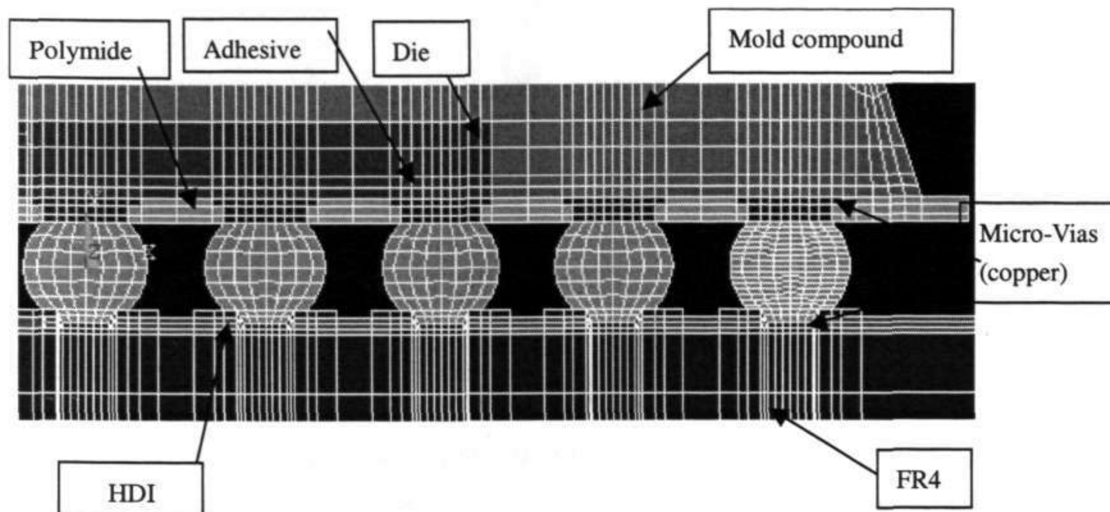

Fig. 8.2-1 2-D Finite Element Model for Micro-BGA

Table 8.2-1 Thermo-mechanical constitutive models of Micro-BGA assembly materials

Material	*Constitutive model*	*Source*
Silicon Die	Elastic-isotropic	[116]
Polyimide	Elastic-isotropic	Vendors data
Mould	Viscoelastic-isotropic	[116]
Copper Pad	Elastic-isotropic	[116]
HDI	Elastic-isotropic	Vendors data
PCB	Temp-dependent elastic, isotropic	[116]
Die Adhesive	Temp-dependent elastic, isotropic	[116]
Sn-3.8Ag-0.7Cu Solder	Viscoplastic	Curve-fitted

In Chapter 7, a new constitutive visco-plastic model was developed to characterize the stress-strain behavior of solder alloys. Hence, based on the incremental form of the new model, a subroutine code was programmed and implemented into the commercial ANSYS FEA software (See Appendix A), to characterize the visco-plastic behavior of Sn-3.8Ag-0.7Cu solder joint in Micro-BGA assembly. Before applying the new model subroutine to real Micro-BGA assembly, a simple tensile test simulation was

ATTENTION: The Singapore Copyright Act applies to the use of this document. Nanyang Technological University Library

conducted to verify the source code. It was found that the calculated stress results from new model simulation compares satisfactory to the Anand model results within 12%. (See Appendix B)

In Micro-BGA assembly simulation, PLANE183 element based on the user defined material subroutine was used for Sn-3.8Ag-0.7Cu lead-free solder. The constants used in the new hardening model were curve fitted in the previous section and they are C1 = 18.59 MPa, C2 =5645 (1/K), C3 = 13.1, C4 = 0.3, C5 =5.5×10^{-4}, respectively.

The FEA output for the U and V displacement fields for the selected solder joint at 75°C and 125°C are shown in Fig. 8.2-2 and 8.2-3. The maximum and minimum values are located at the corners. By comparison to Fig. 8.1-5 and 8.1-6, it can be noticed that the U and V displacement field pattern from the Micro-DISC and FEA results gave similar trend. For 75°C, the largest relative displacements between the diagonal corners are 1.3 m (for U displacement) and 0.99 m (for V) from FEA results, and 1.5 m (for U) and 1.1 m (for V) from correlation results respectively; at 125°C, displacements are 2.9 m(for U) and 2.3 m (for V) for FEA results, and 2.6 m(for U) and 2.8 m (for V) for correlation results. This means that the displacement differences which cause the deformation of the solder ball obtained from FEA and correlation are in satisfactory agreement.

ATTENTION: The Singapore Copyright Act applies to the use of this document. Nanyang Technological University Library

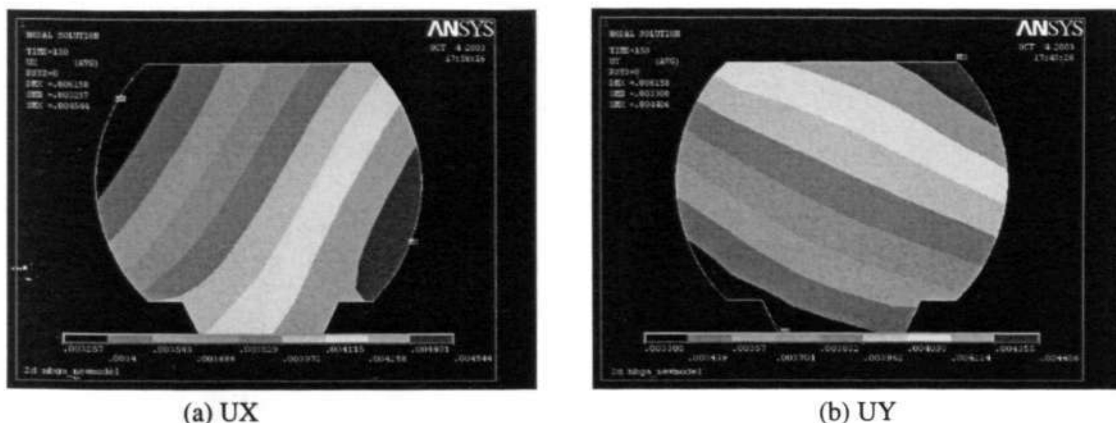

(a) UX (b) UY

Fig. 8.2-2 Displacement fields of the outmost solder ball by FEA (new model) (T=75°C, unit: mm)

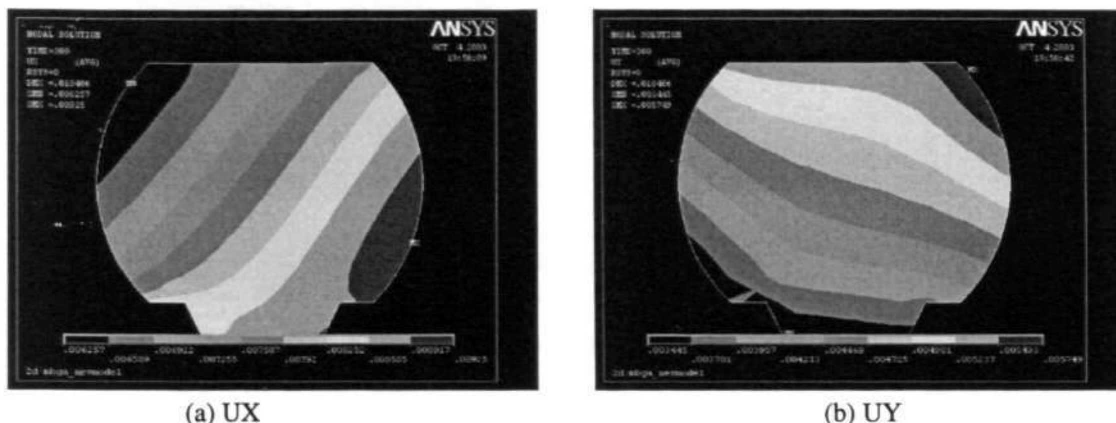

(a) UX (b) UY

Fig. 8.2-3 Displacement fields of the outmost solder ball by FEA (new model) (T=125°C, unit: mm)

The shear strain fields for the solder joint at 75°C and 125°C are illustrated in Fig. 8.2-4 and 8.2-5. As indicated in Fig. 8.2-4, the largest shear strain (in absolute value) at 75°C is about –0.46%, and also located near the bottom left corner of the solder ball compared to the correlation result. The overall shear strain is around -0.1%, which is exactly matched with the correlation value. While for the shear strain at 125°C shown in Fig. 8.2-5, the similar trend can be found. The largest shear strain (in absolute value) is about –1.4%, and the overall strain is around –0.4%. It can be concluded that the overall results from FEA and correlation are in satisfactory agreement. That means the new constitutive model is also a useful tool to characterize the visco-plastic behavior of solder joints in electronic packaging assembly.

ATTENTION: The Singapore Copyright Act applies to the use of this document. Nanyang Technological University Library

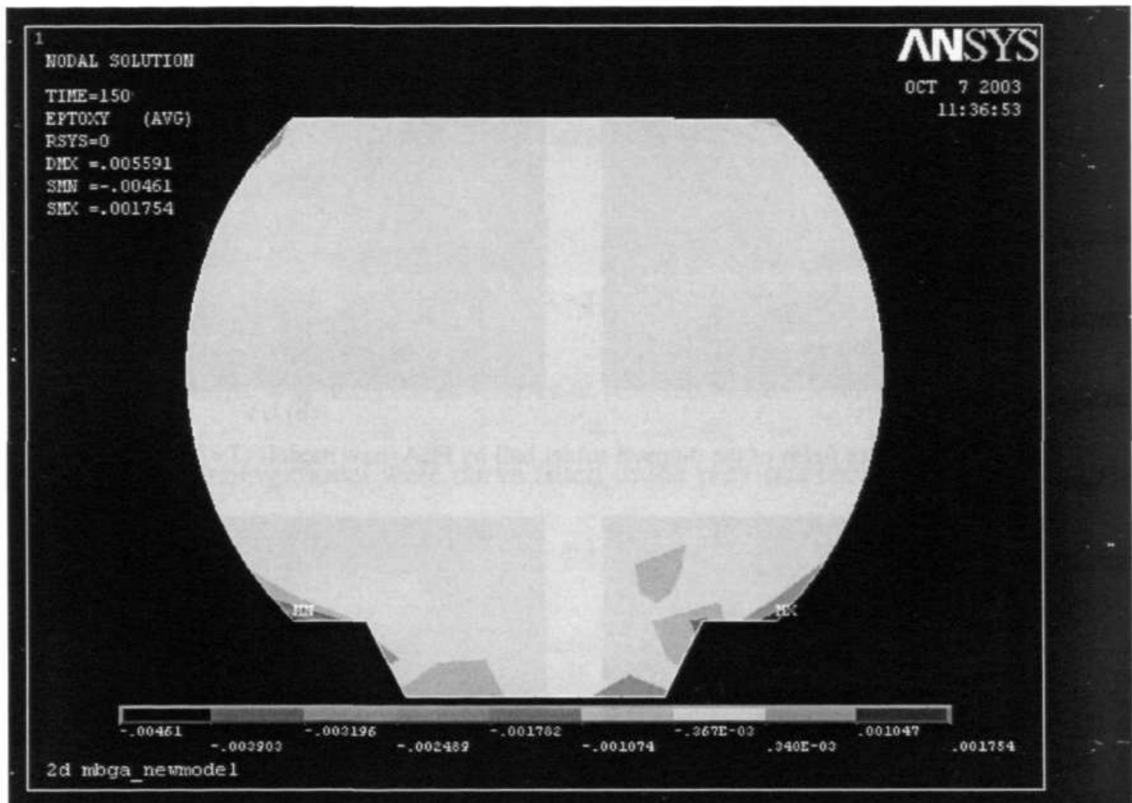

Fig. 8.2-4 Shear strain field of solder ball at 75°C from FEA (new model)

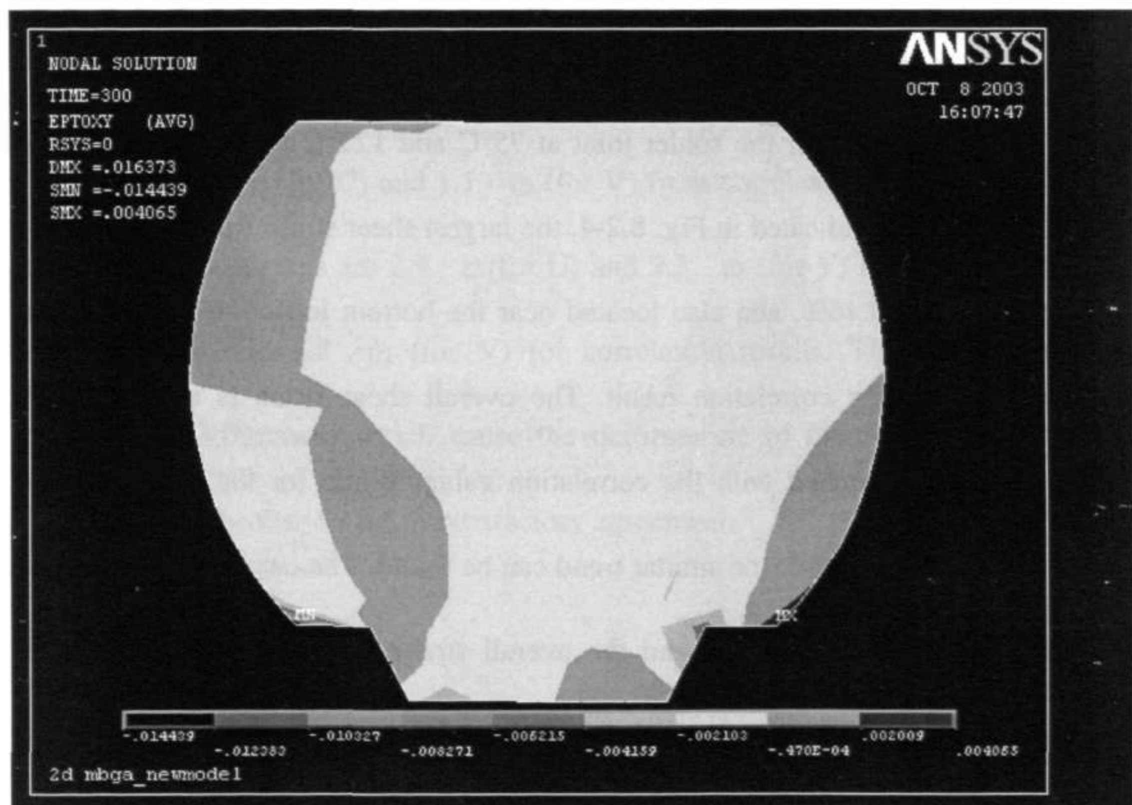

Fig. 8.2-5 Shear strain field of solder ball at 125°C from FEA (new model)

ATTENTION: The Singapore Copyright Act applies to the use of this document. Nanyang Technological University Library

Chapter 9. Conclusion & Recommendation

Mechanics of materials characterization of 95.5Sn-3.8Ag-0.7Cu and 99.3Sn-0.7Cu lead-free solder alloys have been investigated for the mechanical properties, creep and low cycle fatigue behavior. New developments in a visco-plastic constitutive model and a load-drop fatigue model have been documented in detail. Based on the systematic tests and analysis program conducted, the following conclusions can be made.

9.1 Mechanical properties

With reference to the specific research objective (i), the temperature and strain rate dependent tensile properties and stress-strain relations for the two Pb-free solders were investigated and the following conclusions can be made,

1. The values of the mechanical properties of Sn-3.8Ag-0.7Cu and Sn-0.7Cu solder alloys depend strongly on test temperature and strain rate. The experimental results for elastic modulus, yield stress, and UTS have been curve-fitted to comprehensive empirical equations given in Eqs. (4.2.1-4.2.6), respectively.
2. Sn-3.8Ag-0.7Cu and Sn-0.7Cu lead-free solder alloys have better mechanical properties than 63Sn-37Pb solder under the conditions tested here. The author's test data were compared to other reported results.
3. Material constants in Anand visco-plastic model for Sn-3.8Ag-0.7Cu and Sn-0.7Cu lead-free solders were derived and given in Table 4.2-3.

ATTENTION: The Singapore Copyright Act applies to the use of this document. Nanyang Technological University Library

9.2 Creep properties

With reference to the specific research objective (ii), the creep properties for the two Pb-free solders were investigated and the following conclusions can be made,

1. The creep behaviors of Sn-3.8Ag-0.7Cu and Sn-0.7Cu solder alloys depend strongly on test stress level and temperature. The experimental results for steady state creep strain rates had been curve-fitted to a hyperbolic-sine power law model as given in Eq. (5.2.3) and (5.2.4).
2. Sn-3.8Ag-0.7Cu and Sn-0.7Cu lead-free solder alloys have better creep properties than 63Sn-37Pb solder under the conditions tested here. The author's creep test data were compared with other reported solder joint creep results and show similar trends.

9.3 Low cycle fatigue behavior

With reference to the specific research objective (iii), low cycle fatigue behavior for the two Pb-free solders at different temperatures and frequencies were investigated and the following conclusions can be made,

1. Low cycle fatigue models for 95.5Sn-3.8Ag-0.7Cu and 99.3Sn-0.7Cu solder is provided for different temperatures (25°C, 75°C and 125°C) and frequencies (10^{-3}, 10^{-2} and 1Hz). The Coffin-Manson model and Morrow model were used to describe the low cycle fatigue behavior of the two lead-free solder alloys. The fatigue exponent m (or n) and ductility coefficient C (or A) in these models are dependent on temperature and frequency. Frequency-modified Coffin-Manson

ATTENTION: The Singapore Copyright Act applies to the use of this document. Nanyang Technological University Library

model and Morrow model were used to compensate for the frequency effect.

2. Sn-3.8Ag-0.7Cu and Sn-0.7Cu lead-free solder alloys have better fatigue properties than 63Sn-37Pb solder under the conditions tested here. The author's fatigue data show the similar trend with other reported fatigue test results.

9.4 New mechanics models for visco-plastic, fatigue and impact properties

With reference to the specific research objective (iv) and (v), visco-plastic behavior, load drop effects in fatigue and impact property of Sn-3.8Ag-0.7Cu solder were studied, and the conclusions are as follows,

1. A new constitutive model to characterize the visco-plastic behavior of solder material has been developed. It can accurately simulate the strain-stress response over the temperature and strain rate range tested. A hardening-softening parameter and a new strain hardening equation are introduced. The new constitutive model was applied to characterize the Sn-3.8Ag-0.7Cu lead-free solder alloy and implemented as a subroutine in the ANSYS finite element program (See Appendix A).

2. A new low cycle fatigue model has been developed. It overcomes the problem in conventional Coffin-Manson model and Morrow model, where the fatigue behavior at different temperatures and frequencies can be fitted to a master curve with the load drop rate parameter. A damage mechanics approach was developed to calculate the load drop rate at different test conditions. The low cycle fatigue behavior of Sn-3.8Ag-0.7Cu was characterized by the load drop rate fatigue

ATTENTION: The Singapore Copyright Act applies to the use of this document. Nanyang Technological University Library

model.

3. In addition, impact characterization using the Split Hopkinson Pressure Bar impact test provided yield stress for high dynamic strain rates above $10^2 s^{-1}$. The yield stress for Sn-3.8Ag-0.7Cu over a wide strain rate range (from $10^{-4} s^{-1}$ to $10^3 s^{-1}$) is given in Eq. (7.3.2).

9.5 Application to Micro-BGA assembly with Sn-3.8Ag-0.7Cu solder joints

With reference to the specific research objective (vi), micro-deformation analysis of a Micro-BGA assembly was studied by in-situ DIC and FEA methods,

The Micro-BGA assembly with Sn-3.8Ag-0.7Cu lead-free solder was subject to thermal loading and the in-situ strain was measured by the Digital Image Correlation (DIC) method, and compared to FEA analysis. In DIC measurement, the displacement and strain field of the solder joint at 75°C and 125°C were computed. In FEA simulation, the newly developed visco-plastic constitutive model was used to characterize the Sn-Ag-Cu lead-free solder displacement and strain distribution. The FEA results compared fairly well with the in-situ DIC measurement results. It is encouraging that the new visco-plastic constitutive model is able to characterize the non-linear deformation behavior of the solder joints subject to thermal loading.

ATTENTION: The Singapore Copyright Act applies to the use of this document. Nanyang Technological University Library

9.6 Achievements and Recommendations

The key contributions and achievements of this work are noted in the following areas:

1. A systematic study of 95.5Sn-3.8Ag-0.7Cu and Sn-0.7Cu lead-free solders on mechanical properties, creep and low cycle fatigue behavior. Derive mechanics of material models for stress-strain behavior, comprehensive empirical equations for tensile properties, hyperbolic-sine power law models for creep strain rate, material constants for Anand model and fatigue exponent and ductility coefficients in Coffin-Manson and Morrow's models for low cycle fatigue behavior.
2. A new visco-plastic constitutive model has been developed for Sn-3.8Ag-0.7Cu solder and applied to characterize the solder joint non-linear deformation behavior in a Micro-BGA assembly subject to thermal loading.
3. A new load drop rate fatigue model has been developed. This model is more sophisticated than the conventional Coffin-Manson and Morrow models. The fatigue lives at different temperatures and frequencies can be reduced to a master curve with the load drop rate parameter.
4. In-situ micro-deformation analysis of the Micro-BGA assembly under thermal loading was measured by Digital Image Correlation (DIC). The measured strain results compared fairly well with the FEA simulation results using the new visco-plastic constitutive model implemented in a ANSYS subroutine (See Appendix A)
5. A list of journal publication achieved during this project is given in Appendix C.

ATTENTION: The Singapore Copyright Act applies to the use of this document. Nanyang Technological University Library

Some recommendations to improve and make use of the developments made in this project are as follows,

(i) More repeated tests should be conducted to update the database of lead-free solders;

(ii) Specimen of different microstructure is suggested to study the effect of microstructure on mechanical properties, creep and low cycle fatigue behavior;

(iii) The link between the isothermal fatigue micro-mechanism and thermal cycling fatigue micro-mechanism should be investigated.

ATTENTION: The Singapore Copyright Act applies to the use of this document. Nanyang Technological University Library

References:

[1] Tummala R.R., Fundamentals of Microsystems Packaging, McGraw-Hill, 2001.

[2] Miric A.Z. and Grusd A., "Lead-Free Alloy," Soldering & Surface Mount Technology, 1998, pp.19-25.

[3] Toyoda Y., "The Latest Trends in Lead-Free Soldering," Fourth International Symposium on Electronic Packaging Technology, August 2001, Beijing, China.

[4] Edwin Bradley et. al., NEMI Pb-free Task Group Report, 2002 APEX Free Forum January 23, 2002, National Electronics Manufacturing Initiative. http://www.nemi.org.

[5] Frear, D.R., Burchett S.N., Morgan, H.S. and Lau J.H., The Mechanics of Solder Alloy Interconnects, Chapman and Hall, 1994.

[6] Knecht S. and Fox R., "Constitutive relationship and creep-fatigue life model for eutectic tin-lead solder," IEEE Transaction on Components, Hybrids, and Manufacturing Technology, Vol. 13, No. 2, June 1990, pp.424-433.

[7] Darveaux R., "Effect of Simulation Methodology on Solder Joint Crack Growth Correlation", IEEE Proceedings of Electronic Components and Technology Conference, 2000, pp.158-169.

[8] Akay H.U., Paydar N.H. and Bilgic A., "Fatigue Life Prediction for Thermally Loaded Solder Joints Using a Volume-Weighted Averaging Technique," J. Electronic Packaging, Vol. 119, 1997, pp. 228-235.

[9] Akay H, Zhang H, Paydar N. "Experimental Correlations of an Energy-Based Fatigue Life Prediction Method for Solder Joints,", Proceedings of the Pacific Rim/ASME International Intersociety Electronic and Photonic Packaging Conference INTERpack'97, Vol. 2, 1997, pp. 1567–1574.

[10] Darveaux R., Banerji K. and Dody G., "Reliability of Plastic Ball Grid Array Assembly," Ball Grid Array Technology (J. Lau, Editor), McGraw-Hill, Inc. (New York), 1995, pp.379-442.

ATTENTION: The Singapore Copyright Act applies to the use of this document. Nanyang Technological University Library

[11] Shi X.Q., Wang Z.P., Zhou W., H.L.J. Pang and Q.J. Yang, "A New Creep Constitutive Model for Eutectic Solder Alloy," Journal of Electronic Packaging, Vol. 124, June 2002, pp. 85-90.

[12] Anand, L., 1985, "Constitutive equations for hot working of metals," J. Plasticity, No.1, pp.213-231.

[13] Brown S. B., Kwon H. Kim and L. Anand, "An Internal Variable Constitutive Model For Hot Working of Metals," International Journal of Plastic, Vol.5, 1989, pp95-130.

[14] Tachibana Y. and Krempl E., "Modeling of high homologous temperature deformation behavior using the visco plasticity theory based on overstress (VBO): Part I- Creep and tensile behavior," Transactions of ASME, Vol. 117, 1995, pp.456-461.

[15] Tachibana Y. and Krempl E., "Modeling of high homologous temperature deformation behavior using the visco plasticity theory based on overstress (VBO): Part II- Characteristics of the VBO model," Journal of Engineering materials and technology, Vol. 119, 1997, pp.1-6.

[16] Tachibana Y. and Krempl E., "Modeling of high homologous temperature deformation behavior using the visco plasticity theory based on overstress (VBO): Part III- A simplified model," Journal of Engineering materials and technology, Vol. 120, 1998, pp.193-196.

[17] Bor Z. H., "A viscoplasticity theory based on overstress for rate dependent deformation of eutectic lead-tin solder alloy," AMD-Vol. 187, Mechanics and Materials for Electronic Packaging, ASME 1994, pp73-81.

[18] McDowell D. L., "A nonlinear kinematic hardening theory for cyclic thermoplasticity and thermoviscoplasticity," International Journal of Plasticity, 8(1992), pp 695-728.

[19] Wen S.M., Keer L.M. and Mavoori H., "Constitutive and damage model for a lead-free solder," Journal of electronic materials, Vol.30, No.9, 2001, pp 1190-1196.

ATTENTION: The Singapore Copyright Act applies to the use of this document. Nanyang Technological University Library

[20] Busso E.P., Kitano M. and Kumazawa T., "A Visco-Plastic Constitutive Model for 60/40 Tin-Lead Solder Used In IC Package Joints," ASME Journal of Engineering Materials and Technology, Vol. 114, 1992, pp.331-339.

[21] Yaguchi M. and Takahashi Y., "A viscoplastic constitutive model incorporating dynamic strain aging effect during cyclic deformation conditions," International Journal of Plasticity, 16(2000), pp.241-262.

[22] Yaguchi M., Yamamoto M. and Ogata T., "A viscoplastic constitutive model for nickel-base superalloy, part I: Kinematic hardening rule of anisotropic dynamic revoery," International Journal of Plasticity, 18(2002), pp.1083-1109.

[23] Yaguchi M., Yamamoto M. and Ogata T., "A viscoplastic constitutive model for nickel-base superalloy, part II: modeling under anisothermal conditions," International Journal of Plasticity, 18(2002), pp.1111-1131.

[24] Harold J.F. and Robert T.H., "Creep Fatigue Modeling For Solder Joint Reliability Predictions Including the Microstructure Evolution of the Solder," IEEE Transaction on Components, Hybrids, and Manufacturing Technology, Vol. 13, 1990, pp.727-735.

[25] Yasumi U., Shuichi T., Akio I. and Sumio Y., "A Method of Fatigue Life Prediction For Surface-Mount Solder Joints of Electronic Devices by Mechanical Fatigue Test," Advances In Electronic Packaging, ASME, 1993, pp.493-498.

[26] Mavoori H., Vaynman S., Chin J., Moran B. and Fine M.E., "Isothermal Fatigue Life Prediction of Solder Materials," Mechanics and Materials For Electronic Packaging, ASME 1994, pp.165-179.

[27] Lee S.B. and Kim J.K., "A Mechanistic Model For Fatigue Life Prediction of Solder Joints For Electronic Packages," International Journal of Fatigue, 1997, pp.85-91.

[28] Kariya Y. and M. Otsuka, "Mechanical Fatigue Characteristics of Sn-3.5Ag-X(X=Bi, Cu, Zn and In) Solder Alloys," Journal of Electronic Materials, 27(1998), pp.1229-1235.

ATTENTION: The Singapore Copyright Act applies to the use of this document. Nanyang Technological University Library

[29] Masao S. and Hiroki Y., "A Strain Ratio Approach For Assessing Creep-Fatigue Life of 63Sn-37Pb Solder Under Shear Loading," Inter Conference on Thermal Phenomena, 2000, pp.187-192.

[30] Park T.S. and Lee S.B., "Isothermal Low Cycle Fatigue Tests of Sn/3.5Ag/0.75Cu and 63Sn/37Pb Solder Joints under Mixed-Mode Loading Cases," IEEE Proceeding of Electronic Components and Technology Conference, 2002, pp.979-984.

[31] Hong Tang and Cemal Basaran, "Experimental Characterization of Material Degradation of Solder Joint Under Fatigue Loading," 2002 Inter Society Conference on Thermal Phenomena, 2002, pp.896-901.

[32] Schlums H., Tchankow D.S., Meissner B. and Villwock J., "Life Prediction For High Temperature Low Cycle Fatigue and Thermo-Mechanical Fatigue," Proceedings of the Eighth International Fatigue Congress, 2002, pp.1699-1706.

[33] Kanchanomai C., Y. Miyashita and Y. Mutoh, "Low Cycle Fatigue Behavior of Lead-free Solder 96.5Sn/3.5Ag," Journal of Electronic Materials, 31(2002), pp. 142-151.

[34] Kanchanomai C., Yamamoto S., Miyashita Y., Mutoh Y. and McEvily A.J., "Low Cycle Fatigue Test For Solder Using Non-Contact Digital Image Measurement System," International Journal of Fatigue, 2002, pp.57-67.

[35] Kanchanomai C., Miyashita Y. and Mutoh Y., "Low Cycle Fatigue Behavior of Sn-Ag, Sn-Ag-Cu and Sn-Ag-Cu-Bi Lead-free Solders," Journal of Electronic Materials, 31(2002), pp. 456-465.

[36] Yang Q.D., Shim D.J., Spearing S.M., "A cohesive zone model for low cycle fatigue life prediction of solder joints," Microelectronic Engineering 75 (1), JUL 2004, pp. 85-95.

[37] Lee K.O., Yu J., Park T.S., Lee S.B., "Low-cycle fatigue characteristics of Sn-based solder joints," Journal of Electronic Materials 33(4), APR 2004, pp. 249-257.

[38] Coffin L.F., "A Study of the Effects of Cyclic Thermal Stresses on a Ductile

ATTENTION: The Singapore Copyright Act applies to the use of this document. Nanyang Technological University Library

Metal," Trans ASME, 76(1954), pp.931-950.

[39] Manson S.S., "Fatigue a Complex Subject-Some Simple Approximations," Experimental Mechanics, 1965, pp.193-226.

[40] Dieter GE, Mechanical Metallurgy, New York, 1986.

[41] Kilinski TJ, Lesniak JR, Sandor BI, "Modern Approaches to Fatigue Life Prediction of SMT Solder Joints," Lau JH, editor, Solder Joint Reliability Theory and Applications, New York, 1991, pp.384-405.

[42] Solomon H.D., "Predicting Thermal and Mechanical Fatigue Lives from Isothermal Low Cycle Data," Solder Joint Reliability, Edited by J.H. Lau, Van Nostrand Reinhold, New York, Chapter 14, 1991, pp.508-544.

[43] Knecht S. and Fox L., "Integrated Matrix Creep: Application to Accelerated Testing and Lifetime Prediction," Solder Joint Reliability, Edited by J.H. Lau, Van Nostrand Reinhold, New York, Chapter 16, 1991, pp.508-543.

[44] Syed AR, "Thermal Fatigue Reliability Enhancement of Plastic Ball Grid Array (PGBA) Packages," Electronic Components and Technology Conference, 1996, pp.1151-1158.

[45] Syed AR., "Factors Affecting Creep-fatigue Interaction in Eutectic Sn/Pb Solder Joints," Proceedings of the Pacific Rim/ASME International Intersociety Electronic and Photonic Packaging Conference INTERpack'97, Vol. 2, 1997, pp. 467-473.

[46] Pang JHL, Seetoh C.W. and Wang Z.P., "CBGA Solder Joint Reliability Evaluation Based on Elastic-Plastic-Creep Analysis," Journal of Electronic Packaging, Vol. 122, 2000, pp.255-261.

[47] Pang JHL and Chong D.Y.R., "Flip Chip on Board Solder Joint Reliability Analysis Using 2-D and 3-D FEA Models," IEEE Transactions on Advanced Packaging, Vol. 24, No. 4, 2001, pp.499-506.

[48] Pang JHL, Ang K.H., Shi X.Q. and Wang Z.P., "Mechanical Deflection System (MDS) Test and Methodology for PBGA Solder Joint Reliability," IEEE Transactions on Components and Packaging Technologies, Vol. 24, No. 4, 2001,

ATTENTION: The Singapore Copyright Act applies to the use of this document. Nanyang Technological University Library

pp.507-514.

[49] Pang JHL, Chong D.Y.R. and Low T.H., "Thermal Cycling Analysis of Flip-Chip Solder Joint Reliability," IEEE Transactions on Components and Packaging Technologies, Vol. 24, No. 4, 2001, pp.705-712.

[50] Engelmaier W., "Solder Attachment Reliability, Accelerated Testing, and Result Evaluation," Solder Joint Reliability, Edited by J.H. Lau, Van Nostrand Reinhold, New York, Chapter 17, 1991, pp.545-587.

[51] Shi X.Q., Pang H.L.J., Zhou W., Wang Z.P., "Low Cycle Fatigue Analysis of Temperature and Frequency Effects in Eutectic Solder Alloy," International Journal of Fatigue, 2000, pp.217-228.

[52] Shi X.Q., Pang H.L.J., Zhou W., Wang Z.P., "A Modified Energy-Based Low Cycle Fatigue Model for Eutectic Solder Alloy," Scripta Material, Vol. 41, No. 3, 1999, pp.289-296.

[53] Pao Yi-Hsin, "A Fracture Mechanics Approach to Thermal Fatigue Life Prediction of Solder Joints," IEEE Transaction Components, Hybrids, and Manufacturing Technology, Vol. 15, No. 4, 1992, pp.559-570.

[54] Lau J.H., "Thermal Fatigue Life Prediction of Flip Chip Solder Joints by Fracture Mechanics Method," Engineering Fracture Mechanics, Vol. 45, 1993, pp.643-654.

[55] Bernstein H.L., "An Evaluation of Four Creep-Fatigue Models for a Nickel-Base Super alloy," Low cycle Fatigue and Life Prediction, Philadelphia, American Society for Testing and Materials, 1982, pp.105-134.

[56] Kordisch T. and Nowack H., "High Temperature Creep-Fatigue Behavior of Titanium IMI 834," 1996, pp.777-782.

[57] Mcdowell D.L., "Basic Issues in the Mechanics of High Cycle Metal Fatigue," International Journal of Fracture, 1996, pp.103-145.

[58] Pidaparti R.M.V. and Song X., "Fatigue Crack Propagation Life Analysis of Solder Joints Under Thermal Cyclic Loading," Theoretical and Applied Fracture Mechanics, Vol. 24, 1996, pp.157-164.

ATTENTION: The Singapore Copyright Act applies to the use of this document. Nanyang Technological University Library

[59] Nguyen B.N., Onch P.R. and van der Giessen E., "On Higher-Order Crack-Tip Fields in Creeping Solids," Transaction of the ASME, Vol.67, 2000, pp. 372-382.

[60] Liu P.L. and Shang J.K., "Influence of Microstructure on Fatigue Crack Growth Behavior of Sn-Ag Solder Interfaces," Journal of Electronic Materials, Vol. 29, 2000, pp.622-627.

[61] Mutoh Y., Zhao J., Miyashita Y. and Kanchanomai C., "Fatigue Crack Growth Behavior of Lead-Containing and Lead-free solders," Proceedings of International Conference on Advanced in Packaging, December 2001, Singapore, pp.306-315.

[62] Zhao J., Mutoh Y., , Miyashita Y. and Mannan S. L., "Fatigue Crack Growth Behavior of Sn-Ag-Cu and Sn-Ag-Cu-Bi Lead-free solders," Journal of Electronic Materials, August 2002, pp.879-886.

[63] ASTM standards, ASTM E8M: Standard Test Methods for Tension Testing of Metallic Materials [Metric], The American Society for Testing and Materials, Vol. 03.01, 1998.

[64] ASTM standards, ASTM E606: Standard Practice for Strain-Controlled Fatigue Testing, The American Society for Testing and Materials, Vol. 03.01, 1998.

[65] Pang H.L. John, Xiong B.S. and Kurniawijaya H., "Mechanical Strength of Lead-Free Solders," GlobalTRONICS Technology Conference, 2002, Singapore EXPO, September 3-5, pp.113-118.

[66] Pang H.L. John, Xiong B.S., Neo C.C., Zhang X.R., and Low T.H., "Bulk Solder and Solder Joint Properties for Lead-Free Solder 95.5Sn-3.8Ag-0.7Cu Solder Alloy," IEEE Proceedings of 2003 Electronic Components and Technology Conference, pp.673-679, 2003.

[67] John H.L. Pang, B.S Xiong and T.H. Low, "Constitutive Model For Lead-Free 95.5Sn-3.8Ag-0.7Cu Solder Alloy," ICMAT, Singapore, 2003.

[68] X.Q. Shi, W. Zhou, H.L.J. Pang, Z.P. Wang, "Effect of Temperature and Strain Rate on Mechanical Properties of 63Sn/37Pb Solder Alloy," Journal of

ATTENTION: The Singapore Copyright Act applies to the use of this document. Nanyang Technological University Library

Electronic Packaging, Vol. 121, September 1999, pp179-185.

[69] Technical Reports for the Lead Free Solder Project: Properties Reports: "Room Temperature Tensile Properties of Lead-Free Solder Alloys," Lead Free Solder Project CD-ROM, National Center for Manufacturing Sciences (NCMS), 1998.

[70] Foley J.C. et. al., "Analysis of ring and Plug shear strengths for comparison of lead-free solders," JEM vol.29, No.10, 2000, pp1258-1263.

[71] Kariya Y. and Plumbridge J., "Mechanical Properties of Sn-3.0mass%Ag -0.5mass%Cu Alloy," 7th Symposium on Microjoining and Assembly in Electronic, Feburary 1-2, 2001, Yokohama.

[72] Lin J.K., Silva A.D., Frear D., Guo Y., Jang J.W., Li L., Mitchell D., Yeung B., Zhang C., "Characterization of Lead-Free Solders and Under Bump Merallurgies for Flip-Chip Package," Proceedings of IEEE Electronic Components and Technology Conference, 2001, pp.455-462.

[73] Harrison M.R., Vincent J.H. and Steen H.A.H., "Lead-free reflow soldering for electronic assembly," Soldering & Surface Mount Technology, 13/3 2001, pp.21-38.

[74] Plumbridge W.J. and Gagg C.R., "The mechanical properties of lead-containing and lead-free solders-----meeting the environmental challenge," Proc Instn Mech Engrs, Vol. 214, Part L, pp.153-161, 2001.

[75] Suraski D. and Seeling, K., "The Currrent Status of Lead-Free Solder Alloys," IEEE Transactions on Electronics Packaging Manufacturing, Vol.24, No.4, Oct, 2001, pp.244-248.

[76] Amagai M., Watanabe M., Omiya M., Kishimoto K. and Shibuya T., "Mechanical characterization of Sn-Ag-based lead-free solders," Microelectronics reliability, 42(2002), pp.951-966.

[77] Kim K.S., Huh S.H. and Suganuma K., "Effects of Cooling Speed on microstructure and tensile properties of Sn-Ag-Cu alloys," Materials Science and Engineering A333 (2002), pp.106-114.

[78] Wu C.M.L., Yu D.Q., Law C.M.T. and Wang L., "Microstructure and

ATTENTION: The Singapore Copyright Act applies to the use of this document. Nanyang Technological University Library

Mechanical Properties of New Lead-Free Sn-Cu-Re Solder Alloys," JEM, Vol. 31, No. 9, 2002, pp.928-932.

[79] Schubert , A., Dudek, R., Auerswald E., Gollhardt A., Michel B. and Reichl H., "Fatigue life models for SnAgCu and SnPb solder joints evaluated by experiments and simulation," 53th ECTC, New Orlearns, Louisiana USA May 27-30, 2003, Proceedings of IEEE ECTC Conference(2003), pp.603-610.

[80] Hirose A., Yanagawa, H., Ide E. and Kobayashi K. F., "Joint strength and interfacial microstructure between Sn-Ag-Cu and Sn-Zn-Bi solders and Cu substrate," Science and Technology of Advanced Materials, 2004, pp.267-276.

[81] Shohji I., Yoshida T., Takahashi T. and Hioki S., "Tensile properties of Sn-Ag based lead-free solders and strain rate sensitivity," Materials Science and Engineering A366(2004), pp.50-55.

[82] Pang H.L John., Xiong B.S. and Low T.H., "Comprehensive Mechanics Characterization of Lead-Free 95.5Sn-3.8Ag-0.7Cu Solder," Micromaterials and Nanomaterials, Issue 3, 2004, pp.86-93.

[83] Pang H.L. John, Xiong B.S., Neo C.C. and Low T.H., "Mechanical Properties for 95.5Sn-3.8Ag-0.7Cu Lead Free Solder Alloy," IEEE Transactions of Components and Packaging Technologies (Accepted).

[84] Pang H. L. John, Low T. H., Xiong B. S., Xu Luhua and Neo C. C., "Thermal cycling aging effects on Sn–Ag–Cu solder joint microstructure, IMC and strength," Thin Solid Film, Vol. 462-463, September 2004, pp. 370-375.

[85] John H.L. Pang, B.S Xiong and F.X. Che, "Modeling Stress Strain Curves For Lead-Free Sn-3.8Ag-0.7Cu Solder," Proceedings of Eurosime 2004, Brussels, Belgium, May 10-12, 2004, pp.449-453.

[86] Glazer, J., "Metallurgy of low temperature Pb-free solders for electronic assembly", IMR/273, The institute of Materials and ASM International, 1995, pp.65-93.

[87] Liang J., Gollhard N., Lee P.S., Schroeder S.A. and. Morris W.L, "A Study of Fatigue and Creep Behavior of Four High Temperature Solders," Fatigue

ATTENTION: The Singapore Copyright Act applies to the use of this document. Nanyang Technological University Library

Fracture & Engineering Material & Structure, Vol. 19, 1996, pp.1401-1409.

[88] Ren W., Lu M., Liu S. and Shangguan D., "Thermal mechanical property testing of new lead-free solder joints," Soldering and Surface Mount Technology, Vol. 9, No. 3, Oct 1997, pp. 37-40.

[89] Mathew M.D., Movva S., Yang H., and Murty K. L., "Creep of Sn, Sn-3.5Ag and Sn-5Sb Soldering for Electronic Packaging," Creep Behavior of Advanced Materials for 21st Century, Edited by R.S. Mishra, A.K. Mukherjee, and K. L. Murty, The Minerals, Metals & Materials Society, 1999, pp.51-57.

[90] Igoshev V.I. and Kleiman J.I., "Creep Phenomena in Lead-Free Solders," Journal of Electronic Material, Vol. 29, No. 2, 2000, pp.244-250.

[91] Schubert A., Walter H., Dudek R., Michel B., Lefranc G., Otto, J. and Mitic G., "Thermo-mechanical properties and creep deformation of lead-containing and lead-free solders", Proceedings, 2001 International Symposium on Advanced Packaging Materials, pp. 129-134.

[92] Neu R.W., Scott D.T. and Woodmansee M.W., "Thermo-mechanical behavior of 96Sn-4Ag and Castin Alloy", ASME Transactions, Journal of Electronic Packaging, Vol. 123, No. 3 Sep. 2001, pp. 238-246.

[93] Plumbridge W.J., Gagg C.R. and Peters S., "The Creep of Lead-free Solders at Elevated Temperature", Journal of Electronic Materials, Vol. 30, No. 9, 2001.

[94] Guo F., Lucas J.P. and Subramanian K.N., "Creep behavior in Cu and Ag particle-reinforced composite and eutectic Sn-3.5Ag and Sn-4.0Ag-0.5Cu non-composite joints," Journal of Materials Science: Materials in Electronics, Vol. 12 (2001), pp. 27-35.

[95] Woosley A., Swan G., Chong T.S., Matsushita L., Koschmieder T. and Simmons K., "Development of Lead(Pb) and Halogen Free Peripheral Leaded and PBGA Components to Meet MSL3 260C Peak Reflow," Proceedings of Electronics Goes Green, Berlin, 2000, pp. 146-153.

[96] Morris. J.W. Jr., Song H.G. and Fay Hua, "Creep Properties of Sn-rich Joints," IEEE Proceedings of Electronic Components and Technology Conference,

ATTENTION: The Singapore Copyright Act applies to the use of this document. Nanyang Technological University Library

2003, pp.54-57.

[97] Wiese S., Meusel E. and Wolter K.J., "Microstructural Dependence of Constitutive Properties of Eutectic SnAg and SnAgCu solders," IEEE Proceedings of Electronic Components and Technology Conference, 2003, pp.197-206.

[98] Dusek M., Hunt C., Do we know enough about Lead-free solders?, IPC/JEDEDC, October 2003, www.npl.co.uk/ei/.

[99] Lau John, Dauksher W. and Vianco P., "Acceleration Models, Constitutive Equations, and Reliability of Lead-Free Solders and Joints," IEEE Proceedings of 2003 Electronic Components and Technology Conference, pp.229-236, 2003.

[100] Schubert Andreas and Pang John, Lead Free Solder Materials and Reliability Performance, Short Course Notes at 4th Electronics Packaging Technology Conference, Lead-Free Workshop, 10th December 2002.

[101] Pang H.L John., Xiong B.S. and Low T.H., "Creep and Fatigue Properties of Lead Free Sn-3.8Ag-0.7Cu Solder," IEEE Proceedings of 2004 Electronic Components and Technology Conference, pp.1333-1337, June 1-4, 2004.

[102] John H.L. Pang and B.S Xiong, "Comparison of 95.5Sn-3.8Ag-0.7Cu Solder Joint and Bulk Solder Properties," TMS 2004, 133rd Annual Meeting and Exhibition, Charlotte, North Carolina, USA, March 14-18, 2004.

[103] Pang H.L. John, Xiong B.S. and Low T.H., "Low Cycle Fatigue Study of Lead Free 99.3Sn-0.7Cu Solder Alloy," International Journal of Fatigue, Vol. 26, Issue 8, August 2004, pp. 865-872.

[104] Pang H.L. John, Xiong B.S. and Low T.H., "Low Cycle Fatigue Models For Lead Free Solders," Thin Solid Film, Vol. 462-463, September 2004, pp. 408-412.

[105] J.D. Morrow, Cyclic Plastic Strain Energy and Fatigue of Metals, ASTM STP 378, American Society for Testing and Materials, Philadelphia, PA, 1964, 45.

[106] Kairya Y., Hosoi T., Terashima S., Tanaka M. and Suga T., "Fatigue life

ATTENTION: The Singapore Copyright Act applies to the use of this document. Nanyang Technological University Library

enhancement of low sliver content Sn-Ag-Cu flip-chip interconnects by Ni addition," Proceedings of 2004 Inter Society Conference on Thermal Phenomena, pp.103-108, June 1-4, 2004.

[107] Lau H. John, D. Shang Guang, Lau C.Y. Dennis, Kung T.W. Terry and Lee S.W. Ricky, "Thermal-Fatigue life prediction equation for wafer-level chip scale package(WLCSP) lead-free solder joints on lead free printed cirruit board (PCB)," IEEE Proceedings of 2004 Electronic Components and Technology Conference, pp.1563-1569, June 1-4, 2004.

[108] Lin J.K., Jang J.K., Hayes S. and Frear D., "Lead free flip chip interconnect reliability for DCA and FC-PBGA packages," IEEE Proceedings of 2004 Electronic Components and Technology Conference, pp.642-649, June 1-4, 2004.

[109] Chakrabarty J., Applied Plasticity, Springer-Verlag New York, 2000.

[110] Donald C. Stouffer and L. Thomas Dame, Inelastic deformation of metals: models, mechanical properties, and metallurgy, John Wiley & Sons, 1996.

[111] Thomas H. Courtney, Mechanical Behavior of Materials, 1990, McGraw-Hill.

[112] Chaboche J.L., "Continuum Damage Mechanics: Part I — General Concepts," Journal of Applied Mechanics, Vol.55, 1998, pp.59-64.

[113] Chaboche J.L., "Continuum Damage Mechanics: Part II — Damage Growth, Crack Initiation, and Crack Growth," Journal of Applied Mechanics, Vol.55, 1998, pp.65-72.

[114] Lan Hong Dai and Shi-Wei Ricky Lee, "Characterization of Strain Rate-Dependent Behavior of 63Sn-37Pb Solder Alloy," Proceedings of InterPACK'01, July 8-13, Kauai, Hawaii, 2001, pp.1-7.

[115] Tanimura S., Mimura K. and Zhu W.H., "Practical Constitutive Models Covering Wide Ranges of Strain Rates, Strains and Temperature," Key Engineering Materials, 2000, pp.177-180.

[116] Amagai M., Chip Scale Package (CSP) solder joint reliability and modeling, Microelectronics Reliability 39, 1999, pp. 463 – 477.

ATTENTION: The Singapore Copyright Act applies to the use of this document. Nanyang Technological University Library

Appendix A. USERMAT Subroutine Code

This ANSYS subroutine code was programmed for applying the new constitutive model to Finite Element Analysis (FEA). User material subroutine, USERMAT was chosen to implement the new constitutive model subroutine code. The schematic illustration of the subroutine is shown in Fig. 1.

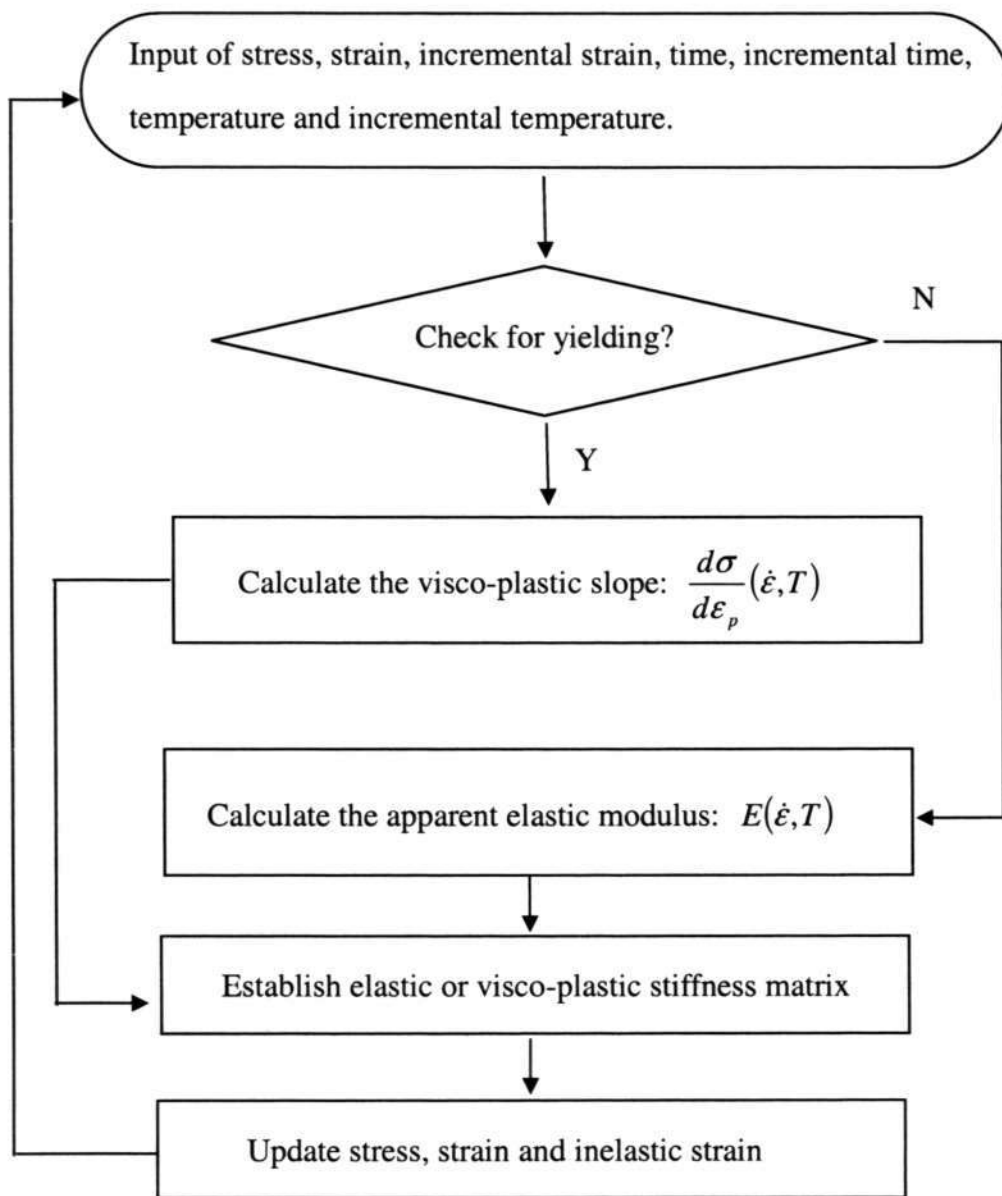

Fig. 1 Schematic illustration of new constitutive model subroutine

ATTENTION: The Singapore Copyright Act applies to the use of this document. Nanyang Technological University Library


```
      subroutine usermat3d(
     &                   matId, elemId,kDomIntPt, kLayer, kSectPt,
     &                   ldstep,isubst,keycut,
     &                   nDirect,nShear,ncomp,nStatev,nProp,
     &                   Time,dTime,Temp,dTemp,
     &                   stress,statev,dsdePl,sedEl,sedPl,epseq,
     &                   Strain,dStrain, epsPl, prop, coords,
     &                   rotateM, defGrad_t, defGrad,
     &                   tsstif, epsZZ,
     &                   var1, var2, var3, var4, var5,
     &                   var6, var7, var8)

#include "impcom.inc"
c
      INTEGER
     &                 matId, elemId,
     &                 kDomIntPt, kLayer, kSectPt,
     &                 ldstep,isubst,keycut,
     &                 nDirect,nShear,ncomp,nStatev,nProp
      DOUBLE PRECISION
     &                 Time,    dTime,   Temp,    dTemp,
     &                 sedEl,   sedPl,   epseq,   epsZZ
      DOUBLE PRECISION
     &                 stress  (ncomp  ), statev  (nStatev),
     &                 dsdePl  (ncomp,ncomp),
     &                 Strain  (ncomp  ), dStrain (ncomp  ),
     &                 epsPl   (ncomp  ), prop    (nProp  ),
     &                 coords  (3),       rotateM (3,3),
     &                 defGrad (3,3),     defGrad_t(3,3),
     &                 tsstif  (2)

c --- parameters
c
      INTEGER          mcomp
      DOUBLE PRECISION HALF, THIRD, ONE, TWO, SMALL, ONEHALF,
     &                 ZERO, TWOTHIRD, ONEDM02, ONEDM05, sqTiny
      PARAMETER        (ZERO       = 0.d0,
     &                 HALF        = 0.5d0,
     &                 THIRD       = 1.d0/3.d0,
     &                 ONE         = 1.d0,
     &                 TWO         = 2.d0,
     &                 SMALL       = 1.d-08,
     &                 sqTiny      = 1.d-20,
     &                 ONEDM02     = 1.d-02,
```

ATTENTION: The Singapore Copyright Act applies to the use of this document. Nanyang Technological University Library


```
     &                   ONEDM05      = 1.d-05,
     &                   ONEHALF      = 1.5d0,
     &                   TWOTHIRD     = 2.0d0/3.0d0,
     &                   mcomp        = 6
     &                   )

      EXTERNAL            vmove, rotVect
      DOUBLE PRECISION sigElp(mcomp), dsdeEl(mcomp,mcomp), G(mcomp),
     &                   sigDev(mcomp), JM     (mcomp,mcomp), dfds(mcomp),
     &                   dsdeVp(mcomp,mcomp), sigvp(mcomp),
     &                        stresslast(mcomp)

      DOUBLE PRECISION var1, var2, var3, var4, var5,
     &                   var6, var7, var8

      DATA G/1.0D0,1.0D0,1.0D0,0.0D0,0.0D0,0.0D0/
c
      INTEGER             i, j
      DOUBLE PRECISION pEl,    qEl,     pleq_t,   sigy_t , sigy,
     &                   dpleq, pleq,
     &                   young, posn,    sigy0,    dsigdep,
     &                   elast1,elast2,
     &                   twoG,   threeG,   oneOv3G, qElOv3G, threeOv2qEl,
     &                   fratio,   con1,     con2, sigts, dqElstrain,
     &                   strainrate, h, tyoung, sstr, qElstrain,
     &                   sigyhistory, visplas1, visplas2, sigyts
c***********************************************************************
c
      keycut     = 0
      dsigdep    = ZERO
      pleq_t     = statev(1)
      pleq       = pleq_t
c *** get Young's modulus and Poisson's ratio, initial yield stress and others
      young      = prop(1)
      posn       = prop(2)
      sigy0      = prop(3)
c *** plastic strain tensor
      do i = 4, ncomp
         statev(i+1) = 0.5d0 * statev(i+1)
      end do
c *** update plastic strain
      call rotVect(rotateM,statev(2),ncomp)
c *** back to engineering strain form
      do i = 4, ncomp
```

ATTENTION: The Singapore Copyright Act applies to the use of this document. Nanyang Technological University Library


```
            statev(i+1) = 2.0d0 * statev(i+1)
         end do
         call vmove(statev(2), epsPl(1), ncomp)
c *** calculate plastic slope
           dqElstrain=
     &    (dStrain(1) - dStrain(2))*(dStrain(1) - dStrain(2))+
     &    (dStrain(1) - dStrain(3))*(dStrain(1) - dStrain(3))+
     &    (dStrain(3) - dStrain(2))*(dStrain(3) - dStrain(2))+
     &    TWOTHIRD*(dStrain(4)**2+dStrain(5)**2+dStrain(6)**2)
         dqElstrain = sqrt( 4.d0/9.d0 * dqElstrain)
       qElstrain=
     &    (Strain(1) - Strain(2))*(Strain(1) - Strain(2))+
     &    (Strain(1) - Strain(3))*(Strain(1) - Strain(3))+
     &    (Strain(3) - Strain(2))*(Strain(3) - Strain(2))+
     &    TWOTHIRD*(Strain(4)**2+Strain(5)**2+Strain(6)**2)
         qElstrain = sqrt( 4.d0/9.d0 * qElstrain)
       strainrate=dqElstrain/dTime
         h=((strainrate/18.59d0)*EXP(5.645d03/Temp))**3.0d-01
         sstr=13.1d0*log10(h+SQRT(h*h+1))
         dsigdep=sstr*5.5d-04/
     &       ((5.5d-04+qElstrain)*(5.5d-04+qElstrain))
         twoG        = young / (ONE+posn)
         threeG      = ONEHALF * twoG
         elast1=young*posn/((1.0D0+posn)*(1.0D0-TWO*posn))
         elast2=HALF*twoG
c *** define tsstif(1) since it is used for calculation of hourglass stiffness
         tsstif(1) = elast2
c
c *** calculate elastic stiffness matrix (3d)
c
         dsdeEl(1,1)=(elast1+TWO*elast2)*G(1)*G(1)
         dsdeEl(1,2)=elast1*G(1)*G(2)+elast2*TWO*G(4)*G(4)
         dsdeEl(1,3)=elast1*G(1)*G(3)+elast2*TWO*G(5)*G(5)
         dsdeEl(1,4)=elast1*G(1)*G(4)+elast2*TWO*G(1)*G(4)
         dsdeEl(1,5)=elast1*G(1)*G(5)+elast2*TWO*G(1)*G(5)
         dsdeEl(1,6)=elast1*G(1)*G(6)+elast2*TWO*G(4)*G(5)
         dsdeEl(2,2)=(elast1+TWO*elast2)*G(2)*G(2)
         dsdeEl(2,3)=elast1*G(2)*G(3)+elast2*TWO*G(6)*G(6)
         dsdeEl(2,4)=elast1*G(2)*G(4)+elast2*TWO*G(1)*G(4)
         dsdeEl(2,5)=elast1*G(2)*G(5)+elast2*TWO*G(1)*G(5)
         dsdeEl(2,6)=elast1*G(2)*G(6)+elast2*TWO*G(2)*G(6)
         dsdeEl(3,3)=(elast1+TWO*elast2)*G(3)*G(3)
         dsdeEl(3,4)=elast1*G(3)*G(4)+elast2*TWO*G(5)*G(6)
         dsdeEl(3,5)=elast1*G(3)*G(5)+elast2*TWO*G(5)*G(3)
```

ATTENTION: The Singapore Copyright Act applies to the use of this document. Nanyang Technological University Library


```
      dsdeEl(3,6)=elast1*G(3)*G(6)+elast2*TWO*G(6)*G(3)
      dsdeEl(4,4)=elast1*G(4)*G(4)+elast2*(G(1)*G(2)+G(4)*G(4))
      dsdeEl(4,5)=elast1*G(4)*G(5)+elast2*(G(1)*G(6)+G(5)*G(4))
      dsdeEl(4,6)=elast1*G(4)*G(6)+elast2*(G(4)*G(6)+G(5)*G(2))
      dsdeEl(5,5)=elast1*G(5)*G(5)+elast2*(G(1)*G(3)+G(5)*G(5))
      dsdeEl(5,6)=elast1*G(5)*G(6)+elast2*(G(4)*G(3)+G(5)*G(6))
      dsdeEl(6,6)=elast1*G(6)*G(6)+elast2*(G(2)*G(3)+G(6)*G(6))
      do i=1,ncomp-1
        do j=i+1,ncomp
          dsdeEl(j,i)=dsdeEl(i,j)
        end do
      end do
c
c *** calculate the trial stress and
c     copy elastic moduli dsdeEl to material Jacobian matrix
      do i=1,ncomp
         sigElp(i) = stress(i)
         do j=1,ncomp
            dsdePl(j,i) = dsdeEl(j,i)
            sigElp(i) = sigElp(i)+dsdeEl(j,i)*dStrain(j)
         end do
      end do
c *** hydrostatic pressure stress
      pEl = -THIRD * (sigElp(1) + sigElp(2) + sigElp(3))
c *** compute the deviatoric stress tensor
      sigDev(1) = sigElp(1) + pEl
      sigDev(2) = sigElp(2) + pEl
      sigDev(3) = sigElp(3) + pEl
      sigDev(4) = sigElp(4)
      sigDev(5) = sigElp(5)
      sigDev(6) = sigElp(6)
c *** compute von-mises stress
      qEl =
     &  sigDev(1) * sigDev(1)+sigDev(2) * sigDev(2)+
     &  sigDev(3) * sigDev(3)+
     &  TWO*(sigDev(4) * sigDev(4)+ sigDev(5) * sigDev(5)+
     &  sigDev(6) * sigDev(6))
      qEl = sqrt( ONEHALF * qEl)
c *** compute current yield stress
     sigy0=(-1.36d-1*(Temp-273)+67.54)*
     &   (strainrate**(5.59d-4*(Temp-273)+0.0675))
     sigy = sigy0+ dsigdep * pleq
c
      fratio = qEl / sigy - ONE
```

ATTENTION: The Singapore Copyright Act applies to the use of this document. Nanyang Technological University Library


```
c *** check for yielding
      IF (sigy .LE. ZERO.or.fratio .LE. -SMALL) GO TO 500
c
      sigy_t = sigy
      threeOv2qEl = ONEHALF / qEl
c *** compute derivative of the yield function
      DO i=1, ncomp
         dfds(i) = threeOv2qEl * sigDev(i)
      END DO
      oneOv3G   = ONE / threeG
      qElOv3G   = qEl * oneOv3G
c *** initial guess of incremental equivalent plastic strain
      dpleq     = qElOv3G - sigy * oneOv3G
      pleq      = pleq_t + dpleq
      sigy      = sigy0 + dsigdep * pleq
c
c ***  update stresses
      DO i = 1 , ncomp
         stress(i) =  sigElp(i) - TWOTHIRD * (qEl-sigy) * dfds(i)
      END DO
c
c ***  update plastic strains
      DO i = 1 , nDirect
         epsPl(i) = epsPl(i) + dfds(i) * dpleq
      END DO
      DO i = nDirect + 1 , ncomp
         epsPl(i) = epsPl(i) + TWO * dfds(i) * dpleq
      END DO
      epseq   = pleq
c *** Update state variables
      statev(1) = pleq
      do i=1,ncomp
         statev(i+1) = epsPl(i)
      end do
c *** Update plastic work
      sedPl = sedPl + HALF * (sigy_t+sigy)*dpleq
c
c *** Material Jcobian matrix
c
      IF (qEl.LT.sqTiny) THEN
         con1 = ZERO
      ELSE
         con1 = threeG * dpleq / qEl
      END IF
```

ATTENTION: The Singapore Copyright Act applies to the use of this document. Nanyang Technological University Library


```
      con2 = threeG/(threeG+dsigdep) - con1
      con2 = TWOTHIRD * con2
      DO i=1,ncomp
         DO j=1,ncomp
            JM(j,i) = ZERO
         END DO
      END DO
      DO i=1,nDirect
         DO j=1,nDirect
            JM(i,j) = -THIRD
         END DO
         JM(i,i) = JM(i,i) + ONE
      END DO
      DO i=nDirect + 1,ncomp
         JM(i,i) = HALF
      END DO
      DO i=1,ncomp
         DO j=1,ncomp
            dsdePl(i,j) =     dsdeEl(i,j) - twoG
     &                 * (   con2 * dfds(i) * dfds(j) + con1 * JM(i,j) )
         END DO
      END DO
c
      goto 600
  500 continue

c *** Update stress in case of elastic/unloading
      do i=1,ncomp
         stress(i) = sigElp(i)
      end do

  600 continue
      sedEl = ZERO
      DO i = 1 , ncomp
         sedEl = sedEl + stress(i)*(Strain(i)+dStrain(i)-epsPl(i))
      END DO
      sedEl      = sedEl * HALF
      statev(nStatev) = sigy
c
 990  CONTINUE
c
      return
      end
```

ATTENTION: The Singapore Copyright Act applies to the use of this document. Nanyang Technological University Library

Appendix B. FEA Simulation of Simple Tension Displacement Case Study

A simple tension displacement simulation was conducted to verify the new visco-plastic model subroutine. A 2-Dimension plane strain model was used to model simple tension displacement. Fig. 1 shows the boundary condition of the simulation. PLANE183 element was used for new model simulation; while VISCO108 element was used for Anand model simulation. The simple tension case study was simulated at different temperatures and strain rates by changing the uniform temperature and loading time, the simulation matrix is shown in Table 1. Each simulation used displacement loading up to 1% strain.

The FEA simulation was also conducted by using Anand model for comparison to the new visco-plastic model results. It was found that both the new visco-plastic model and Anand model simulation results gave a computed stress (at 1% strain) which decrease with temperature and increase with strain rate. The simulation results at 10^{-3} s^{-1} strain rate at different temperatures are shown in Fig. 2. It can be seen that both the models have similar trend and agree fairly well. Fig. 3 shows the comparison of the computed stress at 1% strain in tension for the new model and Anand model results. The new visco-plastic constitutive model show similar trend compared with the Anand model and gave higher computed stress by 12%.

ATTENTION: The Singapore Copyright Act applies to the use of this document. Nanyang Technological University Library

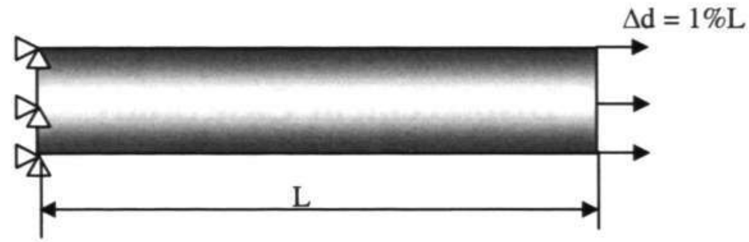

Fig. 1 Boundary condition of tensile simulation

Table 1 Simulation matrix

	25°C	75°C	125°C
10^{-4} s^{-1}	√	√	√
10^{-3} s^{-1}	√	√	√
10^{-2} s^{-1}	√	√	√

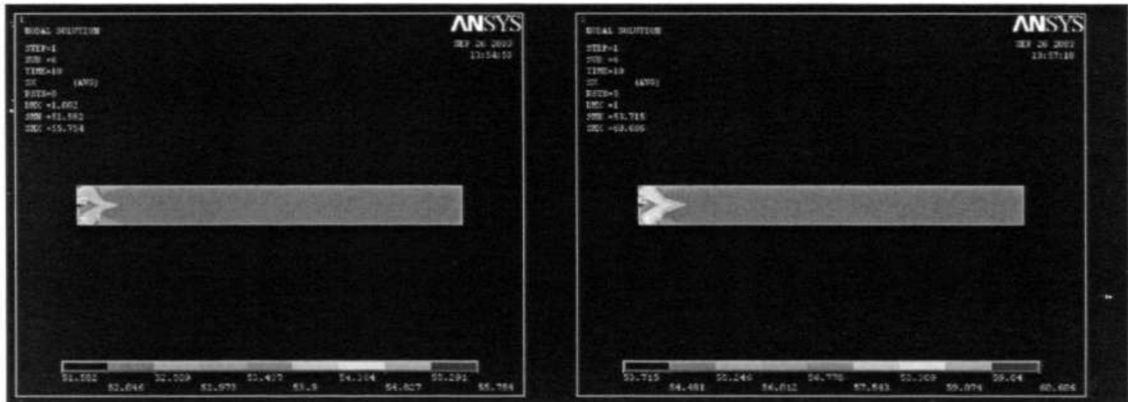

Anand model　　　　Own model

Fig. 2(a) Simple tensile test simulation result at 25°C and strain rate of 10^{-3} s^{-1}

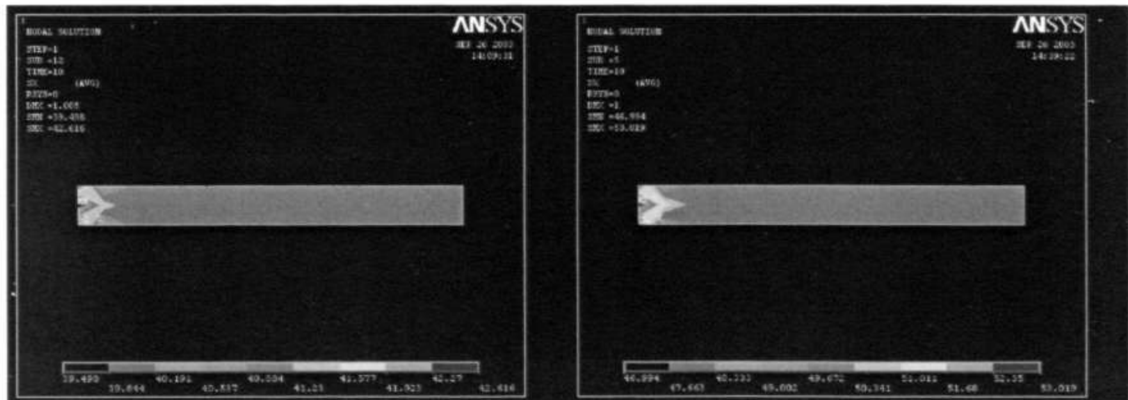

Anand model　　　　Own model

Fig. 2(b) Simple tensile test simulation result at 75°C and strain rate of 10^{-3} s^{-1}

ATTENTION: The Singapore Copyright Act applies to the use of this document. Nanyang Technological University Library

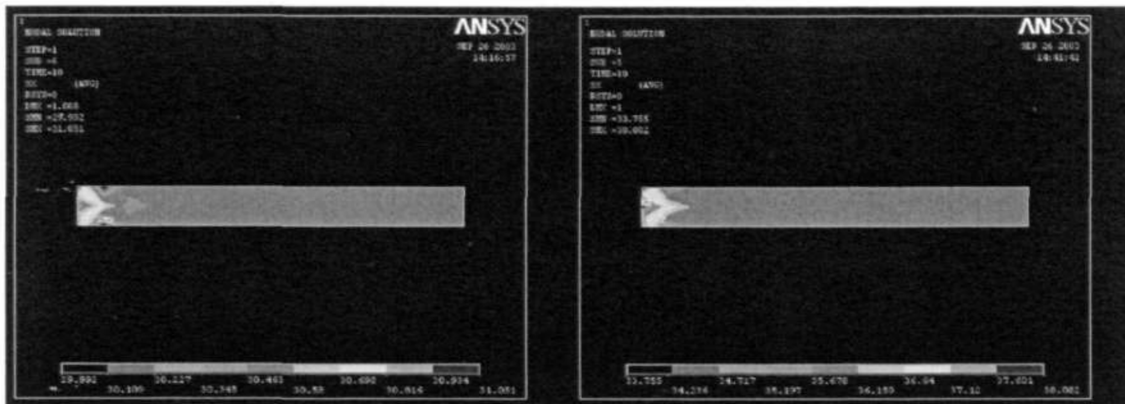

Anand model Own model

Fig. 2(c) Simple tensile test simulation result at 125°C and strain rate of 10^{-3} s^{-1}

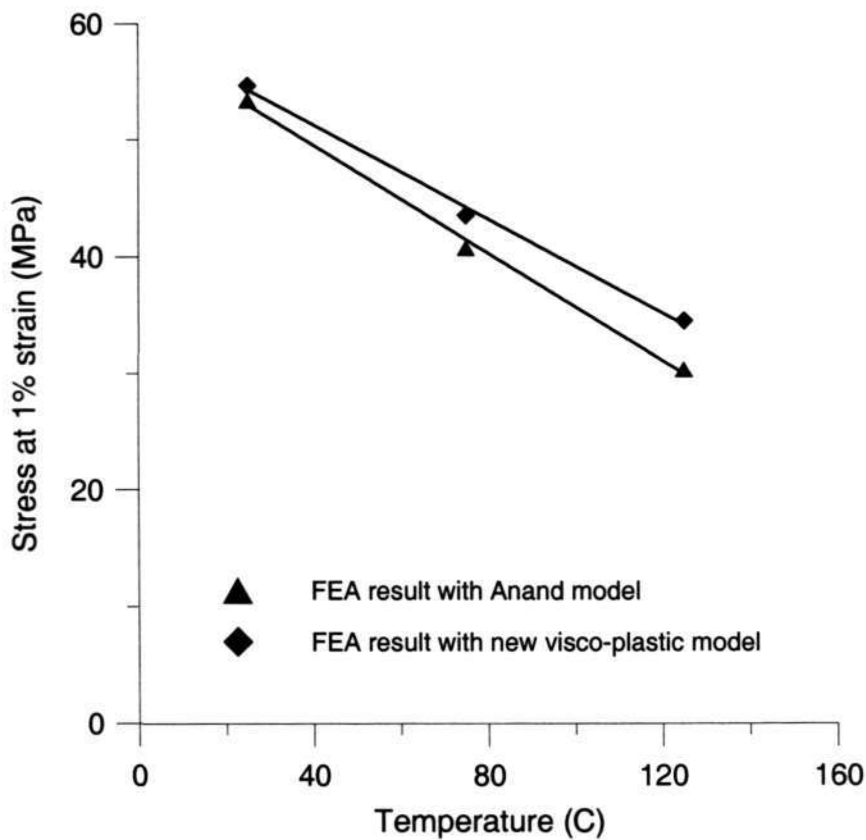

Fig. 3 Comparison of simple tensile test at 10^{-3} s^{-1} and different temperatures

ATTENTION: The Singapore Copyright Act applies to the use of this document. Nanyang Technological University Library

Appendix C. List of Journal Publication

1. Pang H.L. John, **Xiong B.S.** and Low T.H., "Low Cycle Fatigue Study of Lead Free 99.3Sn-0.7Cu Solder Alloy," International Journal of Fatigue, Vol. 26, Issue 8, August 2004, pp.865-872.
2. Pang H.L John., **Xiong B.S.** and Low T.H., "Comprehensive Mechanics Characterization of Lead-Free 95.5Sn-3.8Ag-0.7Cu Solder," Micromaterials and Nanomaterials, Issue 3, 2004, pp.86-93.
3. Pang H.L. John, **Xiong B.S.** and Low T.H., "Low Cycle Fatigue Models For Lead Free Solders," Thin Solid Film, Vol. 462-463, September 2004, pp. 408-412.
4. Pang H. L. John, Low T. H., **Xiong B.S.**, Xu Luhua and Neo C. C., "Thermal cycling aging effects on Sn–Ag–Cu solder joint microstructure, IMC and strength," Thin Solid Film, Vol. 462-463, September 2004, pp. 370-375.
5. Pang H.L. John, **Xiong B.S.**, Neo C.C. and Low T.H., "Mechanical Properties for 95.5Sn-3.8Ag-0.7Cu Lead Free Solder Alloy," IEEE Transactions of Components and Packaging Technologies (Accepted).